Human cerebellum and ventral tegmental area interact during extinction of learned fear

Enzo Nio[1,2], Patrick Pais Pereira[1,2], Nicolas Diekmann[3], Mykola Petrenko[1,2], Alice Doubliez[1,2], Thomas M. Ernst[1,2], Giorgi Batsikadze[1,2], Stefan Maderwald[2], Cornelius Deuschl[4], Metin Üngör[5], Sen Cheng[3], Christian J. Merz[6], Harald H. Quick[2,7], Dagmar Timmann[1,2]

[1] Department of Neurology and Center for Translational Neuro- and Behavioral Sciences (C-TNBS), Essen University Hospital, University of Duisburg-Essen, Essen, Germany;

[2] Erwin L. Hahn Institute for Magnetic Resonance Imaging, University of Duisburg-Essen, Essen, Germany;

[3] Institute for Neural Computation, Faculty of Computer Science, Ruhr University Bochum, Bochum, Germany;

[4] Institute of Diagnostic and Interventional Radiology and Neuroradiology, Essen University Hospital, University of Duisburg-Essen, Essen, Germany;

[5] Department of Psychology, Philipps-University Marburg, Marburg, Germany;

[6] Department of Cognitive Psychology, Institute of Cognitive Neuroscience, Ruhr University Bochum, Bochum, Germany;

[7] High-Field and Hybrid MR Imaging, Essen University Hospital, University of Duisburg-Essen, Essen, Germany

Send correspondence to

Enzo Nio, MSc
Department of Neurology, Essen University Hospital
Hufelandstr. 55
45147 Essen, Germany
Email: enzo.nio@uk-essen.de
Phone: +49 201 723 2594
Fax: +49 201 723 5534

Abstract

The key elements for fear extinction learning are unexpected omissions of expected aversive events, which are considered to be rewarding. Given its reception of reward information, we tested the hypothesis that the cerebellum contributes to reward prediction error processing driving extinction learning via its connections with the ventral tegmental area (VTA). Forty-three young and healthy participants performed a three-day fear conditioning paradigm in a 7T MR scanner. The cerebellum and VTA were active during unexpected omissions of aversive unconditioned stimuli, particularly during initial extinction trials. Increased functional connectivity was observed between the cerebellum and VTA, indicating that the cerebellum could positively modulate VTA activity, which in turn might facilitate dopaminergic signaling during fear extinction learning. These results imply that an interaction between the cerebellum and VTA should be incorporated into the existing model of the fear extinction network.

Introduction

Deficits in learning to extinguish previously associated threat responses to cues that no longer signal danger are thought to be one of the main causes in the development of anxiety disorders, including post-traumatic stress disorder and social anxiety disorder[1]. Exposure therapy addresses this deficit and attempts to compensate for failed or absent extinction learning from the past[2]. This is modeled effectively with extinction training in classical fear conditioning paradigms where the previously paired conditioned stimulus (CS+) is no longer followed by the aversive unconditioned stimulus (US)[3,4]. At the beginning of extinction training the omission of the US is unexpected and this unexpected lack of the US is considered to be rewarding[5–7]. This reward prediction error is thought to drive safety learning. This newly learned safety association should then inhibit the initially learned fear association (which is never fully lost)[8].

The reward system in the brain is primarily associated with the mesolimbic dopamine system[9], i.e., the ventral tegmental area (VTA) and the ventral striatum. In fact, recent rodent studies provide strong evidence that the VTA is central for extinction learning, and that (reward) prediction errors are encoded in a subset of VTA neurons[5–7,10]. Importantly, new evidence indicates that the cerebellum receives reward signals[11–13], and has direct efferent connections with the mesolimbic dopaminergic system, in particular the VTA[14–17].

Functional magnetic resonance imaging (fMRI) findings in healthy human participants suggest that the cerebellum is involved in processing of prediction errors in fear conditioning[18,19]. Ernst et al.[18] studied acquisition of learned fear responses using a partial reinforcement rate, i.e., a subset of CS+ trials were not reinforced during acquisition training. Cerebellar activations were strongest in the unreinforced CS+ trials, when the US was expected but did not occur. An unreinforced CS+ trial can be considered as a very first extinction trial, and cerebellar activations may reflect prediction errors driving extinction learning. Likewise, recordings from the VTA in rodents showed strong activations at the time the US is expected and does not occur during initial extinction trials[6,10]. The aim of the present fMRI study is therefore to test the hypothesis that the cerebellum contributes to fear extinction learning via its connection to the VTA.

In contrast to the previous one-day study design[18], here we used a three-day design with acquisition training on day 1, extinction training on day 2 and a recall test on day 3. This multi-day study design allowed enough time for consolidation of both fear and extinction memory traces. Furthermore, to increase the size of the reward prediction error at the initial US omission in extinction training trials, a full (100%) reinforcement rate was used during acquisition training. Previous studies showed significant spontaneous recovery of learned fear in initial recall test trials (unreinforced CS+) following extinction training in humans, which allowed us to test for cerebellar activations related to reward prediction errors also on day 3. Additionally, after the recall test on day 3, a reacquisition phase with a partial reinforcement rate (i.e., with unexpected US omissions between reinforced trials) and a subsequent reextinction phase were realized. Taken together, we were able to access cerebellar activity related to the unexpected omission of the US at various points during the experiment. We used a deep reinforcement learning model fitted to trial-by-trial skin conductance response (SCR) data to compute individual prediction errors. 7T fMRI allowed us to assess VTA activation. Results showed significant functional interaction between the cerebellum and VTA related to prediction errors, particularly during initial extinction trials. These findings suggest that the cerebellum contributes to extinction learning via the VTA, and thus supports safety learning inhibiting the initial fear association.

Results

Behavioral data

SCR data is reported below, pupil size data is provided in the supplementary information (Supplementary figure 1, Supplementary table 1). Statistical analysis of SCR data is summarized in Supplementary table 2.

Skin conductance responses (SCRs)

During habituation (day 1), SCRs did not differ between CS+ and CS- (Figure 1, top row). SCRs for both stimuli decreased significantly in habituation trials. Non-parametric ANOVA-type statistics revealed a significant effect for Time (early vs. late; F_1 = 26.49; p<.001) but not for Stimulus (CS+ vs. CS-; F_1 = 1.19; p=0.28) or the Stimulus x Time interaction (F_1 = 0.06; p=0.80).

During fear acquisition training (day 1), participants underwent a fully reinforced, semi-instructed differential fear conditioning protocol. Participants quickly learned the associations, and their responses decreased as expected due to habituation effects (Figure 1, top row). SCRs for the CS+ were significantly higher than for the CS- and decreased in late trials. Non-parametric ANOVA-type statistics revealed a significant effect of Stimulus (CS+ vs. CS-; F_1 = 16.28; p<.001) and Time (early vs. late; F_1 = 24.49; p<.001). No significant Stimulus x Time interaction was observed (F_1 = 3.33; p=0.07).

During extinction training (day 2), SCRs were significantly higher for the CS+ than for the CS– only in initial extinction trials (Figure 1, top row). Non-parametric ANOVA-type statistics revealed a significant effect of Stimulus (CS+ vs. CS-; F_1 = 6.57; p=0.01) and Time (early vs. late; F_1 = 21.10; p<.001). The Stimulus x Time interaction was not significant (F_1 = 2.83; p=0.09). For pupil size responses (PSRs), the Stimulus x Time interaction was significant (F_1 = 4.28; p=0.039). Post-hoc tests showed that PSR related to the CS+ was significantly lower during late extinction compared to early (least squares means test; p < .001), but not for PSR related to the CS- (least squares means test; p = 0.64; see supplementary materials), indicating extinction learning towards the CS+.

During the recall test (day 3), SCRs for CS+ were significantly higher than for CS- (Figure 1, bottom row). In late recall, no difference between SCRs for CS+ and CS- were observed. Non-

parametric ANOVA-type statistics revealed a significant main effect of Stimulus (CS+ vs. CS-; F_1 = 4.19; p=0.04), Time (early vs. late; F_1 = 32.47, p<0.001) and a Stimulus x Time interaction (F_1 = 5.27; p=0.02). Post-hoc tests revealed that SCRs for CS+ were significantly higher than for CS- in early trials (least squares means test; p < .001) but not in late trials (least squares means test; p = 0.98). SCRs for both stimuli significantly decreased in late trials compared to early trials (least squares means test; both: p < .001).

During reacquisition on day 3, SCRs for the CS+ were significantly higher than for the CS- and decreased for both stimuli in late reacquisition (Figure 1, bottom row). Non-parametric ANOVA-type statistics revealed a significant effect of Stimulus (CS+ vs. CS-; F_1 = 26.65, p<0.001), Time (early vs. late; F_1 = 30.37, p<0.001) and a Stimulus x Time interaction (F_1 = 6.34, p=0.01). Post-hoc tests showed that both stimuli were higher in early vs late reacquisition training (CS- early vs. CS- late; p = 0.02; CS+ early vs. CS+ late; p < .001), and a significant difference between stimulus types early and late (all p values < .001).

During reextinction on day 3, SCRs related to the CS+ were significantly higher than for the CS- although the difference was small (Figure 1, bottom row). Non-parametric ANOVA-type statistics revealed a significant main effect of Stimulus (CS+ vs. CS-; F_1 = 4.3; p=0.04), but not for Time (early vs. late; F_1 = 0.2; p=0.65) nor for the Stimulus x Time interaction (F_1 = 1.1; p=0.29). For PSRs, the Stimulus x Time interaction was significant (F_1 = 4.43; p=0.035), and PSRs related to the CS+ were significantly higher than to the CS- in early trials, but not in late trials (see supplementary materials).

In the last phase on day 3, three CS+ trials were unexpectedly reinforced ("unexpected US phase"). SCRs for the CS+ were significantly higher than for the CS- (Figure 1, bottom row). Non-parametric ANOVA-type statistics revealed a significant main effect of Stimulus (CS+ vs. CS-; F_1 = 5.68; p=0.02), but neither for Time (early vs. late; F_1 = 0.26; p=0.61) nor for the Stimulus x Time interaction (F_1 = 2.81; p=0.09).

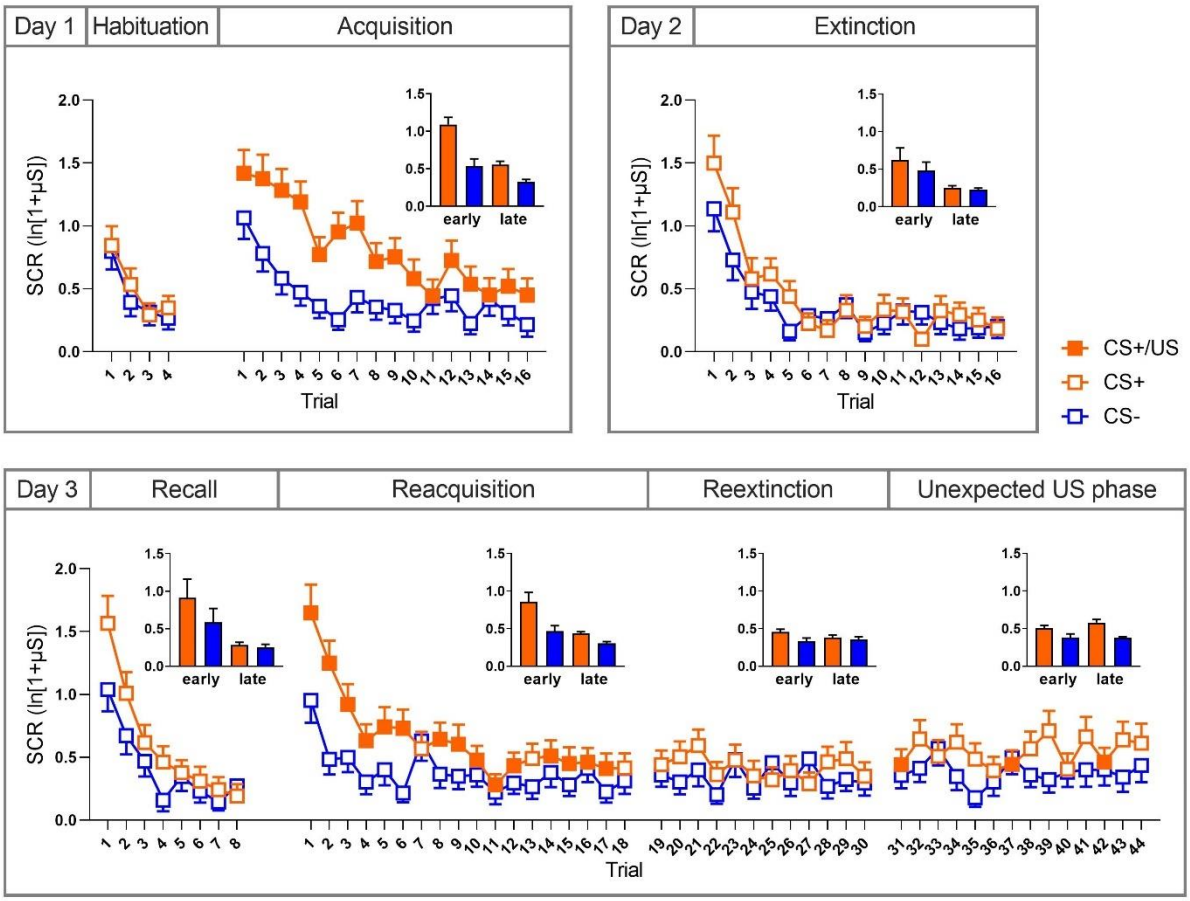

Figure 1*: Skin conductance responses (SCRs) for each trial, with CS+ (shown in orange) and CS- (shown in blue) responses paired in blocks. Reinforcement of the CS+ by a US (CS+/US) is indicated by filled squares. The CS- is never reinforced. Bar plots on the top right show early and late mean responses for both CS+ and CS-. On day 1, there was no differentiation between CS+ and CS- in the habituation phase, with significant differentiation emerging during acquisition training. On day 2, there was a loss of differentiation during extinction training. On day 3, during the initial recall test, participants exhibited spontaneous recovery, i.e., a return of differential responses after extinction training. During initial reacquisition, there were again differential responses to the CS+ and CS-, which decreased in reextinction and the unexpected US phase. Mean values are shown with error bars representing the standard error of the mean. CS: Conditioned stimulus; US: Unconditioned stimulus; SCR: Skin conductance response; µS: microSiemens.*

Self-reports

Valence, arousal, fear and US expectancy ratings of the CS+ did not differ significantly from the CS- before acquisition training (Supplementary table 3,4). Following acquisition training, the CS+ was rated as more arousing, fearful and unpleasant compared to the CS-. Participants expected the US to follow the CS+ but not the CS-. Although less pronounced, these CS+/CS- differentiations persisted after extinction training and recall test. The difference between CS+ and CS- increased at the end of day 3, when CS+/US pairings were reintroduced.

Non-parametric ANOVA-type statistics showed a significant main effect of Stimulus, Time and a Stimulus x Time interaction (all $p<0.001$; Supplementary table 4). Post-hoc tests revealed significant differences between stimulus type (CS+, CS-) following acquisition training, extinction training, recall test and at the end of day 3 but not after habituation.

fMRI results

Analysis of BOLD fMRI responses revealed significant activations related to the prediction, the presentation and the unexpected omission of the US (Figure 2). Our primary focus was on activations related to the unexpected omission of the US, which could be detected across four distinct phases: extinction training, recall test, reacquisition, and reextinction (Figure 3). Statistical analyses are summarized in Supplementary table 5-9.

Activations related to US prediction (CS+ > CS- and CS+ x prediction)

In the event-based analysis, there was no significantly higher activation in the cerebellum during the CS+ compared to the CS- (CS+ > CS-) during acquisition or extinction training. In the same contrast, the lateral VTA exerted significant differential activations during acquisition (Figure 2A; threshold free cluster enhancement (TFCE) and family-wise error (FWE) corrected $p<0.05$), but not during extinction training. Trend-level results showed differential cerebellar activation in posterolateral regions (lobule VI, Crus I, Crus II, lobule VIIb and VIIa; Figure 2A, D; uncorrected $p<0.05$) during acquisition training, which match results obtained by Ernst and colleagues (2019).

In the parametric modulation analysis, there were significant activations in the cerebellum (lobule and vermis I-VI), deep cerebellar nuclei (DCN) and VTA negatively associated with CS+ prediction value modulation during acquisition training (CS+ x prediction; Figure 2B), whereas there were significant positively associated activations during extinction training (Figure 2E; lobule VI and Crus I bilaterally, right lobule V and VTA). Parametric modulation results indicate that early CS+ presentations are paired with high cerebellar activations in both acquisition and extinction training, with prediction values being low during early and high during late acquisition, whereas prediction values are high during early and low during late extinction (Figure 5C). In other words, the activations were negative due to high activations of early CS+

compared to late CS+ events with prediction values taking the opposite course (i.e., low during early acquisition and high during late acquisition).

Activations related to US presentation (US post CS+ > no US post CS-)

During acquisition training, significant activations related to the presentation of the US (US post CS+ > no US post CS-) were widespread and included the whole cerebellum and VTA (Figure 2C,F). Cerebellar activations extended to the DCN. Peak activations in the cerebellum were found ipsilateral to the US (electrical stimulation applied to right hand).

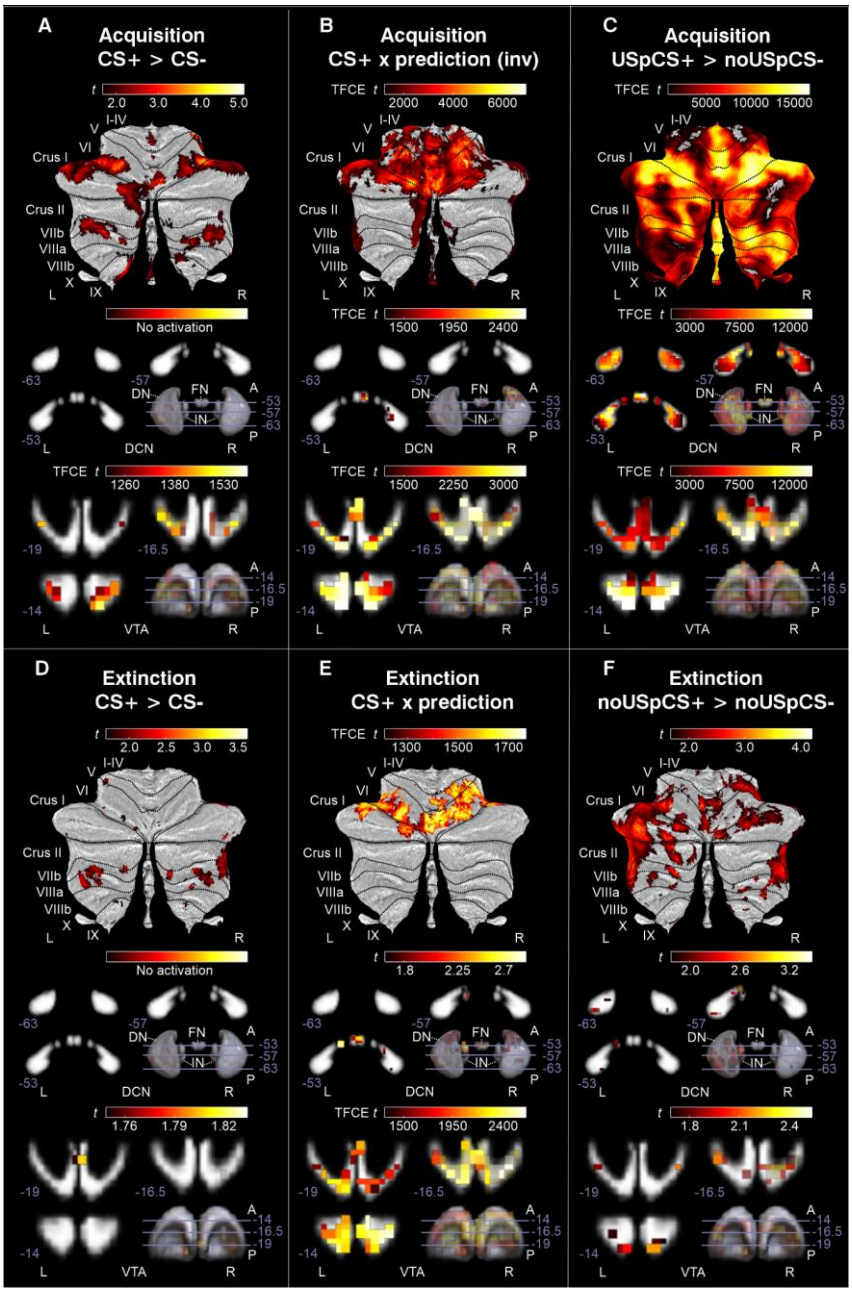

***Figure 2**: Cerebellar cortex, DCN and VTA fMRI activations related to the prediction and presentation of the US. Cerebellar cortex activations are shown on cerebellar flatmaps (SUIT;* Diedrichsen & Zotow, 2015)*, while VTA and DCN activations are displayed on coronal slices progressing from posterior to anterior with MNI y-coordinates indicated on the left-bottom for each slice. A 3D rendering in the bottom right shows the slice locations within the probabilistic DCN and VTA atlases (see methods for atlas generation). **A**: The event-based CS+ > CS- prediction contrast showed trend-level activations in posterolateral lobules and the VTA; no DCN activations were found. **B**: Inverse activations were found in the parametric modulation analysis of CS+ x prediction showing activations mainly in the anterior cerebellum, the paravermis, lobule VI and Crus I, and VTA, with trend-level activations in the DCN. **C**: The presentation of the US elicited widespread cerebellar, DCN and VTA activation. **D**: The event-based CS+ > CS- contrast in extinction training showed trend-level activations in lobule VIIb, VIIIa and VIIIb and the central VTA, and no activations in the DCN. **E**: The parametric modulation contrast CS+ x prediction showed activations in lobule VI and Crus I, vermis, and VTA, as well as trend-level activations in the DCN. **F**: Trend-level activations to the omission of the US in extinction training were shown in the cerebellum, DCN and VTA. VTA: Ventral tegmental area; DCN: Deep cerebellar nuclei; DN: Dentate nucleus; IN: Interposed nucleus; FN: Fastigial nucleus; CS: Conditioned stimulus; noUSpCS: Omission of unconditioned stimulus post CS; L: left; R: right; MNI: Montreal Neurological Institute standard brain; SUIT: Spatially unbiased atlas template of the cerebellum; TFCE t: threshold-free cluster-enhanced test-statistic.*

Activations related to the unexpected omission of the US (first 3 no US post CS+ > no US post CS- and no US post CS+ x prediction error)

Considering the whole extinction training phase, trend-level results showed activations in posterolateral lobules and the VTA related to the omission of the US (no US post CS+ > no US post CS-; Figure 2F). When focusing specifically on the early trials in extinction training to quantify activations related to the unexpected omission of the US, we found significant activations in both event-based and parametric modulation analyses.

In the event-based analysis, the cerebellar cortex, DCN and VTA showed significant activations related to unexpected omissions of the US in initial trials for all four phases (first 3 no US post CS+ > no US post CS-; extinction training, recall test, reacquisition and reextinction; Figure 3A-D). The location of activations was consistent across phases, with highest activations in left posterolateral lobule VI and Crus I. Activations in the left posterolateral cerebellar cortex were paired with high activations in the left dentate nucleus. The VTA was bilaterally activated.

In the parametric modulation analysis, significant activations were found in the cerebellum for unexpected omissions during extinction training and the recall test (Figure 3E,F), and showed trend-level activations during reacquisition and reextinction (Figure 3G,H). The highest activations were again found in left lobule VI and Crus I. In the DCN, significant activations were found during extinction training with peak activations in the left dentate, with trend-level results in the recall test. In the VTA, results were significant during extinction training (Figure 3E), with trend-level activations during the recall test, reacquisition and reextinction.

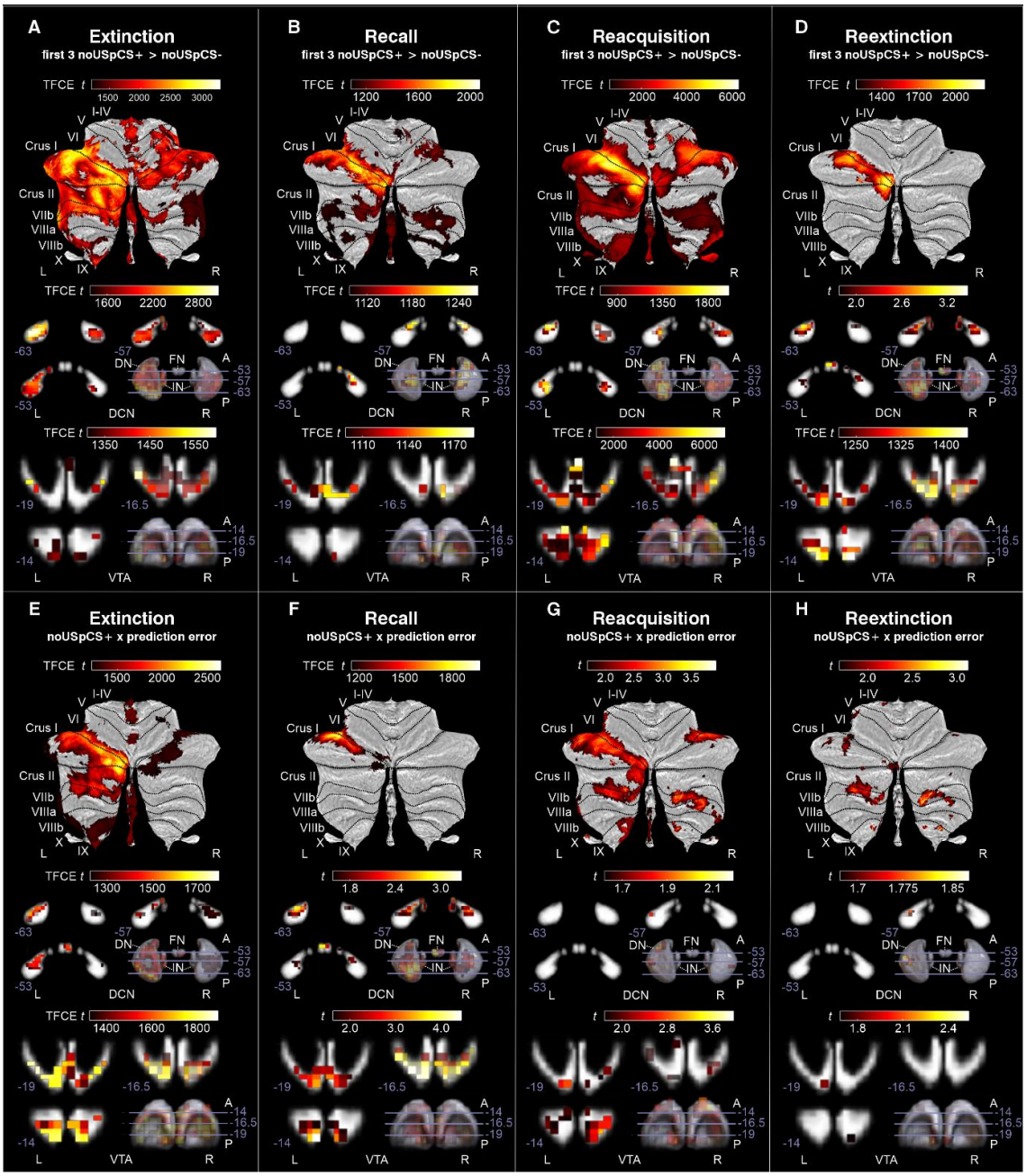

Figure 3*: Cerebellar cortex, DCN and VTA fMRI activations to the unexpected omission of the US. Cerebellar cortex activations are shown on cerebellar flatmaps (SUIT[20]), while VTA and DCN activations are displayed in coronal slices progressing from posterior to anterior with MNI y-coordinates indicated on the left-bottom for each slice. A 3D rendering in the bottom right shows the slice locations within the probabilistic DCN and VTA atlas (see methods for atlas generation).* ***A-D****: Event-based contrasts of the first 3 unexpected omissions showed activations in the cerebellar cortex, DCN and VTA for all four phases. Activations in the DCN during reextinction were trend-level. Activations were most consistent in left lobule VI and Crus I, with DCN activation mainly in the left dentate, while VTA activations were bilateral.* ***E-H****: Parametric modulation contrasts related to prediction errors from unexpected US omissions showed activations in all four phases in the cerebellum, DCN and VTA. Activations in reacquisition and reextinction were trend-level. Activations during the recall test in the DCN and VTA were trend-level. Activations were most consistently found in lobule VI and Crus I, in addition activations were found in the vermis, Crus II and lobule VIIb. VTA: Ventral tegmental area; DCN: Deep cerebellar nuclei; DN: Dentate nucleus; IN: Interposed nucleus; FN: Fastigial nucleus; CS: Conditioned stimulus; noUSpCS: Omission of unconditioned stimulus post CS; L: left; R: right; MNI: Montreal Neurological Institute standard brain; SUIT: spatially unbiased atlas template of the cerebellum; TFCE t: threshold-free cluster-enhanced test-statistic.*

PPI: Functional connectivity during unexpected US omissions between the cerebellum and VTA

Next, we aimed to assess functional interactions between the cerebellum and VTA using psychophysiological interaction (PPI), using the VTA as a seed region. In the parametric modulation analysis, we observed trend-level positive functional connectivity in left lobule VI and Crus I for extinction training, recall test, reacquisition and reextinction (Figure 4A; Supplementary table 7,8). When combining the contrasts by summing, the combination of all four phases showed similar positive functional connectivity between the cerebellar cortex and the VTA in lobule VI and Crus I, but only on a trend-level (Figure 4B). No activations were seen in the DCN.

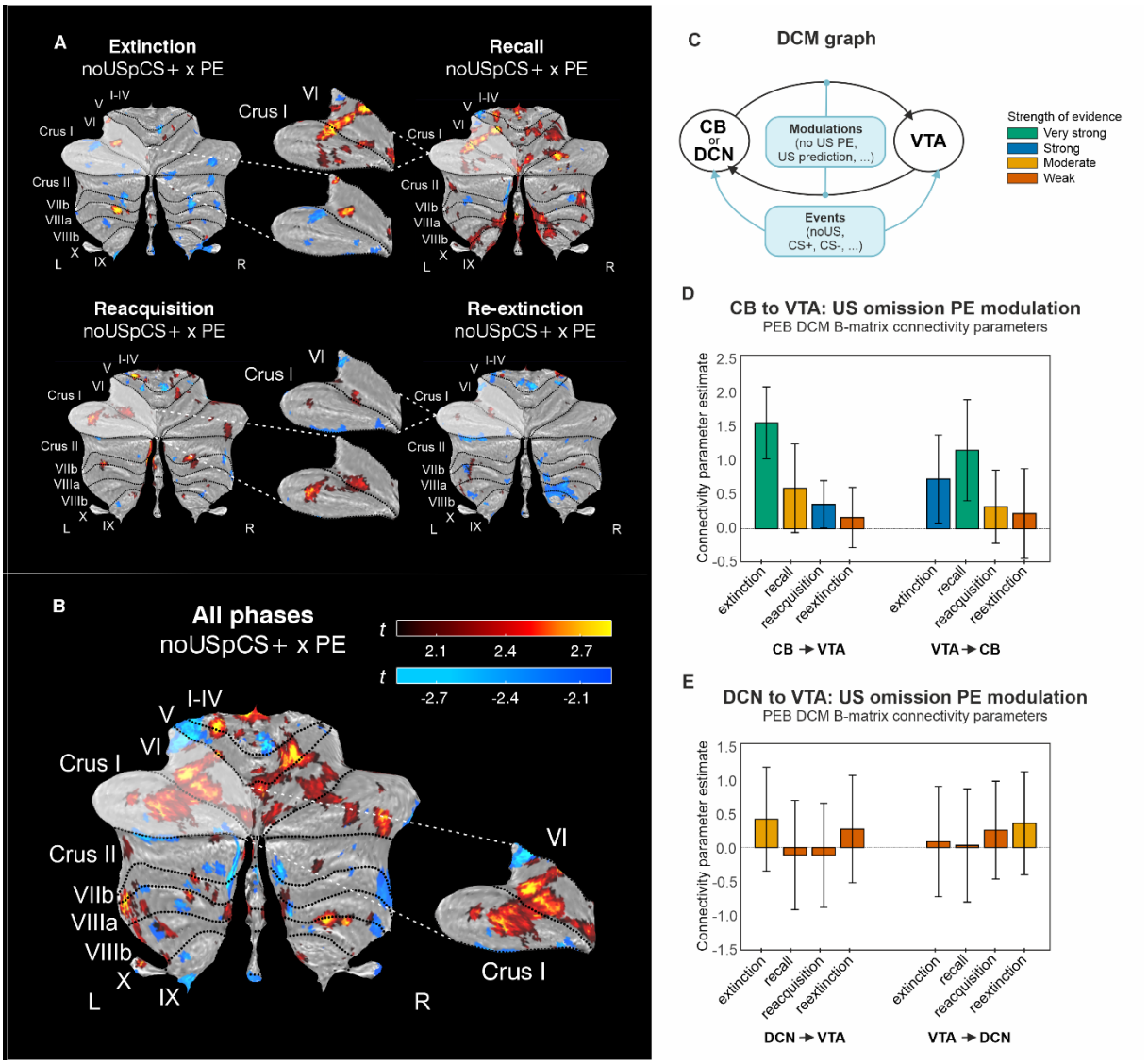

***Figure 4**: Functional connectivity analysis using PPI and DCM. **A,B**: Trend-level activations in the cerebellum found by PPI analysis using the VTA as a seed region, shown on cerebellar flatmaps [20]. To highlight activations, a zoomed cutout of lobule VI and Crus I is also shown. **A**: Trend-level connectivity with VTA is found in lobule VI and Crus I for extinction training, the recall test, reacquisition and reextinction using PPI of the unexpected US omission contrasts from the parametric modulation analysis with a VTA seed. **B**: Summary of trend-level PPI results by summing all contrasts in A. **C-E**: DCM analysis showed significant modulation of cerebellar cortex (CB) to VTA connections with prediction errors during unexpected omission events. **C**: DCM model is shown, modulations act on both the CB/DCN to VTA as well as the VTA to CB/DCN connections. Events, i.e., US post CS+, no US post CS+, no US post CS-, CS+ and CS- for each phase, are provided as inputs to both nodes. Colors of bars are determined by the posterior probability calculated in the PEB analysis (very strong: P>0.99; strong: 0.95<P<0.99; moderate: 0.75<P<0.95; weak: P<0.75). Very strong and strong results are considered significant, moderate results are considered trend-level. **D**: Significant modulations during extinction training, the recall test and reacquisition. The strongest result was found during extinction training in the connection from the cerebellum to VTA. **E**: Trend-level results showed connectivity from the DCN to VTA in extinction, and from the VTA to DCN in reextinction. PPI: Psychophysiological interaction; DCM: Dynamic causal modeling; PEB: Parametric Empirical Bayes; PE: Prediction error; P: Posterior probability; VTA: Ventral tegmental area; CB: Cerebellar region in lobule VI and Crus I consistently active during unexpected US omissions; US: unconditioned stimulus; L: left; R: right; SUIT: spatially unbiased atlas template of the cerebellum; t: test-statistic.*

DCM: Functional connectivity during unexpected US omissions between the cerebellum and VTA

In the dynamic causal modeling (DCM) parametric modulation analysis, unexpected omissions significantly positively modulated both the connection from cerebellar cortex (CB) to VTA and VTA to CB during extinction training (Figure 4D; very strong evidence, posterior probability $P>0.99$, strong evidence: $0.95<P<0.99$). In the recall test, the VTA to CB connection was positively modulated. In reacquisition, the CB to VTA connection was positively modulated. Results were less strong for the other unexpected omission modulations, with trend-level moderate evidence for the CB to VTA connection in the recall test and the VTA to CB connections in reacquisition, and weak evidence for both CB to VTA and VTA to CB connections in reextinction (Figure 4D; moderate $0.75<P<0.95$; weak $P<0.75$). In the model incorporating the DCN and VTA, there was a trend-level modulation from the DCN to the VTA during extinction training, as well as a trend-level modulation from the VTA to the DCN during reextinction (Figure 4E; moderate significance, $0.75<P<0.95$).

Discussion

The cerebellum and VTA were active during unexpected omissions of aversive unconditioned stimuli, particularly during initial extinction trials. Importantly, increased functional connectivity was observed between the cerebellum and VTA, indicating that during unexpected omissions in extinction training, the cerebellum could positively modulate VTA activity. These results support the view that an interaction between the cerebellum and VTA should be incorporated into the existing model of the fear extinction network. Furthermore, given that the unexpected omission of an aversive stimulus can be considered rewarding, data suggest that the cerebellum contributes to reward processing in humans, and that this may be one way how the cerebellum modulates non-motor functions, in our case the control of emotions. Our findings build on previous research in rodents showing that the cerebellum modulates addictive, social and depression-like behavior via direct projection to VTA in rodents[16,21].

Cerebellar activations were most prominent in trials with maximum prediction errors, i.e., during the initial extinction training phase, but were also seen in early recall, reacquisition and early reextinction. The activations in lobule VI and Crus I are consistent with previous findings by Ernst et al.[18] during unexpected omissions in a partially reinforced acquisition phase.

Additionally, other studies have reported activations in these regions during the prediction of the US in extinction training[22–25] and during unexpected omissions of aversive stimuli[26–29]. More broadly, activations in lobule VI and Crus I have been observed during US prediction[30], particularly in the early phases of acquisition training. Conversely, unexpected rewards lead to activation in Crus I[31], and a meta-analysis implicated left lobule VI and Crus I in both the anticipation and processing of rewarding outcomes[32]. Anticipation-related activations were more hemispheric, whereas rewarding outcome activations were more paravermal.

Activated areas in more lateral parts of lobule VI and Crus I overlap with multi-demand regions[33], whereas activations neighboring the vermis overlap with emotional regions[34]. The main components of the multi-demand (or executive) neural network are working memory, attention and inhibition[35]. Thus, attention-related processes involved in fear conditioning may

also contribute to cerebellar activations. Attention-related processes have been related to the salience of the stimulus[36], but are also thought to change when a cue is followed by an unexpected outcome with more attention being paid in the next trial[37,38]. Attention related processes may therefore contribute to activations in the more lateral cerebellar parts of lobule VI/Crus I. However, unexpected omission of the US should lead to increased attention to the CS in the next trial and therefore increased activation towards the CS (which was not the case) and not at the time the US was presented and did not occur.

Our findings of increased activation in the VTA related to the unexpected omission of the aversive US aligns well with rodent data[6,7]. In rodents, it has been shown that dopamine neurons in the VTA are active in initial extinction trials, and that lack of this dopamine signal prevents extinction learning[5,6,39]. In a more recent study, Salinas-Hernandez et al.[10] observed that these dopamine neurons project to extinction-related neurons of the nucleus accumbens, and receive input from the dorsal raphe. Our data show that the VTA is also involved in extinction learning in humans, and provide first evidence that the VTA receives input from the cerebellum during extinction learning. Esser et al.[40] found that the administration of L-Dopa in healthy human participants enhanced activation of the nucleus accumbens which was functionally coupled with the VTA at the time of unexpected omission of the US in early extinction learning, which is in good agreement with our findings.

The unexpected omission of the aversive US is thought to be rewarding and fMRI signals in the cerebellum and VTA may be related to reward prediction errors. Whereas the VTA has long been known to process rewards, and fMRI data in humans indicate that the VTA is active related to the unexpected presentation of rewards[41,42], the cerebellum has only recently been found to process reward signals in rodents[11,13,43]. FMRI signals are known to be driven by synaptic input[44–46]. In the cerebellum this is mainly related to mossy fiber input to the cerebellar cortex[47]. There is evidence, however, that granule cell activity also modulates vasodilatation and likely contributes to fMRI BOLD signals in the cerebellar cortex[48,49]. Likewise, recent evidence suggests that activation of dopamine neurons in the VTA leads to increased BOLD signals using DREADD-fMRI in rodents[50]. Human fMRI-PET studies have shown that VTA BOLD activation in response to rewards correlates with increases in dopamine in the

striatum, suggesting that the fMRI signal in the SN/VTA is related to dopaminergic neuron activity[42,51]. FMRI signals in the cerebellar cortex and VTA may therefore reflect incoming reward-related signals, prediction error processing or, maybe most likely, both. The origin of the afferent reward signals to the cerebellum remains unclear; while an early study showed afferent connections from the VTA to the cerebellum[52], this finding has not been replicated in more recent research[53]. However, preliminary evidence from Guarque-Chabrera et al.[54] suggests the existence of a connection from the VTA to the cerebellum.

In rodents, a subset of VTA dopamine neurons has been found to be active when the US is expected and does not occur, and are therefore considered to represent prediction error signals driving extinction learning[6,10]. The VTA, however, also contains neurons which are active during the presentation and prediction of threat[55,56], and likewise we observed fMRI activation of the VTA related to threat prediction and presentation. Cerebellar activations and their interactions are likely not limited to reward prediction errors; they may also be related to unexpected presentation of aversive stimuli. Because aversive stimulus presentation results in pronounced cerebellar activations, we were unable to separate cerebellar activation related to the unexpected (initial acquisition trials) and the expected (late acquisition trials) presentation of the US.

Although, the present findings are consistent with the interpretation of prediction error related activations in the VTA (and cerebellum), based on the present fMRI data, we cannot decide whether activations reflect surprise signals (i.e., unsigned prediction error related signals) or signed prediction error signals[37,57–59]. Rodent data show that cerebellar neurons in the cortex and nuclei increase activations both related to the unexpected presentation and omission of reward signals[60], which would indicate that the cerebellum primarily contributes to unsigned (reward) prediction errors. Likewise, a meta-analysis of human prediction error showed that activations in the cerebellum were more consistently related to unsigned prediction errors[61].

Results showed significant functional interaction between the cerebellum and VTA related to prediction errors in unexpected omission trials in extinction training, which was further confirmed by similar functional interactions in spontaneous recovery trials on day 3, and

unexpected omissions of the US in unreinforced trials in a partially reinforced reacquisition phase. Predictive output of the cerebellum may be linked to the timing of the unconditioned response and therefore its omission and may help to refine prediction error signals in the VTA.

Notably, the unexpected US omission area in the cerebellum was more prominent on the left, while we applied the US to the right. In our previous work it was also the left cerebellum which was mainly activated, however, stimulation was always done on the left[18,62]. As outlined above, we believe that cerebellar activation is reward related. In a recent meta-analysis of fMRI data in monetary reward tasks, reward outcome was also related to the left cerebellum (i.e., lobule VI in the cerebellar hemisphere and vermis)[32]. There is good evidence that emotional information is most prominently processed in the right cerebral hemisphere[63,64]. The present data suggest that emotional processing may also be lateralized in the cerebellum, with the left cerebellar hemisphere projecting to the right cerebral cortex and vice versa. Lateralization of positive emotions to left cerebellar lobule VI has also been reported by Liu et al.[65]. Furthermore, emotion-related tasks resulted in increased activity of the left cerebellar hemisphere in patients with anorexia nervosa compared to controls[66]. Meta-analyses of fMRI studies of emotional tasks, however, report mostly bilateral cerebellar activations with no clear lateralization[67–69]. These studies primarily focused on emotion recognition tasks. Future research should explore the lateralization of emotional processing in the cerebellum using a variety of emotional tasks. In addition to emotions, there is also a preference of the right cerebral hemisphere for the ventral fronto-parietal attention network, which has been related to the detection of potentially harmful events[70]. Thus, as outlined above, attention-related processes involved in fear conditioning may also contribute to (lateralized) cerebellar activations.

In the following, we discuss potential limitations of our study. Firstly, while we demonstrated functional connectivity in the DCM analysis, the results were weaker with PPI. PPI is known to frequently lack power and to have a high proportion of false negatives[71,72], particularly for event-based designs. Additionally, the low number of unexpected events in our experiment, due to the 100% reinforcement/non-reinforcement rates in acquisition training (which was designed to induce maximum prediction error in the initial extinction trials), may have made

detecting activation challenging. Furthermore, a lack of specificity of the unexpected omission condition to the cerebellum-VTA interaction may have contributed. As the PPI regressor is demeaned, any persistent activation (i.e., due to an anatomical connection) will decrease detected connectivity. Because cerebellar and VTA activation co-occur not only in response to unexpected US omissions, but also to US presentation and prediction, this lack of specificity could have weakened our results. The same reasons apply for the lack of observation in functional connectivity between the DCN and the VTA.

Secondly, in the DCM analysis, we observed strong modulation related to unexpected US omissions when using the cerebellar cortex and VTA as volumes of interest (VOIs), but observed only trend-level results when substituting the cerebellar cortex with the DCN. This is likely explained due to the high iron content in the DCN causing susceptibility artefacts and reducing signal[73]. Although we opted for a whole-brain sequence with a conventional echo-time in order to generate a dataset of general value, future studies could opt for lower echo times and optimize for detection of signal in the DCN[74].

Thirdly, the extent of the VTA varies depending on the MRI atlas used. The VTA in the atlas from Pauli et al.[75] is about 4 times smaller than the VTA in the atlas by Trutti et al.[76] due to different VTA definitions used. Our average volumes are in good accordance with Trutti et al.[76], which in turn is in good accordance with histological data. The VTA and its boundaries, particularly laterally, are not clearly visible on MRI scans and were identified by using landmarks such as the substantia nigra, red nucleus, interpeduncular fossa and the cerebral aqueduct. We have approximated the VTA region as closely as we could, but cannot rule out imperfect masks, especially at both lateral ends of the VTA.

In conclusion, our study provides evidence that the cerebellum contributes to fear extinction learning via its connections with the VTA, possibly by modulating dopaminergic VTA neurons processing (reward) prediction errors driving fear extinction learning. Previous studies found that the cerebellum modulates addictive and social behavior via direct projection to VTA in rodents. Our findings extent this observation to the control of emotions. Added knowledge to the fear extinction network, on the other hand, may provide new ways of improving exposure

therapy by targeting the dopaminergic system or stimulating the cerebellum specifically during unexpected learning events.

Online Methods

Preregistration

This study was preregistered on OSF on 16/11/2023[77]. The preregistration document can be viewed at https://osf.io/n4df3/?view_only=d541dc3b6a304e31a16eadd3a02f152f.

The preregistration outlines the methods explained here, and includes the main hypotheses. Adjustments were made to specific parts of the methods, which include the optimized localization of the VTA and DCN by manual drawing by an expert annotator, and the inclusion as volumes of interest (VOIs) in the functional connectivity analyses.

Participants

Experiment power estimate and number of participants

Experiment power was estimated based on previous fear conditioning data acquired at 7T fMRI[18] using the FMRIPower toolbox (fmripower.org)[78]. Considering first level unexpected US omission contrasts during a partially reinforced acquisition training and aiming for a power of 80% at $p<.005$ for a one-sided hypothesis test, group sizes were estimated to 41 participants for Crus I ipsilaterally to US presentation (effect size 0.56 in units of standard deviations). To account for potential dropouts and outliers, 50 participants were initially recruited. However, only 44 successfully completed the three-day study, with reasons for non-completion including Covid-related issues (1 participant), problems with the Digitimer equipment (3 participants), and failure to attend on day 3 (2 participants). Additionally, one participant dropped out due to a shimming failure, resulting in a final sample size of 43 participants.

Exclusion criteria and demographic information

Participants were between 20 and 35 years old (23 men, 20 women, mean age: 24.7 (SD = 3.4) years), fluent in German, non-smokers, reported no intake of medication or illicit drugs affecting the central nervous system, had no history of neurological or mental disorders for themselves or their first-degree relatives, and had no previous participation in similar learning experiments. Additionally, female participants were not pregnant, breastfeeding, or using hormonal contraceptives. Before the experiment, participants completed the Depression Anxiety Stress Scale (DASS21G)[79]. Participants who scored higher than 20 for depression, 14

for anxiety or 25 for stress components were excluded from the study. All participants were right-handed based on the Edinburgh handedness inventory[80]. Participants were asked to refrain from alcohol consumption the night before the experiment. Informed consent was obtained from all participants. The study was approved by the local ethics committee and conducted in accordance with the Declaration of Helsinki.

Fear conditioning paradigm

Participants underwent a three-day differential fear conditioning paradigm. The paradigm presentation was controlled by a computer running Presentation (version 21.0, Neurobehavioral System Inc, Berkeley, CA). Participants were shown two visual stimuli (square and diamond) as CS (CS+ and CS-) and informed that electrical stimulations would be applied during the experiment. Three types of trials were used: reinforced CS+ (CS+ paired with the US; CS+/US), unreinforced CS+ (no US) and unreinforced CS-. The CS- was never reinforced.

The paradigm consisted of seven phases separated over three days (Figure 5A). On day 1, the experiment started with a habituation phase consisting of 8 unreinforced CS- and CS+ trials (4 CS+ trials, 4 CS- trials, presented in semi-randomized order). This phase is intended to decrease novelty effects and enable participants to acclimate to the scanner environment and presentation of visual stimuli. The habituation phase was followed by acquisition training consisting of 32 trials with fully reinforced CS+ (16 CS+/US, 16 CS- trials), during which the fear association was learned. On day 2, extinction training was applied which consisted of 32 unreinforced trials (16 CS+, 16 CS-). On day 3, the recall test, reacquisition, reextinction and the unexpected US phase were applied. The recall test consisted of 16 unreinforced trials (8 CS+, 8 CS-). This phase tested the recall of extinguished fear responses and showed spontaneous recovery (see Results). Reacquisition, reextinction, and the unexpected US phases were done in a single continuous fMRI run without pauses between sequences. The partially reinforced reacquisition phases consisted of 36 trials (15 CS+/US trial, 3 CS+, 18 CS-) with 3 unexpected omissions of the US, reextinction consisted of 24 trials (12 CS+, 12 CS-) and the unexpected US phase consisted of 28 trials (3 CS+/US trial, 11 CS+, 14 CS-) with 3 unexpected reinforced CS+ trials (Figure 5A). Learned fear responses were measured by skin conductance responses (SCRs) and pupil size reactions (PSRs) in each trial. The reacquisition,

reextinction and unexpected US phases were included to increase the number of trials with high prediction errors (i.e., discrepancy between US expectation and actual US presentation).

We used the model from Batsikadze et al.[28] to optimize our experimental design. Values for US prediction and US prediction error produced by the model were recorded during simulation. Simulations were repeated for different paradigm CS sequences, and the sequence which required a short number of trials and still yielded high prediction errors was selected.

A

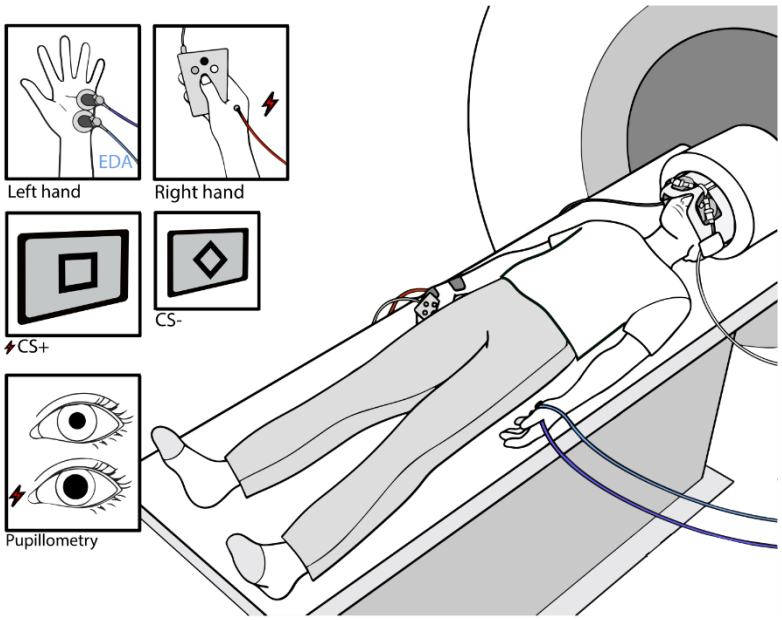
EDA
Left hand
Right hand
CS+
CS-
Pupillometry

B

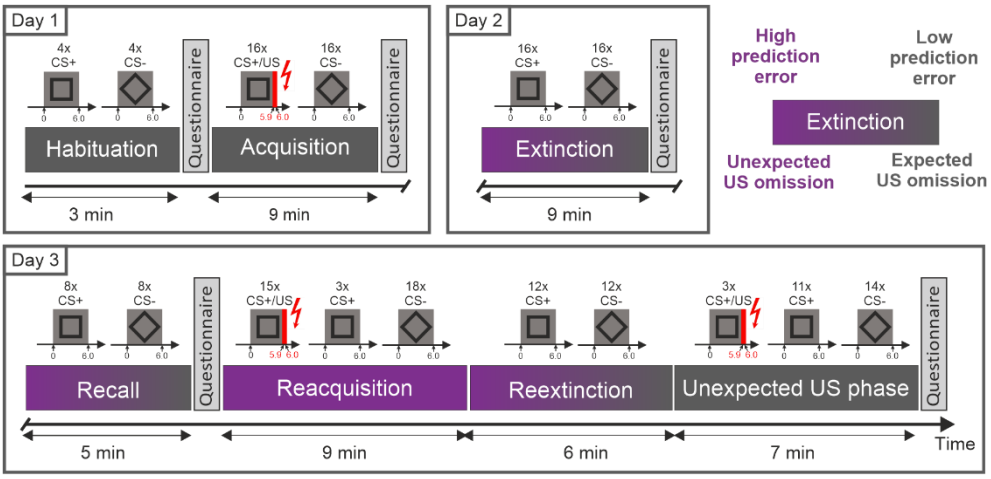
Day 1
4x CS+
4x CS-
16x CS+/US
16x CS-
Habituation
Questionnaire
Acquisition
Questionnaire
3 min
9 min
Day 2
16x CS+
16x CS-
Extinction
Questionnaire
9 min
High prediction error
Low prediction error
Extinction
Unexpected US omission
Expected US omission
Day 3
8x CS+
8x CS-
15x CS+/US
3x CS+
18x CS-
12x CS+
12x CS-
3x CS+/US
11x CS+
14x CS-
Recall
Questionnaire
Reacquisition
Reextinction
Unexpected US phase
Questionnaire
5 min
9 min
6 min
7 min
Time

C

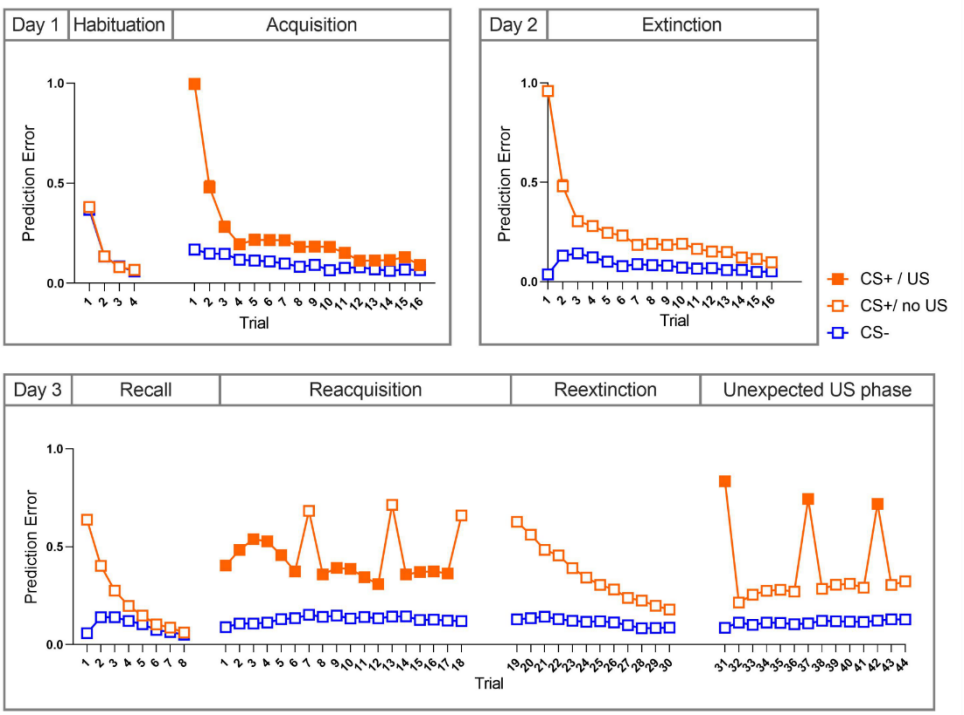
Day 1
Habituation
Acquisition
Prediction Error
Trial
Day 2
Extinction
Prediction Error
Trial
CS+ / US
CS+/ no US
CS-
Day 3
Recall
Reacquisition
Reextinction
Unexpected US phase
Prediction Error
Trial

***Figure 5A**: Overview of the three-day fear conditioning paradigm. Day 1 consists of habituation and acquisition training, day 2 consists of extinction training, and day 3 consists of the recall test, reacquisition, reextinction and the unexpected US phase. In acquisition training, the CS+ is reinforced 100% of the time, while reacquisition and the unexpected US phases contain 3 unexpected US omissions and 3 unexpected US presentations, respectively, with respective reinforcement rates of 83.3% and 21.4%. Extinction, the recall test, reacquisition and reextinction are marked in purple to indicate that these phases are of interest when studying unexpected US omissions. Extinction, recall test and reextinction show a gradient, as in these phases the US omissions are gradually less unexpected (as opposed to distinct unexpected US omission events during the partially reinforced reacquisition phase). **5B**: Schematic of participant lying in the MRI scanner. EDA was measured on the left-hand hypothenar eminence (EDA; blue and purple cables). The US was applied to the first dorsal interosseous muscle area of the right hand; red cable). The button box was held in the right hand. Dielectric bags and cushions were included to reduce susceptibility artifacts and head movement. The participants viewed a screen placed at the end of the scanner bore through mirrors, and the eyes were simultaneously imaged and tracked by an infrared camera. **5C**: Mean absolute prediction error values for each trial estimated from SCRs, with CS+ and CS- responses paired in blocks. Reinforcement of the CS+ by a US (CS+/US) is indicated by filled squares. Prediction and prediction error values were estimated over 200 iterations. CS: Conditioned stimulus; US: Unconditioned stimulus; EDA: Electrodermal activity.*

The CS+ and CS- were presented in equal numbers during the first and second half of each phase, regardless of whether the CS+ was followed by a US or not. Counterbalancing was implemented for the visual CS (CS+ square and CS- diamond, or CS+ diamond and CS- square) as well as for the order of presentation of the CS during the unreinforced habituation, extinction training, and recall test phases (i.e., CS+ presented first or CS- presented first). The reinforced acquisition training and reacquisition phases always started with a CS+. The two orders of CS presentation were pseudorandomly generated, similar to Ernst et al.[18]. Participants were instructed to pay attention to any possible connection between the CS and US presentations. They were also informed that the patterns of CS and US presentations would stay the same across all phases. However, they were not told about the CS/US contingencies or the timing and occurrence of the US.

In the analysis, the focus was on trials containing unexpected omissions of the US (CS+/no US) with high prediction error values. These trials occurred during early extinction, early recall, reacquisition and the reextinction phase.

CS visual stimuli

Visual stimuli were displayed on an fMRI monitor (BOLD-screen 32, Cambridge Research Systems Ltd., Rochester, UK) placed at the end of the scanner bore which was projected to the participant using a mirror system (Figure 5B). Two pictures of black geometric figures (a square and a diamond shape) on a gray background were used as CS+ and CS-. Both CS were presented for 6 s. The period of the CS was shortened from 8 s used in our previous study[18] to

6 s to decrease the length of the experiment, while still being able to assess SCRs[4]. In the periods between visual stimuli a fixation cross was shown (time of ITI: varies between 9 s and 13.5 s).

US aversive stimulus

In reinforced CS+ trials, the visual stimulus co-terminated with the presentation of the aversive US, an electric shock (100 ms) applied to the first dorsal interosseous muscle area of the right hand via a 6.5 mm concentric surface electrode (WASP electrode, Specialty Developments, Bexley, UK). The US was produced by a high voltage DC stimulator (DS7A, Digitimer Ltd., London, UK) and consisted of four consecutive 500 µs current pulses (maximum output voltage: 400 V) with an inter pulse interval of 33 ms. The location of the US electrode was kept constant across all days of measurement by marking the electrode position with a permanent marker on day 1 and 2. Before the first experimental phase began, the individual electrical stimulation intensity threshold was calibrated to be perceived as 'very unpleasant but not painful'. To reach the threshold, the current strength was progressively increased and modulated according to each participant's feedback. The calibrated US intensity was increased by 20 % to compensate for possible habituation to the US, which could result in a weakening of the conditioned responses as successfully done in previous studies of our group[28,81]. The US intensity remained the same for the three days of the experiment (mean US intensity: 3.8 (SD = 2.9) mA, range 0.6-19.2 mA).

Physiological data acquisition

During each phase, SCRs and pupil size were recorded. SCRs were acquired with appropriate hardware filters sampling at 2 kHz through an MP160 Data Acquisition Hardware unit (BIOPAC Systems Inc, Goleta, CA). Two SC electrodes were attached to the left-hand hypothenar eminence. Pupil size was measured using an MRI compatible eye tracking system (Avotec Inc, Stuart, FL). Calibration of the eye tracking system was performed prior to each phase to track gaze position on the screen.

Self-reports

After each learning phase, participants completed questionnaires using a 4-button fiberoptic response device (Current Designs, Haverford, PA). The Likert scale questionnaires assessed

self-reports such as arousal (rated on a 1-9 scale from 1: "very calm" to 9: "very nervous"), valence (rated on a 1-9 scale from 1: "comfortable" to 9: "uncomfortable"), and fear (rated on a 1-9 scale from 1: "not afraid" to 9: "very afraid") related to the visual stimuli. The questionnaires also included questions about US perception and CS-US contingency. Additionally, participants completed standardized questionnaires before the start of the experiment to assess handedness, depression, anxiety, and stress levels. All participants were screened for contraindications of 7T MRI.

Skin conductance analysis

To eliminate high frequency artefacts, skin conductance data was first low-pass filtered at 10 Hz (62nd-order Blackman FIR filter) in MATLAB (Release 2022b, RRID:SCR_001622, The MathWorks Inc., Natick, MA). SCRs were defined as the maximum trough-to peak-amplitude within a given time interval after CS onset using semi-automated peak detection implemented in a MATLAB-based EDA-Analysis App[82]. A minimum amplitude criterion of 0.01 µS was used as the SCR detection threshold. In each trial, SCRs were evaluated for two distinct time windows: the conditioned response within a time window of 1.0 s to 5.9 s after CS onset and the unconditioned response within a time window of 6 s to 10 s after CS onset (irrespective of whether a US was presented). To account for between-subjects variance, the resulting raw SCR amplitudes were increased by 1 µS and normalized through a logarithmic transformation (LN(1+SCR))[83,84].

Pupil size analysis

Preprocessing of the raw pupil size data was performed to detect and remove blinks[85]. Trials with fewer than 50% of their data points remaining after blink removal were excluded from the analysis. For each trial, the baseline was computed as the mean pupil size during the 500 ms period prior to CS onset. The baseline was subtracted from the corresponding pupil size and the result was divided by the baseline to compute the pupil size response[86,87]. The mean pupil size response for CS+ and CS- trials were calculated in the time windows from 4 to 5.9 s and 6.0 to 8.0 s for the CS and US pupil size response, respectively. Pupil size responses during possible US presentation were excluded (5.9 to 6 s). The time window for the CS was chosen based on Jentsch et al.[86] who observed the largest differentiation between CS+ and CS- 2 s

prior to the US. The US time window was chosen to match the CS time window. For valid trials, a missing pupillometric data point was considered as 'not a number value' to not influence the pupil size mean computation[87].

Behavioral statistical analysis

For physiological data, due to non-normal distribution (SCR and PSR: Shapiro-Wilk test, $p < 0.001$), statistical analysis was performed using the ANOVAF option in the PROC Mixed procedure in SAS Studio 3.8 (SAS Institute Inc., Cary, NC, USA). This method is suggested for addressing skewed distributions, outliers, or small sample sizes. To ensure more reliable results, an ANOVA-type statistic (ATS) was applied, with the denominator degrees of freedom set to infinity[88–90] as the use of finite denominator degrees of freedom can result in increased type I errors[91]. The ATS was calculated for each phase (habituation, acquisition training, extinction training, recall test, reacquisition, reextinction, unexpected US phase), with stimulus type (CS+, CS-) and block (early vs. late) as within-subjects factor and SCRs or PSRs as dependent variables.

For analyses of self-reports, an ATS with repeated measures was calculated with stimulus type and phase as within-subjects factor and ratings (valence, arousal, fear and US expectancy) as dependent variables.

For behavioral results, a $p<0.05$ criterion was used to determine if results were significantly different from those expected if the null hypotheses were correct. Post-hoc comparisons were calculated using least square means tests and were adjusted for multiple comparisons using the Tukey-Kramer method.

Computational modeling

An artificial agent was trained to predict the likelihood of a shock for a given visual input in a virtual version of the experiment as in Batsikadze et al.[28]. The model was based on reinforcement learning[92] and consisted of a deep neural network (DNN)[93]. The model hyper-parameters were fit to SCRs recorded in the experiment, which served as a read-out of the participants' expectation of an US.

The same simplified visual stimuli for trial stimuli s_t and the same encoding for reinforcement signals r_t were used as in Batsikadze et al.[28]. We employed the same network architecture, which comprised two hidden fully connected layers with 64 units each and an output layer with activation function φ. For each of the two trial sequences experienced by the participants, 25 randomly initialized agents were trained during the fitting of hyper-parameters, and 100 randomly initialized agents were trained to derive trial-by-trial values for predictions v_t and prediction errors δ_t from the best fit. On each trial t, the agent stored an experience tuple $e_t = (s_t, r_t, \delta_t)$ in memory for later replay[94]. The agents were trained using the backpropagation algorithm[95] on batches of experiences of size b, which were sampled randomly from memory with a probability that was proportional to a priority score p:

$$P(e_k) = \frac{p_k}{\sum_{j=1}^{T} p_j}$$

Priority scores depended on the experiences' recency λ^{τ}, where τ is the time passed since the experience and λ is a decay factor. Optionally, the priority could additionally depend on the magnitude of US prediction error, i.e., $p = |\delta|\lambda^{\tau}$ [96]. The parameter RPE ∈ {Yes, No} indicates whether the replay priorities also depended on the magnitude of the US prediction error. The number of replays i was varied to control the degree of learning on each trial.

While the previous model could account for ABA renewal[28], it cannot account for spontaneous recovery in the AAA paradigm, because, in the model, extinction in the same context overwrites the association formed during acquisition. Hence, we extended the model by an additional replay phase, which takes place between habituation, acquisition, extinction, recall and reextinction phases, and serves to recover the initially acquired association. This replay phase prioritized experiences according to the reinforcement r_k received in a trial and consisted of a total 100 replays of batches of size 128. Reactivation probabilities for these replays were computed as follows:

$$P(e_k) = \frac{e^{\beta r_k}}{\sum_{j=1}^{T} e^{\beta r_j}}$$

where β denotes the inverse temperature and controls the relative difference of reactivation probabilities.

Hyper-parameter fitting

We averaged SCRs from CS+ and CS- trials separately for each trial sequence and applied min-max scaling. The averaged SCRs were accordingly defined as $\bar{Y}_l = (\bar{y}_{+,1}, \ldots, \bar{y}_{+,N}, \bar{y}_{-,1}, \ldots, \bar{y}_{-,N})$, where $\bar{y}_{+,n}$ and $\bar{y}_{-,n}$ are the averaged SCRs for the n-th CS+ and n-th CS- presentations across all participants who completed a given trial sequence l, respectively. Analogously, the averaged US predictions of the model were defined as $\bar{V}_l(b, \lambda, i, \beta, RPE, \varphi) = (\bar{v}_{+,1}, \ldots, \bar{v}_{+,N}, \bar{v}_{-,1}, \ldots, \bar{v}_{-,N})$, where $\bar{v}_{+,n}$ and $\bar{v}_{-,n}$ are the averaged US predictions for the n-th CS+ and CS- presentations across all model instances who were trained on a given trial sequence l, respectively. The goodness of fit was defined as:

$$\bar{F}(b, \lambda, i, \beta, RPE, \varphi) = \sum_{l=1}^{L} w_l \left(\|\bar{Y}_l - \bar{V}_l(b, \lambda, i, \beta, RPE, \varphi)\| + P_{Acq} + P_{Gen} + P_{Ext} + P_{Ren} + P_{Rex} \right)$$

where w_l is the number of participants who experienced trial sequence l. To ensure that the overall learning curve in the model resembled that of the participants, we added the following penalty terms, if the model failed to

1. learn that CS+ is followed by the US: $P_{Acq} = \begin{cases} 0, \bar{v}_{Acq,End} \geq 0.5 \\ 1, \bar{v}_{Acq,End} < 0.5 \end{cases}$ where $\bar{v}_{Acq,End}$ is the average US prediction over the last 2 CS+ presentations of acquisition training.
2. show the CR at the start of extinction training: $P_{Gen} = \begin{cases} 0, \bar{v}_{Ext,Start} \geq 0.5 \\ 1, \bar{v}_{Ext,Start} < 0.5 \end{cases}$ where $\bar{v}_{Ext,Start}$ is the average US prediction over the first 2 CS+ presentations of extinction training.
3. successfully extinguish the CR during extinction training: $P_{Ext} = \begin{cases} 0, \bar{v}_{Ext,End} < 0.1 \\ 1, \bar{v}_{Ext,End} \geq 0.1 \end{cases}$ where $\bar{v}_{Ext,End}$ is the average US prediction over the last 2 CS+ presentations of extinction training.

4. show renewal of the CR: $P_{Ren} = \begin{cases} 0, \bar{v}_{Rec,Start} \geq 0.5 \\ 1, \bar{v}_{Rec,Start} < 0.5 \end{cases}$ where $\bar{v}_{Rec,Start}$ is the average US prediction over the first 2 CS+ presentations of recall.
5. successfully extinguish the CR during recall: $P_{Rex} = \begin{cases} 0, \bar{v}_{Rec,End} \leq 0.1 \\ 1, \bar{v}_{Rec,End} > 0.1 \end{cases}$ where $\bar{v}_{Rec,End}$ is the average US prediction over the last 2 CS+ presentations of recall

A grid search was conducted over the hyper-parameter sets shown in Table 1. The model with the best goodness-of-fit was then chosen to derive trial-by-trial values for US predictions and prediction errors. Prediction errors were used for parametric modulation of fMRI data to test hypotheses related to prediction error processing of the cerebellum and VTA.

Table 1: Modeling. Parameters the grid search was run for.

Grid Search Parameters	
b (batch size)	{1, 16, 32, 64}
λ (decay factor)	{0.5, 0.525, 0.55, ..., 0.95, 0.975, 1}
i (training repeats)	{1, 2, 3, 4, 5, 6, 7, 8, 9, 10}
β (inverse temperature)	{0, 0.5, 1, 1.5, 2, 2.5, 3, 3.5, 4, 4.5, 5}
RPE	{Yes, No}
φ	{ELU, Sigmoid}

MRI acquisition

All MRI imaging data was collected while participants were lying supine in the 7T MRI scanner (MAGNETOM Terra, Siemens Healthineers AG, Forchheim, Germany). A 1-channel transmit/32-channel receive head RF coil (Nova Medical Inc., Wilmington MA, USA), was used. Two dielectric pads for signal homogenization were placed on either side of each participant's upper neck[97]. Depending on head size, further cushioning was added to prevent participant head movement and discomfort.

Whole brain functional MRI acquisition was performed with a 3-dimensional echo planar image sequence[98] with an isotropic voxel size of 1.5 mm. The sequence was run for each phase (habituation, 98 volumes; acquisition training, 354 volumes; extinction training, 350 volumes; recall test, 182 volumes; reacquisition, reextinction and unexpected US phases; 938 volumes).

Imaging parameters were as follows: TR/TE, 1620/20 ms; flip angle, 11°; phase encoding acceleration factor, 2; 3D acceleration factor, 3; slice partial Fourier factor, 7/8; acquisition matrix, 140 × 140; number of slices, 96.

After acquisition training on day 1, a transversal QSM ASPIRE sequence was acquired[99,100] with an isotropic voxel size of 0.7 mm. Further imaging parameters were as follows: TR/TE1/TE2/TE3/TE4/TE5, 28/5/10/15/20/25 ms; flip angle 15°; phase encoding acceleration factor, 3; slice partial Fourier factor, 6/8; acquisition matrix, 320 × 280; number of slices, 256; TA, 10:52 min.

After the acquisition of the QSM ASPIRE sequence, a sagittal MP2RAGE sequence including fat navigators[101–103] was acquired with an isotropic voxel size of 0.75 mm. Further imaging parameters were as follows: TR/TE, 6000/1.85 ms; TI1/TI2, 800/2750 ms; flip angles 1/2, 4°/5°; phase encoding acceleration factor, 3; acquisition matrix, 340 × 340; number of slices, 256; TA, 14:58 min.

Image processing

Motion correction of MP2RAGE volumes including fat navigators was performed using offline reconstruction with the Retro-MoCo toolbox for MATLAB provided by David Gallichan (version23 0.9.0dev, https://github.com/dgallichan/retroMoCoBox.git). A T1 map was generated from the motion corrected MP2RAGE with the MP2RAGE-utils package implemented in MATLAB (release 1.0, https://github.com/srikash/MP2RAGE-utils). The MP2RAGE was normalized to MNI-space using the CAT12 (CAT12, release 1450)[104] toolbox in SPM12 (Wellcome Department of Cognitive Neurology, London, UK).

Functional MRI volumes were brain extracted with BET (Brain Extraction Tool)[105] in FSL (Release 6.0.1, RRID:SCR_002823, Centre for Functional MRI of the Brain, Oxford, UK). Motion and distortion correction was performed for each fMRI run with ANTs (Version 2.3.5, RRID:SCR_004757, University of Pennsylvania, Philadelphia, USA)[106]. A 5-volume fMRI sequence preceding each run with phase encoding in the opposite direction was used for the distortion correction. All volumes were coregistered to a T1 map derived from the acquired MP2RAGE with ANTs. The CAT12 processing of the MP2RAGE was used to normalize fMRI

data. A 4.5 mm Gaussian kernel was used for smoothing. Motion nuisance regressors (3 translations, 3 rotations) were derived from ANTS affine transformation matrices output.

fMRI analysis

The 1st level analysis was done in MNI space, defining conditions for both the CS and US window (i.e., CS+, CS-, US post CS+, no US post CS+, no US post CS-) separately for each phase. Regressors were calculated from the conditions in SPM12 by convolving a canonical hemodynamic response function with events, which were modelled as delta functions in an event-based design (i.e., the duration of each event is 0 s). Beta weights were fitted for each regressor by a general linear model for each voxel fMRI time series. Contrasts were computed as linear combinations of beta weights. Contrasts included main effects of conditions, CS differentiation (CS+ > CS-, CS- > CS+), unexpected omission of the US (no US post CS+ > no US post CS-) and US presentation (US post CS+ > no US post CS-). Values in contrast maps were converted to t-statistic values in first level analysis. Contrast maps are combined and used in a one-sample t-test for second level analysis in SPM12. Tests for significance ($p<0.05$) were done after threshold-free cluster enhancement (TFCE toolbox in SPM12, R174, http://dbm.neuro.uni-jena.de/tfce/) and family-wise error (FWE) corrections. Any trend-level results refer to significance tests without TFCE and FWE corrections ($p<0.05$). For the cerebellar cortex, results were visualized on cerebellar flatmaps using the SUIT toolbox in SPM12 [20]. For the cerebellar nuclei and VTA, results were visualized in coronal slices and 3D renderings generated in MRIcroGL[107] using custom probabilistic atlases (described in "Volume of interest definition"). To acquire cerebellar anatomical region labels, activation maps were projected onto the SUIT atlas volume (Cerebellum-SUIT.nii, Diedrichsen, 2006).

Event-based analysis

In addition to main effects of conditions (e.g., during acquisition training), events were additionally separated over time for each experimental phase. For fear acquisition training, extinction training, recall test, reacquisition, reextinction and the unexpected US phase, events were grouped in two equal-size blocks representing early and late halves of those phases (e.g., the 8 first CS+ trials of fear acquisition training correspond to early acquisition and the 8 last CS+ trials of fear acquisition training correspond to late acquisition). Trials with

unexpected events—such as unexpected US presentations or omissions—were treated as separate single trial regressors. These included the initial three trials of acquisition training, extinction training, recall test, reacquisition and reextinction and specific events such as the three unexpected US omissions in reacquisition. Notably, all single trials comprised CS+ trials, with CS- trials also being modeled as single trials to facilitate paired analysis.

Parametric modulation analysis

Parametric modulation of fMRI data was performed with prediction and prediction error values in all learning phases derived from our computational model. CS+ and CS- events were modulated with prediction values, while US omission and presentation events were modulated with prediction error values (Figure 5C). Events were not further divided within phases (e.g., no early or late halves or separation of the first three trials). Modulations were done separately for each phase, except for reacquisition, reextinction and the unexpected US phase which were modulated together as they were part of the same fMRI run.

Volumes of interest (VOI) definition

A global conjunction between unexpected US omission parametric modulation contrasts during extinction, the recall test and reacquisition was multiplied with a cerebellum mask and showed a region in lobule VI and Crus I. This region was used as a cerebellar cortex (lobule VI and Crus I) volume of interest (VOI). Deep cerebellar nuclei (DCN) and VTA VOIs were drawn for each participant. Drawing of the DCN (i.e., the left and right dentate, globose, emboliform and fastigial nuclei) was done by an expert annotator using both MP2RAGE and QSM information in ITK-SNAP (version 3.8.0)[109]. The nuclei of the DCN were combined into a single bihemispheric VOI. Drawing of the VTA was done by adjusting estimated masks with both MP2RAGE and QSM information, using the red nuclei, substantia nigra, the cerebral aqueduct and interpeduncular fossa as landmarks. Initial masks were estimated for the VTA by inversely transforming the probabilistic atlas by Trutti et al.[76] thresholded at a probability of $p>0.4$. All drawn masks were transformed into MNI space. After transformation to MNI space, a probabilistic atlas was generated by averaging binary masks for each structure across participants. The probabilistic atlas was thresholded so that the volume of each structure matched the average volume across participants. For drawing of globose, emboliform and

fastigial nuclei, the thresholded atlas was inversely transformed from MNI to T1 space in order to add missing nuclei for each participant with lower quality QSM data. The VTA VOI was used as a seed region in the PPI analysis. In addition, the cerebellar cortex (CB), DCN and VTA VOIs were used as nodes in the 2-node dynamic causal modelling (DCM) networks. The DCN and VTA VOIs were used as masks for displaying fMRI activations in coronal slices and 3D renderings.

Functional connectivity: PPI

For the PPI analysis, the VTA VOI was used to extract time series with SPM12 in MNI space. Time series were used as physiological regressors, and psychophysiological regressors were added for each condition using the gPPI toolbox[110]. Both first- and second-level analyses were performed with the same contrasts as defined in the parametric modulation (e.g., no US x prediction error during extinction) analysis. To summarize connectivity in the parametric modulation analysis, all contrasts related to unexpected US omissions were combined in a single contrast within the gPPI toolbox.

Functional connectivity: DCM

To calculate dynamic causal models (DCMs), the cerebellar cortex (CB) and VTA VOIs were used to extract time series in a concatenated version of the event based and parametric modulation models using SPM12[111–113]. Each condition was defined as input to the CB and VTA nodes (i.e., CS+, CS-, US post CS+, no US post CS+, no US post CS-), while each prediction or prediction error related event-based contrast (i.e., CS+ > CS-, no US post CS+_first3 > no US post CS-) or parametric modulation (i.e., no US prediction error) could modulate the reciprocal intrinsic connections. Recurrent connections were active but were not modulated. Parametric Empirical Bayes (PEB) was used for analysis on the second level[114]. All DCM and PEB analyses were done within SPM12.

References

1. Grupe, D. W. & Nitschke, J. B. Uncertainty and anticipation in anxiety: An integrated neurobiological and psychological perspective. *Nat. Rev. Neurosci.* **14**, 488–501 (2013).

2. Papalini, S., Beckers, T. & Vervliet, B. Dopamine: from prediction error to psychotherapy. *Transl. Psychiatry* **10**, (2020).

3. Milad, M. R. & Quirk, G. J. Fear Extinction as a Model for Translational Neuroscience: Ten Years of Progress. *Annu. Rev. Psychol.* **63**, 129–151 (2012).

4. Lonsdorf, T. B. *et al.* Don't fear 'fear conditioning': Methodological considerations for the design and analysis of studies on human fear acquisition, extinction, and return of fear. *Neurosci. Biobehav. Rev.* **77**, 247–285 (2017).

5. Luo, R. *et al.* A dopaminergic switch for fear to safety transitions. *Nat. Commun.* **9**, 1–11 (2018).

6. Salinas-Hernández, X. I. *et al.* Dopamine neurons drive fear extinction learning by signaling the omission of expected aversive outcomes. *Elife* **7**, 1–25 (2018).

7. Kalisch, R., Gerlicher, A. M. V. & Duvarci, S. A Dopaminergic Basis for Fear Extinction. *Trends Cogn. Sci.* **23**, 274–277 (2019).

8. Craske, M. G., Liao, B., Brown, L. & Vervliet, B. Role of Inhibition in Exposure Therapy. *J. Exp. Psychopathol.* **3**, 322–345 (2012).

9. Schultz, W. & Dickinson, A. Neuronal Coding of Prediction Errors. *Annu. Rev. Neurosci* **23**, 473–500 (2000).

10. Salinas-Hernández, X. I., Zafiri, D., Sigurdsson, T. & Duvarci, S. Functional architecture of dopamine neurons driving fear extinction learning. *Neuron* **111**, 3854-3870.e5 (2023).

11. Wagner, M. J., Kim, T. H., Savall, J., Schnitzer, M. J. & Luo, L. Cerebellar granule cells encode the expectation of reward. *Nature* **544**, 96–100 (2017).

12. Heffley, W. & Hull, C. Classical conditioning drives learned reward prediction signals in

climbing fibers across the lateral cerebellum. *Elife* **8**, 1–21 (2019).

13. Kostadinov, D., Beau, M., Pozo, M. B. & Häusser, M. Predictive and reactive reward signals conveyed by climbing fiber inputs to cerebellar Purkinje cells. *Nat. Neurosci.* **22**, 950–962 (2019).

14. Snider, R. S. & Maiti, A. Cerebellar contributions to the papez circuit. *J. Neurosci. Res.* **2**, 133–146 (1976).

15. Watabe-Uchida, M., Zhu, L., Ogawa, S. K., Vamanrao, A. & Uchida, N. Whole-Brain Mapping of Direct Inputs to Midbrain Dopamine Neurons. *Neuron* **74**, 858–873 (2012).

16. Carta, I., Chen, C. H., Schott, A. L., Dorizan, S. & Khodakhah, K. Cerebellar modulation of the reward circuitry and social behavior. *Science (80-.).* **363**, (2019).

17. Pisano, T. J. *et al.* Homologous organization of cerebellar pathways to sensory, motor, and associative forebrain. *Cell Rep.* **36**, (2021).

18. Ernst, T. M. *et al.* The cerebellum is involved in processing of predictions and prediction errors in a fear conditioning paradigm. (2019) doi:10.7554/eLife.46831.001.

19. Ploghaus, A. *et al.* Dissociating pain from its anticipation in the human brain. *Science (80-.).* **284**, 1979–1981 (1999).

20. Diedrichsen, J. & Zotow, E. Surface-based display of volume-averaged cerebellar imaging data. *PLoS One* **10**, 1–18 (2015).

21. Baek, S. J., Park, J. S., Kim, J., Yamamoto, Y. & Tanaka-Yamamoto, K. VTA-projecting cerebellar neurons mediate stress-dependent depression-like behaviors. *Elife* **11**, 1–38 (2022).

22. Linnman, C. *et al.* Resting Amygdala and Medial Prefrontal Metabolism Predicts Functional Activation of the Fear Extinction Circuit. *Am. J. Psychiatry* **169**, 415–423 (2012).

23. Kattoor, J. *et al.* Cerebellar contributions to different phases of visceral aversive extinction learning. *Cerebellum* **13**, 1–8 (2014).

24. Faul, L. *et al.* Proximal threats promote enhanced acquisition and persistence of reactive fear-learning circuits. *Proc. Natl. Acad. Sci. U. S. A.* **117**, 16678–16689 (2020).

25. Labrenz, F. *et al.* Temporal dynamics of fMRI signal changes during conditioned interoceptive pain-related fear and safety acquisition and extinction. *Behav. Brain Res.* **427**, (2022).

26. Ploghaus, A. *et al.* Learning about pain: The neural substrate of the prediction error for aversive events. *Proc. Natl. Acad. Sci. U. S. A.* **97**, 9281–9286 (2000).

27. Yágüez, L. *et al.* Brain response to visceral aversive conditioning: A functional magnetic resonance imaging study. *Gastroenterology* **128**, 1819–1829 (2005).

28. Batsikadze, G. *et al.* The cerebellum contributes to context-effects during fear extinction learning: A 7T fMRI study. *Neuroimage* **253**, 119080 (2022).

29. Doubliez, A. *et al.* The cerebellum and fear extinction: evidence from rodent and human studies. *Front. Syst. Neurosci.* **17**, 1–8 (2023).

30. Fullana, M. A. *et al.* Neural signatures of human fear conditioning: An updated and extended meta-analysis of fMRI studies. *Mol. Psychiatry* **21**, 500–508 (2016).

31. Ramnani, N., Elliott, R., Athwal, B. S. & Passingham, R. E. Prediction error for free monetary reward in the human prefrontal cortex. *Neuroimage* **23**, 777–786 (2004).

32. Kruithof, E. S., Klaus, J. & Schutter, D. J. L. G. The human cerebellum in reward anticipation and outcome processing: An activation likelihood estimation meta-analysis. *Neurosci. Biobehav. Rev.* **149**, 105171 (2023).

33. Nettekoven, C. *et al.* A hierarchical atlas of the human cerebellum for functional precision mapping. *Nat. Commun.* **15**, 8376 (2024).

34. Guell, X., Gabrieli, J. D. E. & Schmahmann, J. D. Triple representation of language, working memory, social and emotion processing in the cerebellum: convergent evidence from task and seed-based resting-state fMRI analyses in a single large cohort. *Neuroimage* **172**, 437–449 (2018).

35. Camilleri, J. A. *et al.* Definition and characterization of an extended multiple-demand network. *Neuroimage* **165**, 138–147 (2018).

36. Rescorla, R. A. & Wagner, A. R. A theory of Pavlovian conditioning: The effectiveness of reinforcement and non-reinforcement. *Class. Cond. Curr. Res. Theory* (1972).

37. Pearce, J. M. & Hall, G. A model for Pavlovian learning: Variations in the effectiveness of conditioned but not of unconditioned stimuli. *Psychol. Rev.* **87**, 532–552 (1980).

38. Koenig, S., Uengoer, M. & Lachnit, H. Attentional bias for uncertain cues of shock in human fear conditioning: Evidence for attentional learning theory. *Front. Hum. Neurosci.* **11**, 1–13 (2017).

39. Cai, L. X. *et al.* Distinct signals in medial and lateral VTA dopamine neurons modulate fear extinction at different times. *Elife* **9**, 75–103 (2020).

40. Esser, R., Korn, C. W., Ganzer, F. & Haaker, J. L-DOPA modulates activity in the vmPFC, nucleus accumbens, and VTA during threat extinction learning in humans. *Elife* **10**, 1–21 (2021).

41. D'Ardenne, K., McClure, S. M., Nystrom, L. E. & Cohen, J. D. BOLD responses reflecting dopaminergic signals in the human ventral tegmental area. *Science (80-.).* **319**, 1264–1267 (2008).

42. Schott, B. H. *et al.* Mesolimbic functional magnetic resonance imaging activations during reward anticipation correlate with reward-related ventral striatal dopamine release. *J. Neurosci.* **28**, 14311–14319 (2008).

43. Kostadinov, D. & Häusser, M. Reward signals in the cerebellum: Origins, targets, and functional implications. *Neuron* **110**, 1290–1303 (2022).

44. Logothetis, N. K. & Wandell, B. A. Interpreting the BOLD signal. *Annu. Rev. Physiol.* **66**, 735–769 (2004).

45. Logothetis, N. K., Pauls, J., Augath, M., Trinath, T. & Oeltermann, A. Neurophysiological investigation of the basis of the fMRI signal. *Nature* **412**, 150–157 (2001).

46. Logothetis, N. K. What we can do and what we cannot do with fMRI. *Nature* **453**, 869–878 (2008).

47. Peelen, M. V. eLife assessment: Selective recruitment of the cerebellum evidenced by task-dependent gating of inputs. at https://doi.org/10.7554/eLife.96386.3.sa0 (2024).

48. Gagliano, G. *et al.* Non-Linear Frequency Dependence of Neurovascular Coupling in the Cerebellar Cortex Implies Vasodilation–Vasoconstriction Competition. *Cells* **11**, (2022).

49. Mapelli, L. *et al.* Granular layer neurons control cerebellar neurovascular coupling through an NMDA receptor/NO-dependent system. *J. Neurosci.* **37**, 1340–1351 (2017).

50. Zheng, N. *et al.* Investigations of brain-wide functional and structural networks of dopaminergic and CamKIIα-positive neurons in VTA with DREADD-fMRI and neurotropic virus tracing technologies. *J. Transl. Med.* **21**, 1–14 (2023).

51. Düzel, E. *et al.* Functional imaging of the human dopaminergic midbrain. *Trends Neurosci.* **32**, 321–328 (2009).

52. Ikai, Y., Takada, M., Shinonaga, Y. & Mizuno, N. Dopaminergic and non-dopaminergic neurons in the ventral tegmental area of the rat project, respectively, to the cerebellar cortex and deep cerebellar nuclei. *Neuroscience* **51**, 719–728 (1992).

53. Li, C. *et al.* Purkinje cell dopaminergic inputs to astrocytes regulate cerebellar-dependent behavior. *Nat. Commun.* **14**, (2023).

54. Guarque-Chabrera, J., Oñate, M., Vera, J. & Khodakhah, K. Exploring monosynaptic midbrain-to-deep cerebellar nuclei projections. in *Abstracts, Neuroscience 2024* (Chicago, IL, 2024).

55. Jo, Y. S., Heymann, G. & Zweifel, L. S. Dopamine Neurons Reflect the Uncertainty in Fear Generalization. *Neuron* **100**, 916-925.e3 (2018).

56. Moriya, S. *et al.* Acute Aversive Stimuli Rapidly Increase the Activity of Ventral Tegmental Area Dopamine Neurons in Awake Mice. *Neuroscience* **386**, 16–23 (2018).

57. Rouhani, N. & Niv, Y. Signed and unsigned reward prediction errors dynamically

enhance learning and memory. *Elife* **10**, 1–28 (2021).

58. Montague, P. R., Dayan, P. & Sejnowski, T. J. A framework for mesencephalic dopamine systems based on predictive Hebbian learning. *J. Neurosci.* **16**, 1936–1947 (1996).

59. Barto, A. G. Adaptive Critics and the Basal Ganglia. in *Models of Information Processing in the Basal Ganglia* 215–232 (The MIT Press, 1994). doi:10.7551/mitpress/4708.003.0018.

60. Hull, C. Prediction signals in the cerebellum: Beyond supervised motor learning. *eLife* vol. 9 at https://doi.org/10.7554/eLife.54073 (2020).

61. Corlett, P. R., Mollick, J. A. & Kober, H. Meta-analysis of human prediction error for incentives, perception, cognition, and action. *Neuropsychopharmacology* **47**, 1339–1349 (2022).

62. Batsikadze, G. *et al.* Mild deficits in fear learning: Evidence from humans and mice with cerebellar cortical degeneration. *eneuro* **29**, ENEURO.0365-23.2023 (2024).

63. Gainotti, G. Emotions and the Right Hemisphere: Can New Data Clarify Old Models? *Neuroscientist* **25**, 258–270 (2019).

64. Güntürkün, O., Ströckens, F. & Ocklenburg, S. Brain lateralization: A comparative perspective. *Physiol. Rev.* **100**, 1019–1063 (2020).

65. Liu, G. *et al.* Praising others differently: Neuroanatomical correlates to individual differences in trait gratitude and elevation. *Soc. Cogn. Affect. Neurosci.* **13**, 1225–1234 (2018).

66. Zhong, S., Su, T., Gong, J., Huang, L. & Wang, Y. Brain functional alterations in patients with anorexia nervosa: A meta-analysis of task-based functional MRI studies. *Psychiatry Res.* **327**, 115358 (2023).

67. E, K., Chen, S. A., Ho, M. R. & Desmond, J. E. A meta-analysis of cerebellar contributions to higher cognition from PET and fMRI studies. *Hum. Brain Mapp.* **35**, 593–615 (2014).

68. Stoodley, C. J. & Schmahmann, J. D. Functional topography in the human cerebellum: A

meta-analysis of neuroimaging studies. *Neuroimage* **44**, 489–501 (2009).

69. Pierce, J. E., Thomasson, M., Voruz, P., Selosse, G. & Péron, J. Explicit and Implicit Emotion Processing in the Cerebellum: A Meta-analysis and Systematic Review. *Cerebellum* **22**, 852–864 (2023).

70. Bartolomeo, P. & Seidel Malkinson, T. Hemispheric lateralization of attention processes in the human brain. *Curr. Opin. Psychol.* **29**, 90–96 (2019).

71. Friston, K. . *et al.* Psychophysiological and Modulatory Interactions in Neuroimaging. *Neuroimage* **6**, 218–229 (1997).

72. O'Reilly, J. X., Woolrich, M. W., Behrens, T. E. J., Smith, S. M. & Johansen-Berg, H. Tools of the trade: Psychophysiological interactions and functional connectivity. *Soc. Cogn. Affect. Neurosci.* **7**, 604–609 (2012).

73. Diedrichsen, J. *et al.* Imaging the deep cerebellar nuclei: A probabilistic atlas and normalization procedure. *Neuroimage* **54**, 1786–1794 (2011).

74. de Hollander, G., Keuken, M. C., van der Zwaag, W., Forstmann, B. U. & Trampel, R. Comparing functional MRI protocols for small, iron-rich basal ganglia nuclei such as the subthalamic nucleus at 7 T and 3 T. *Hum. Brain Mapp.* **38**, 3226–3248 (2017).

75. Pauli, W. M., Nili, A. N. & Tyszka, J. M. A high-resolution probabilistic in vivo atlas of human subcortical brain nuclei. *Sci. Data* **5**, 180063 (2018).

76. Trutti, A. C. *et al.* A probabilistic atlas of the human ventral tegmental area (VTA) based on 7 Tesla MRI data. *Brain Struct. Funct.* **226**, 1155–1167 (2021).

77. Nio, E. *et al.* 7T fMRI study on extinction learning in young and healthy participants. *Cent. Open Sci.* (2023) doi:https://doi.org/10.17605/OSF.IO/2PXWE.

78. Mumford, J. A. A power calculation guide for FMRI studies. *Soc. Cogn. Affect. Neurosci.* **7**, 738–742 (2012).

79. Henry, J. D. & Crawford, J. R. The short-form version of the Depression anxiety stress scales (DASS-21): Construct validity and normative data in a large non-clinical sample.

Br. J. Clin. Psychol. **44**, 227–239 (2005).

80. Oldfield, R. C. The assessment and analysis of handedness: The Edinburgh inventory. *Neuropsychologia* **9**, 97–113 (1971).

81. Inoue, L. *et al.* Interaction of fear conditioning with eyeblink conditioning supports the sensory gating hypothesis of the amygdala in men. *eNeuro* **7**, 1–15 (2020).

82. Otto, T., Wolf, O. T. & Merz, C. J. EDA-Analysis App (5.11). *Zenodo* (2023) doi:10.5281/zenodo.7965376.

83. Boucsein, W. *Electrodermal Activity: Second Edition*. *Electrodermal Activity: Second Edition* vol. 9781461411 (2012).

84. Venables, P. H. & Christie, M. J. Electrodermal activity. *Tech. Psychophysiol.* **54**, (1980).

85. Kret, M. E. & Sjak-Shie, E. E. Preprocessing pupil size data: Guidelines and code. *Behav. Res. Methods* **51**, 1336–1342 (2019).

86. Jentsch, V. L., Wolf, O. T. & Merz, C. J. Temporal dynamics of conditioned skin conductance and pupillary responses during fear acquisition and extinction. *Int. J. Psychophysiol.* **147**, 93–99 (2020).

87. Mathôt, S., Fabius, J., van Heusden, E. & Van der Stigchel, S. Safe and sensible baseline correction of pupil-size data. *Behav. Res. Methods* 94–106 (2018).

88. Brunner, E., Domhof, S. & Langer, F. Nonparametric analysis of longitudinal data in factorial experiments. (2002) doi:http://ci.nii.ac.jp/ncid/BA54899817.

89. Shah, D. a & Madden, L. V. Nonparametric analysis of ordinal data. *Phytopathology* **94**, 33–43 (2004).

90. Noguchi, K., Gel, Y. R., Brunner, E. & Konietschke, F. nparLD : An R Software Package for the Nonparametric Analysis of Longitudinal Data in Factorial Experiments . *J. Stat. Softw.* **50**, (2012).

91. Bathke, A. C., Schabenberger, O., Tobias, R. D. & Madden, L. V. Greenhouse-Geisser adjustment and the ANOVA-type statistic: Cousins or twins? *Am. Stat.* **63**, 239–246

(2009).

92. Sutton, R. S. & Barto, A. G. *Reinforcement Learning: An Introduction*. (MIT press, 2018).

93. LeCun, Y., Bengio, Y. & Hinton, G. Deep learning. *Nature* **521**, 436–444 (2015).

94. Lin, L.-J. Self-improvement Based On Reinforcement Learning, Planning and Teaching. in *Machine Learning Proceedings 1991* vol. 321 323–327 (Elsevier, 1991).

95. Rumelhart, D. E., Hinton, G. E. & Williams, R. J. Learning representations by back-propagating errors. *Nature* **323**, 533–536 (1986).

96. Schaul, T., Quan, J., Antonoglou, I. & Silver, D. Prioritized Experience Replay. at https://arxiv.org/abs/1511.05952 (2016).

97. Teeuwisse, W. M., Brink, W. M. & Webb, A. G. Quantitative assessment of the effects of high-permittivity pads in 7 Tesla MRI of the brain. *Magn. Reson. Med.* **67**, 1285–1293 (2012).

98. Stirnberg, R. & Stöcker, T. Segmented K-space blipped-controlled aliasing in parallel imaging for high spatiotemporal resolution EPI. *Magn. Reson. Med.* **85**, 1540–1551 (2021).

99. Eckstein, K. *et al.* Computationally Efficient Combination of Multi-channel Phase Data From Multi-echo Acquisitions (ASPIRE). *Magn. Reson. Med.* **79**, 2996–3006 (2018).

100. Eckstein, K. *et al.* Improved susceptibility weighted imaging at ultra-high field using bipolar multi-echo acquisition and optimized image processing: CLEAR-SWI. *Neuroimage* **237**, 118175 (2021).

101. Gallichan, D. & Marques, J. P. Optimizing the acceleration and resolution of three-dimensional fat image navigators for high-resolution motion correction at 7T. *Magn. Reson. Med.* **77**, 547–558 (2017).

102. Marques, J. P. *et al.* MP2RAGE, a self bias-field corrected sequence for improved segmentation and T1-mapping at high field. *Neuroimage* **49**, 1271–1281 (2010).

103. Gallichan, D., Marques, J. P. & Gruetter, R. Retrospective correction of involuntary

microscopic head movement using highly accelerated fat image navigators (3D FatNavs) at 7T. *Magn. Reson. Med.* **75**, 1030–1039 (2016).

104. Gaser, C. *et al.* CAT: a computational anatomy toolbox for the analysis of structural MRI data. *Gigascience* **13**, 2022.06.11.495736 (2024).

105. Jenkinson, M., Pechaud, M. & Smith, M. BET2: MR-based estimation of brain, skull and scalp surfaces. *Elev. Annu. Meet. Organ. Hum. Brain Mapping.* (2005).

106. Tustison, N. J. *et al.* Large-scale evaluation of ANTs and FreeSurfer cortical thickness measurements. *Neuroimage* **99**, 166–179 (2014).

107. Brett, M., Leff, A. P., Rorden, C. & Ashburner, J. Spatial normalization of brain images with focal lesions using cost function masking. *Neuroimage* **14**, 486–500 (2001).

108. Diedrichsen, J. A spatially unbiased atlas template of the human cerebellum. *Neuroimage* **33**, 127–138 (2006).

109. Yushkevich, P. A. *et al.* User-guided 3D active contour segmentation of anatomical structures: Significantly improved efficiency and reliability. *Neuroimage* **31**, 1116–1128 (2006).

110. McLaren, D. G., Ries, M. L., Xu, G. & Johnson, S. C. A generalized form of context-dependent psychophysiological interactions (gPPI): A comparison to standard approaches. *Neuroimage* **61**, 1277–1286 (2012).

111. Friston, K. J., Harrison, L. & Penny, W. Dynamic causal modelling. *Neuroimage* **19**, 1273–1302 (2003).

112. Stephan, K. E. *et al.* Ten simple rules for dynamic causal modeling. *Neuroimage* **49**, 3099–3109 (2010).

113. Zeidman, P. *et al.* A guide to group effective connectivity analysis, part 1: First level analysis with DCM for fMRI. *Neuroimage* **200**, 174–190 (2019).

114. Zeidman, P. *et al.* A guide to group effective connectivity analysis, part 2: Second level analysis with PEB. *Neuroimage* **200**, 12–25 (2019).

Acknowledgements

We would like to thank our technician Beate Brol for the drawing and adjustment of DCN and VTA masks. Additionally, we would like to thank Greta Wippich for providing helpful illustrations. The MAGNETOM Terra 7T MRI system used in the study was funded by the Deutsche Forschungsgemeinschaft (DFG, German Research Foundation), grant number 432647511. This project has received funding from the DFG (project number 316803389 – SFB1280), the European Union's Horizon 2020 research and innovation program under the Marie Skłodowska-Curie grant agreement No 956414 and an individual scholarship for Patrick Pais Pereira from the Hans-Böckler-Stiftung.

Supplementary information

Pupil size responses (PSRs)

During habituation on day 1, PSRs related to the CS+ and CS- did not differ significantly (non-parametric ANOVA-type statistic, main effects, all $p>0.2$).

During fear acquisition training on day 1, PSRs were significantly higher in CS+ trials than in CS- trials, and PSR was more pronounced in early compared to late trials. Non-parametric ANOVA-type statistics revealed a significant main effect of Stimulus (CS+ vs. CS-; $F_1 = 39.51$; $p<0.001$) and Time (early vs. late; $F_1 = 24.31$; $p<0.001$). No significant Stimulus x Time interaction was observed ($F_1 = 0.58$; $p=0.45$).

During extinction training on day 2, PSRs for CS+ significantly decreased early vs late but there were no differences between early and late trials for CS-. Non-parametric ANOVA-type statistics revealed a significant main effect of Time (early vs. late; $F_1 = 18.21$; $p<0.001$) and a significant Stimulus x Time interaction ($F_1 = 4.28$; $p=0.04$). No significant main effect of Stimulus was observed (CS+ vs. CS-; $F_1 = 1.12$; $p=0.29$). Post-hoc tests showed that PSRs related to the CS+ were significantly lower during late extinction compared to early (least squares means test; $p<0.001$). This result was not observed for PSRs related to the CS- (least squares means test; $p=0.64$).

During the recall test on day 3, PSRs for the CS+ were significantly higher than for the CS- in both early and late trials, though the difference was less pronounced in late trials. The PSRs for the CS+ were significantly higher in early compared to late trials. Non-parametric ANOVA-type statistics revealed a significant effect of Stimulus (CS+ vs. CS-; $F_1 = 6.59$; $p=0.01$) and Time (early vs. late; $F_1 = 6.41$; $p=0.01$) and a significant Stimulus x Time interaction ($F_1 = 4.87$; $p=0.03$). Post-hoc tests showed that PSRs related to the CS+ were significantly higher than towards the CS- early but not late (least squares means test; early $p<0.05$; late $p=0.86$) and that the PSRs related to the late CS+ were significantly lower than early (least squares means test; $p<0.05$)

During reacquisition on day 3, PSRs for CS+ were significantly higher in early trials, but no significant difference in PSRs for CS- early vs late was observed. PSRs for CS+ and CS- were

significantly different between early and late. Non-parametric ANOVA-type statistics reveal a significant effect of Stimulus (CS+ vs. CS-; F_1 = 47.87; p<0.001), Time (early vs. late; F_1 = 4.54; p=0.03) and Stimulus x Time interaction (F_1 = 7.7; p=0.006). Post-hoc tests using the least squares means test showed that PSRs related to the CS+ were higher early in the phase (least square means test; p=0.004) but not the CS- (least square means test; p=0.97). Stimulus types were significantly different both early and late (least square means test; CS+ vs. CS-; all: p<0.008).

During reextinction on day 3, PSRs for CS+ were significantly higher than for CS- early, but the difference became insignificant in late trials. Non-parametric ANOVA-type statistics revealed a significant main effect of Stimulus (CS+ vs. CS-; F_1 = 9.1; p=0.003) and a Stimulus x Time interaction (F_1 = 4.43; p=0.04), but not a significant main effect of Time (early vs. late; F_1 = 0.83, p=0.36). Post-hoc test showed a significant difference between the CS+ and CS- early but not late (least squares means test; early: p=0.01; late: p=0.77).

During the unexpected US phase on day 3, PSRs for the CS+ were higher than for the CS-. Non-parametric ANOVA-type analysis revealed a significant main effect of Stimulus (CS+ vs. CS-; F_1 = 17.35; p<0.001), but not of Time (early vs. late; F_1 = 0.83; p=0.363) and the Stimulus x Time interaction (F_1 = 0.03; p=087)

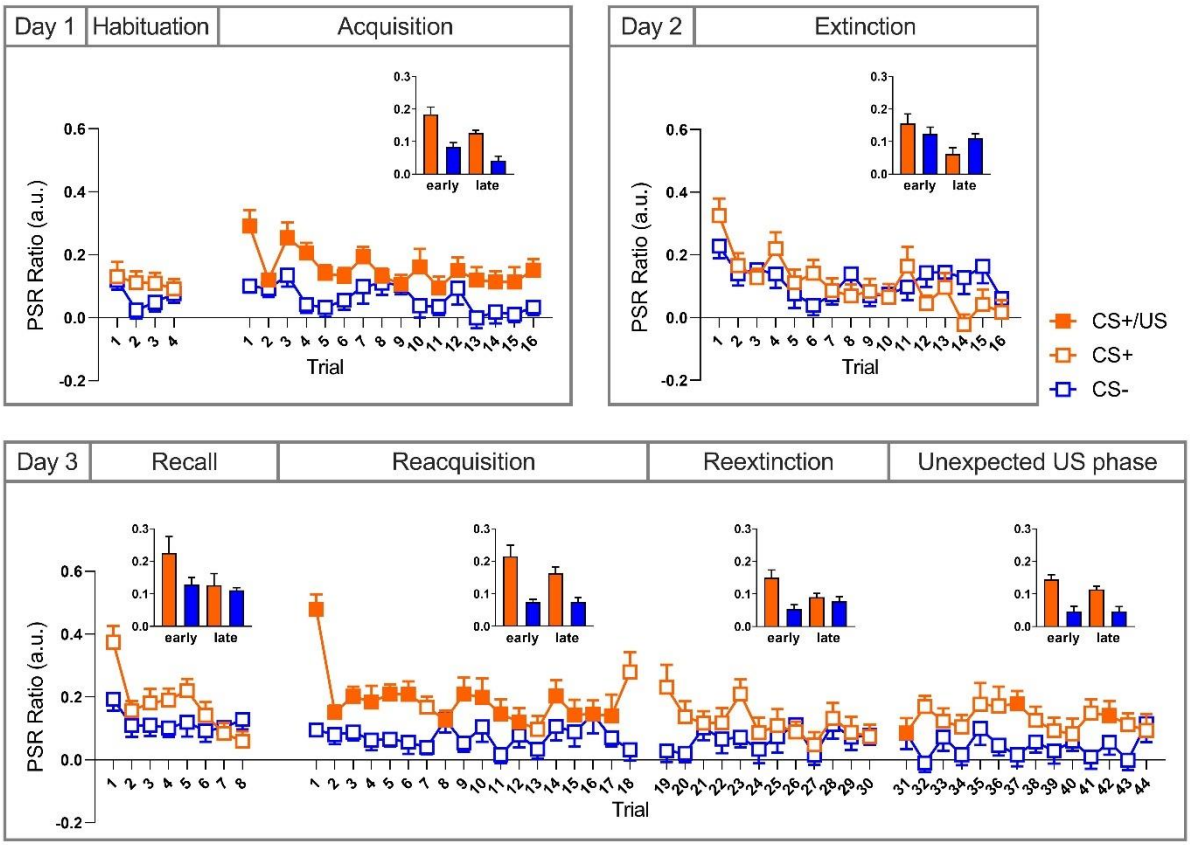

Supplementary figure 1*: Pupil size responses for each trial, with CS+ and CS- responses paired in blocks. Bar plots on the top right show early and late mean responses for both CS+ and CS-. Reinforcement of the CS+ by a US (CS+/US) is indicated by filled squares. On day 1, there was no differentiation between CS+ and CS- in the habituation phase, with significant differentiation emerging during acquisition training. On day 2, there was a loss of differentiation during extinction training. On day 3, during initial recall, participants exhibited spontaneous recovery, i.e., a return of differential responses after extinction training. During initial reacquisition, there were again differential responses to the CS+ and CS-, which decreased in reextinction and the unexpected US phase. Mean values are shown with error bars representing the standard error of the mean. CS: Conditioned stimulus; US: Unconditioned stimulus; PSR: Pupil size response.*

Supplementary table 1: Non-parametric ANOVA results for pupil size responses

Factor	**Numerator Df**	***F***	***P***
		Habituation	
Stimulus	1	1.65	0.2
Time	1	0.26	0.609
Stimulus x Time	1	0.04	0.849
		Fear acquisition training	
Stimulus	1	39.51	**<0.001*** **
Time	1	24.31	**<0.001*** **
Stimulus x Time	1	0.58	0.446
		Extinction training	
Stimulus	1	1.12	0.29
Time	1	18.21	**<0.001*** **
Stimulus x Time	1	4.28	**0.038***
		Recall	
Stimulus	1	6.59	**0.01***
Time	1	6.41	**0.011***
Stimulus x Time	1	4.87	**0.027***
		Reacquisition	
Stimulus	1	47.87	**<0.001*** **
Time	1	4.54	**0.033***
Stimulus x Time	1	7.70	**0.006***
		Reextinction	
Stimulus	1	9.10	**0.003***
Time	1	0.83	0.364
Stimulus x Time	1	4.43	**0.035***
		Unexpected US phase	
Stimulus	1	17.35	**<0.001*** **
Time	1	0.83	0.363

Stimulus x Time	1	0.03	0.872

* Significant results at $p<0.05$.

*** Significant results at $p<0.001$.

Supplementary table 2: Non-parametric ANOVA results for skin conductance responses

Factor	**Numerator Df**	***F***	***p***
		Habituation	
Stimulus	1	1.19	0.276
Time	1	26.49	**<0.001*** **
Stimulus x Time	1	0.06	0.802
		Fear acquisition training	
Stimulus	1	16.28	**<0.001*** **
Time	1	24.94	**<0.001*** **
Stimulus x Time	1	3.33	0.068
		Extinction training	
Stimulus	1	6.57	**0.01***
Time	1	21.10	**<0.001*** **
Stimulus x Time	1	2.83	0.092
		Recall	
Stimulus	1	4.19	**0.041***
Time	1	32.47	**<0.001*** **
Stimulus x Time	1	5.27	**0.022***
		Reacquisition	
Stimulus	1	26.65	**<0.001*** **
Time	1	30.37	**<0.001*** **
Stimulus x Time	1	6.34	**0.012***
		Reextinction	
Stimulus	1	4.30	**0.038***
Time	1	0.20	0.653

Stimulus x Time	1	1.10	0.294
		Unexpected US phase	
Stimulus	1	5.68	**0.017***
Time	1	0.26	0.611
Stimulus x Time	1	2.81	0.094

* Significant results at $p<0.05$.

*** Significant results at $p<0.001$.

Supplementary table 3: Self-reports results summary

Median and interquartile range of arousal, fear, US expectancy, and valence ratings post habituation, acquisition training, extinction training, recall test and at the end of day 3.

Stimulus	Time of assessment				
	Post habituation	Post acquisition	Post extinction	Post recall	End of day 3
Arousal ratings (1 – very calm, 9 – very excited)					
CS+	2 (1-3)	6 (5-7)	3 (1-6)	3 (1-6)	7 (4-7)
CS-	2 (1-4)	2 (1-3)	1 (1-3)	1 (1-3)	1 (1-2)
Fear ratings (1 – not afraid, 9 – very afraid)					
CS+	1 (1-2)	6 (3-6)	2 (1-5)	2 (1-4)	5 (3-7)
CS-	1 (1-2)	1 (1-2)	1 (1-2)	1 (1-2)	1 (1-2)
US expectancy (1 – US not expected, 5 – unsure, 9 – US expected)					
CS+	1 (1-2)	9 (9-9)	3 (1-5)	3 (1-5)	6 (5-7)
CS-	1 (1-2)	1 (1-2)	1 (1-1)	1 (1-2)	1 (1-2)
Valence ratings (1 - unpleasant, 9 – very pleasant)					
CS+	7 (5-8)	3 (2-4)	5 (4-7)	6 (5-8)	3 (3-5)
CS-	7 (5-9)	8 (6-9)	7 (5-9)	8 (6-9)	8 (6-9)

Interquartile range is shown in parenthesis.

Statistically significant differences between CS+ and CS- are indicated in bold (least squares means tests; $p<0.01$)

Supplementary table 4: Non-parametric ANOVA results for self-reports

Results of non-parametric ANOVA-type statistic for arousal, fear, valence, and US expectancy ratings.

Factor	Df	F	p
Arousal			
Stimulus	1	128.71	<0.001*
Time	3.51	16.31	<0.001*
Stimulus x Time	3.29	35.06	<0.001*
Fear			
Stimulus	1	105.13	<0.001*
Time	3.32	18.60	<0.001*
Stimulus x Time	3.4	34.47	<0.001*
Valence			
Stimulus	1	124.79	<0.001*
Time	3.39	19.80	<0.001*
Stimulus x Time	3.11	51.42	<0.001*
US expectancy			
Stimulus	1	451.62	<0.001*
Time	2.4	62.78	<0.001*
Stimulus x Time	2.8	187.33	<0.001*

* Significant results at $p<0.001$.

Supplementary table 5: FMRI activations related to the prediction and presentation of the US. TFCE and FWE corrected.

FMRI activation clusters (p<0.05, FWE and TFCE corrected) related to the prediction and presentation of the US in the cerebellar cortex, DCN and VTA (Figure 2). Up to three maxima in each cluster are shown separated by at least 8 mm. Coordinates are indicated in MNI space (x,y,z). The cluster size is shown by number of voxels (volume of 1 voxel = 3.375 mm^3). US: Unconditioned stimulus; CS: Conditioned stimulus; VTA: Ventral tegmental area; DCN: Deep cerebellar nuclei; DN: Dentate nucleus; IN: Interposed Nucleus; FN: Fastigial nucleus; MNI: Montreal Neurological Institute standard brain; TFCE t: Threshold-free cluster-enhanced t-statistic; p_{FWE}: family-wise error corrected p-value.

Index	Location (lobule, DCN, VTA)	Side	MNI coordinates/mm			Cluster size (number of voxels)	p_{FWE}	TFCE t
			x	y	z			
CS+ > CS- during acquisition (Figure 2A), t-test, TFCE, p<0.05, FWE corr.								
1	VTA	right	4.0	-16.0	-13.0	27	0.016	1599
2	VTA	left	-6.5	-17.5	-11.5	14	0.021	1503
3	VTA	left	-2.0	-17.5	-10.0	1	0.036	1293
CS+ x prediction (inverted) during acquisition (Figure 2B), t-test, TFCE, p<0.05, FWE corr.								
1	Extended cluster	left VI (2109), right VI (1758), right V (1324), left Crus I (1315), white matter (802), left V (748), right I-IV (643), left Crus II (506), right Crus I (453), vermal VI (380), left I-IV (366), left VIIb (137), left VIIIa (90), vermal VIIIa (57), vermal IX (53), left IX (46), right DN (40), vermal X (38), right IX (35), vermal VIIIb (33), vermal VIIb (23), right VIIIa (15), right X (7), right VIIb (5), right FN (5), vermal Crus I (3), vermal Crus II (2), left DN (2), left FN (2)						
	VI	right	25.0	-61.0	-16.0	10997	<0.001	6919
	VI	right	31.0	-55.0	-19.0		<0.001	6890
	V	right	19.0	-52.0	-13.0		<0.001	6636
2	Extended cluster	right VTA (70), left VTA (67)						
	VTA	left	-2.0	-16.0	-14.5	137	0.001	3389
	VTA	right	8.5	-19.0	-13.0		0.001	3202
US post CS+ > no US post CS- during acquisition (Figure 2C), t-test, TFCE, p<0.05, FWE corr.								
1	Extended cluster	left Crus I (4514), white matter (4220), left VI (3448), right VI (3362), right Crus I (2954), left Crus II (2681), right Crus II (2223), right V (1615), left VIIb (1503), right						

		VIIb (1494), right VIIIa (1382), right I-IV (1368), left V (1251), left I-IV (1147), left VIIIa (1102), right VIIIb (1054), left VIIIb (889), right IX (816), vermal VI (806), left IX (723), vermal VIIIa (452), left DN (308), vermal IX (297), right DN (283), left X (267), right X (252), vermal VIIIb (226), vermal Crus II (168), vermal X (98), vermal VIIb (69), left IN (24), right IN (24), left FN (9), vermal Crus I (8), right FN (8)						
	VI	Right	31.0	-70.0	-22.0	41045	<0.001	16742
	VIIb	Right	20.5	-70.0	-49.0		<0.001	16480
	VI	Right	23.5	-68.5	-28.0		<0.001	16166
2	VTA	Left	-0.5	-16.0	-14.5	156	0.001	13357
	VTA	Right	7.0	-16.0	-10.0		0.001	13090
CS+ > CS- during extinction (Figure 2D), t-test, TFCE, p<0.05, FWE corr.								
	No significant voxels							
CS+ x prediction during extinction (Figure 2E), t-test, TFCE, p<0.05, FWE corr.								
1	Extended cluster	left VTA (72), right VTA (63)						
	VTA	right	7.0	-16.0	-11.5	135	0.002	2603
	VTA	left	-3.5	-16.0	-13.0		0.003	2495
2	Extended cluster	right VI (894), left VI (805), right V (410), left Crus I (197), vermal VI (167), left V (40), right I-IV (17), white matter (14), right Crus I (5), left I-IV (3)						
	VI	left	-27.5	-67.0	-19.0	2552	0.004	2328
	VI	right	31.0	-65.5	-19.0		0.004	2298
	VI	right	31.0	-55.0	-19.0		0.004	2295
3	I-IV	left	-3.5	-46.0	-4.0	10	0.009	1990
4	V	left	-17.0	-44.5	-13.0	1	0.029	1457
5	I-IV	right	4.0	-53.5	-10.0	4	0.05	1223
No US post CS+ > no US post CS- during extinction (Figure 2F), t-test, TFCE, p<0.05, FWE corr.								
	No significant voxels							

Supplementary table 6: FMRI activations related to the prediction and presentation of the US. Uncorrected.

FMRI activation clusters (p<0.05, uncorrected) related to the prediction and presentation of the US in the cerebellar cortex, DCN and VTA (Figure 2). Up to three maxima in each cluster are shown separated by at least 8 mm. Coordinates are indicated in MNI space (x,y,z). The cluster size is shown by number of voxels (volume of 1 voxel = 3.375 mm^3). US: Unconditioned stimulus; CS: Conditioned stimulus; VTA: Ventral tegmental area; DCN: Deep cerebellar nuclei; DN: Dentate nucleus; IN: Interposed Nucleus; FN: Fastigial nucleus; MNI: Montreal Neurological Institute standard brain; t: t-statistic; p_{unc}: uncorrected p-value.

Index	Location (lobule, DCN, VTA)	Side	MNI coordinates/mm			Cluster size (number of voxels)	p_{unc}	t
			x	y	z			
CS+ > CS- during acquisition (Figure 2A), t-test, p<0.05, uncorrected								
1	Extended cluster	right VI (701), right Crus I (259), white matter (4), right V (2), right VIIIa (2), right X (1)						
	VI	right	35.5	-53.5	-29.5	969	<0.001	5.05
	VI	right	34.0	-34.0	-35.5		<0.001	4.13
	VI	right	28.0	-65.5	-22.0		0.001	3.21
2	Extended cluster	left VI (425), left Crus I (386), left Crus II (2)						
	VI	left	-29.0	-62.5	-22.0	813	<0.001	4.48
	Crus I	left	-47.0	-44.5	-32.5		<0.001	3.82
	VI	left	-35.0	-55.0	-28.0		<0.001	3.70
3	Extended cluster	right VTA (62), left VTA (47)						
	VTA	right	4.0	-16.0	-13.0	109	<0.001	4.31
	VTA	left	-6.5	-17.5	-11.5		<0.001	4.30
4	Extended cluster	left Crus I (346), left VI (144), left Crus II (131), vermal VI (96), right VI (51), white matter (6)						
	VI	right	8.5	-76.0	-16.0	774	<0.001	3.97
	Crus I	left	-18.5	-80.5	-31.0		<0.001	3.56
	Crus II	left	-5.0	-77.5	-38.5		0.007	2.57
5	Extended cluster	left VIIb (369), left Crus II (44), left VIIIa (30)						
	VIIb	left	-33.5	-64.0	-58.0	443	0.001	3.40
	VIIb	left	-42.5	-59.5	-55.0		0.001	3.23
	VIIb	left	-38.0	-52.0	-50.5		0.004	2.78
6	Extended cluster	right VIIb (150), right VIIIa (146)						
	VIIIa	right	34.0	-58.0	-55.0	296	0.001	3.39
	VIIb	right	40.0	-50.5	-53.5		0.001	3.17
7	Extended cluster	left IX (117), vermal IX (63), white matter (14), left VIIIb (4), vermal X (4)						
	IX	left	-8.0	-56.5	-40.0	202	0.001	3.18
	IX	vermal	-2.0	-55.0	-32.5		0.008	2.51
8	Extended cluster	right VIIIa (94), right VIIb (46)						
	VIIIa	right	8.5	-71.5	-53.5	140	0.002	2.99
	VIIIa	right	22.0	-65.5	-56.5		0.003	2.87
9	Extended cluster	left VIIIa (44), left VIIb (15)						

	VIIb	left	-18.5	-71.5	-58.0	59	0.003	2.94
	VIIIa	left	-11.0	-68.5	-56.5		0.033	1.87
10	I-IV	left	-0.5	-49.0	-20.5	60	0.005	2.69
11	IX	right	10.0	-58.0	-47.5	75	0.005	2.68
12	V	left	-0.5	-62.5	-1.0	19	0.008	2.52
13	Crus II	right	4.0	-83.5	-40.0	24	0.011	2.38
14	white matter		28.0	-52.0	-46.0	16	0.014	2.28
15	Crus II	right	46.0	-59.5	-50.5	14	0.015	2.23
16	VIIIb	right	20.5	-59.5	-49.0	33	0.018	2.16
17	VIIIb	left	-12.5	-58.0	-49.0	10	0.028	1.97
18	X	left	-20.0	-34.0	-47.5	3	0.032	1.90
19	Crus II	right	10.0	-89.5	-37.0	2	0.033	1.87
20	VIIIa	left	-9.5	-70.0	-55.0	2	0.033	1.87
21	IX	right	8.5	-49.0	-55.0	2	0.04	1.78
22	VIIIb	left	-20.0	-37.0	-50.5	1	0.042	1.76
23	IX	right	10.0	-55.0	-55.0	4	0.042	1.76
24	white matter		10.0	-71.5	-35.5	4	0.043	1.75
25	VIIIa	right	31.0	-46.0	-55.0	1	0.044	1.73
26	white matter		-9.5	-50.5	-28.0	1	0.045	1.73
27	I-IV	left	-2.0	-56.5	0.5	1	0.045	1.73
28	Crus I	right	26.5	-83.5	-22.0	1	0.046	1.71
29	Crus II	left	-41.0	-46.0	-46.0	2	0.046	1.71
30	VIIIa	left	-6.5	-71.5	-52.0	1	0.047	1.71
31	V	left	-29.0	-31.0	-31.0	1	0.047	1.70
CS+ x prediction during acquisition (Figure 2B), t-test, p<0.05, uncorrected								
1	Extended cluster	left VI (2607), right VI (2099), left Crus I (1857), right V (1449), white matter (1256), left V (944), right I-IV (886), right Crus I (780), left Crus II (651), left I-IV (510), vermal VI (436), left VIIb (182), right Crus II (181), vermal IX (140), left VIIIa (120), vermal VIIIa (111), right VIIb (110), left IX (82), right IX (80), right DN (77), vermal VIIIb (61), vermal X (53), right VIIIa (39), vermal VIIb (38), right VIIIb (27), left DN (19), right X (13), vermal Crus II (12), right FN (7), vermal Crus I (4), left FN (4), left IN (3)						
	VI	right	25.0	-59.5	-16.0	14838	<0.001	6.47
	VI	right	31.0	-55.0	-19.0		<0.001	6.32
	V	right	1.0	-62.5	-1.0		<0.001	6.15
2	Extended cluster	right VTA (72), left VTA (69)						
	VTA	left	-2.0	-20.5	-17.5	141	<0.001	5.05
	VTA	left	-2.0	-16.0	-8.5		<0.001	4.78
	VTA	right	8.5	-19.0	-13.0		0.001	3.45
3	Extended cluster	right Crus II (258), right VIIb (210), right Crus I (14), right VIIIa (11)						
	Crus II	right	43.0	-55.0	-47.5	493	<0.001	3.76

	Crus II	right	43.0	-67.0	-53.5		0.003	2.85
	VIIb	right	31.0	-71.5	-50.5		0.011	2.38
4	Extended cluster	left VIIIa (82), left VIIb (12)						
	VIIIa	left	-27.5	-56.5	-56.5	94	0.002	2.99
	VIIIa	left	-36.5	-53.5	-58.0		0.04	1.78
5	VIIb	left	-30.5	-74.5	-55.0	80	0.003	2.85
6	IX	left	-11.0	-49.0	-46.0	89	0.004	2.75
7	VIIIb	right	23.5	-46.0	-58.0	16	0.007	2.56
8	Extended cluster	left Crus I (73), left Crus II (9)						
	Crus I	left	-45.5	-67.0	-43.0	82	0.008	2.52
	Crus I	left	-36.5	-61.0	-40.0		0.021	2.09
9	IX	right	8.5	-50.5	-59.5	29	0.009	2.44
10	Crus II	right	28.0	-85.0	-47.5	27	0.01	2.41
11	VIIIa	right	20.5	-62.5	-52.0	45	0.012	2.35
12	VIIIb	left	-24.5	-44.5	-58.0	13	0.014	2.28
13	VIIIb	left	-24.5	-38.5	-53.5	8	0.014	2.28
14	I-IV	left	-11.0	-46.0	-7.0	2	0.016	2.21
15	Crus I	right	37.0	-65.5	-41.5	29	0.02	2.12
16	I-IV	left	-0.5	-52.0	2.0	1	0.022	2.07
17	I-IV	left	-0.5	-46.0	-5.5	8	0.028	1.96
18	X	right	23.5	-34.0	-47.5	1	0.036	1.84
19	I-IV	right	8.5	-46.0	-4.0	1	0.037	1.83
20	IX	left	-8.0	-52.0	-59.5	3	0.038	1.81
21	VIIb	left	-41.0	-52.0	-55.0	2	0.039	1.80
22	VIIIa	right	10.0	-70.0	-56.5	1	0.046	1.71
23	Crus I	left	-53.0	-55.0	-35.5	1	0.048	1.69
24	VIIIb	right	16.0	-44.5	-50.5	1	0.049	1.68
US post CS+ > no US post CS- during acquisition (Figure 2C), t-test, p<0.05, uncorrected								
1	Extended cluster	left Crus I (4378), white matter (3746), left VI (3367), right VI (3353), right Crus I (2720), left Crus II (2536), right Crus II (2069), right V (1592), left VIIb (1456), right VIIb (1455), right VIIIa (1352), right I-IV (1314), left V (1157), left I-IV (1098), right VIIIb (1034), left VIIIa (983), left VIIIb (828), vermal VI (799), right IX (748), left IX (668), vermal VIIIa (452), left DN (308), vermal IX (296), right DN (278), left X (257), right X (246), vermal VIIIb (224), vermal Crus II (168), vermal X (83), vermal VIIb (69), left IN (24), right IN (24), left FN (9), vermal Crus I (8), right FN (8)							
	VIIb	right	20.5	-70.0	-49.0	39107	<0.001	10.43
	VI	right	31.0	-70.0	-22.0		<0.001	9.82
	VIIb	left	-17.0	-70.0	-49.0		<0.001	8.89
2	Extended cluster	right VTA (81), left VTA (75)						
3	VTA	left	-0.5	-16.0	-14.5	156	<0.001	6.77
	VTA	right	7.0	-16.0	-10.0		<0.001	5.07

	IX	right	4.0	-46.0	-43.0	5	0.012	2.35
CS+ > CS- during extinction (Figure 2D), t-test, p<0.05, uncorrected								
1	Extended cluster	right VIIb (96), right VIIIa (53), right Crus II (3)						
	VIIb	right	34.0	-73.0	-56.5	152	<0.001	3.62
	VIIIa	right	31.0	-58.0	-52.0		0.016	2.21
2	VIIb	right	23.5	-73.0	-58.0	16	0.004	2.80
3	Crus II	left	-15.5	-80.5	-46.0	50	0.004	2.76
4	VIIIa	left	-29.0	-49.0	-49.0	49	0.006	2.64
5	VIIb	left	-33.5	-62.5	-53.5	139	0.006	2.60
6	Crus II	right	13.0	-77.5	-46.0	38	0.007	2.56
7	Extended cluster	white matter (25), right Crus II (20), right Crus I (16), right VI (15), right VIIb (14), right VIIIa (1)						
	Crus II	right	38.5	-49.0	-44.5	91	0.008	2.53
	VI	right	32.5	-46.0	-37.0		0.012	2.36
8	Crus I	right	50.5	-61.0	-41.5	12	0.015	2.25
9	VI	left	-33.5	-34.0	-32.5	19	0.016	2.21
10	VIIIa	right	23.5	-62.5	-56.5	14	0.016	2.20
11	white matter		-18.5	-31.0	-37.0	3	0.02	2.11
12	X	right	16.0	-40.0	-47.5	5	0.021	2.10
13	white matter		20.5	-34.0	-40.0	12	0.024	2.04
14	VIIb	right	41.5	-50.5	-53.5	2	0.026	1.99
15	white matter		-12.5	-37.0	-40.0	4	0.027	1.98
16	IX	right	8.5	-53.5	-55.0	13	0.027	1.98
17	VTA	right	5.5	-19.0	-16.0	5	0.027	1.98
18	VIIb	left	-11.0	-74.5	-55.0	2	0.028	1.96
19	VI	right	8.5	-76.0	-16.0	6	0.029	1.94
20	VI	left	-15.5	-77.5	-20.5	7	0.03	1.93
21	VI	left	-29.0	-58.0	-29.5	5	0.03	1.92
22	IX	left	-5.0	-52.0	-44.5	4	0.034	1.87
23	IX	left	-6.5	-59.5	-53.5	2	0.036	1.83
24	white matter		14.5	-40.0	-40.0	1	0.036	1.83
25	VI	right	37.0	-37.0	-34.0	2	0.037	1.82
26	X	left	-27.5	-35.5	-43.0	1	0.038	1.81
27	VTA	right	1.0	-19.0	-10.0	3	0.038	1.81
28	VI	left	-20.0	-67.0	-25.0	6	0.038	1.81
29	VI	left	-36.5	-40.0	-28.0	2	0.039	1.80
30	VIIIb	left	-11.0	-56.5	-56.5	5	0.039	1.80
31	VIIIb	vermal	1.0	-65.5	-49.0	2	0.042	1.76
32	VIIb	left	-11.0	-77.5	-52.0	1	0.042	1.76

33	Crus I	left	-39.5	-50.5	-40.0	1	0.043	1.75
34	VI	right	16.0	-74.5	-16.0	1	0.044	1.73
35	white matter		-11.0	-41.5	-38.5	1	0.047	1.70
36	Crus II	left	-23.0	-79.0	-50.5	1	0.047	1.70
CS+ x prediction during extinction (Figure 2E), t-test, p<0.05, uncorrected								
1	Extended cluster	left VTA (75), right VTA (74)						
	VTA	right	7.0	-16.0	-11.5	149	<0.001	5.64
	VTA	left	-5.0	-16.0	-13.0		<0.001	4.90
2	Extended cluster	left VI (1484), right VI (1377), white matter (711), right V (627), left Crus I (490), right IX (488), left IX (467), right VIIIa (410), right VIIb (380), right VIIIb (246), left VIIIb (234), vermal VI (225), right I-IV (183), right Crus II (178), left I-IV (155), vermal IX (143), vermal X (104), left V (85), right Crus I (84), left X (63), vermal VIIIb (47), right X (46), right DN (37), left DN (32), vermal VIIIa (27), left Crus II (22), left IN (18), left VIIIa (12), left VIIb (7), left FN (6), right FN (3), right IN (2)						
	white matter		5.5	-68.5	-11.5	8393	<0.001	5.03
	VIIIb	left	-18.5	-43.0	-46.0		<0.001	4.68
	VI	left	-5.0	-77.5	-17.5		<0.001	4.61
3	Extended cluster	left Crus II (198), left VIIb (55), vermal Crus II (9)						
	Crus II	left	-0.5	-80.5	-38.5	262	0.002	3.07
	VIIb	left	-12.5	-76.0	-47.5		0.004	2.80
	Crus II	left	-21.5	-76.0	-47.5		0.024	2.03
4	I-IV	left	-3.5	-46.0	-4.0	25	0.002	3.04
5	Extended cluster	left VIIb (162), left VIIIa (51)						
	VIIb	left	-32.0	-61.0	-55.0	213	0.006	2.65
	VIIb	left	-38.0	-55.0	-52.0		0.007	2.58
	VIIb	left	-21.5	-71.5	-56.5		0.01	2.43
6	X	right	20.5	-34.0	-46.0	12	0.007	2.57
7	V	left	-17.0	-44.5	-13.0	5	0.01	2.40
8	Crus I	right	41.5	-53.5	-37.0	13	0.011	2.38
9	Crus I	right	40.0	-74.5	-22.0	13	0.024	2.03
10	X	left	-18.5	-34.0	-47.5	5	0.025	2.01
11	Crus II	left	-32.0	-74.5	-50.5	9	0.025	2.01
12	V	left	-21.5	-46.0	-16.0	1	0.034	1.87
13	DN	right	16.0	-59.5	-38.5	3	0.034	1.87
14	V	left	-23.0	-50.5	-16.0	1	0.038	1.81
15	Crus I	right	47.5	-53.5	-34.0	1	0.038	1.81
16	VI	vermal	5.5	-71.5	-25.0	4	0.038	1.81
17	Crus II	left	-33.5	-77.5	-53.5	2	0.039	1.80
18	Crus II	right	34.0	-76.0	-52.0	3	0.039	1.79

19	white matter		-17.0	-31.0	-35.5	2	0.039	1.79
20	I-IV	right	2.5	-41.5	-16.0	1	0.041	1.77
21	Crus I	left	-45.5	-43.0	-31.0	1	0.044	1.74
No US post CS+ > no US post CS- during extinction (Figure 2F), t-test, p<0.05, uncorrected								
1	Extended cluster	left Crus I (1015), white matter (539), left VI (451), left Crus II (386), left VIIb (58), left VIIIa (34), left DN (34), left V (22), left IX (8)						
	VI	left	-24.5	-55.0	-31.0	2547	<0.001	4.20
	Crus I	left	-41.0	-58.0	-37.0		<0.001	3.84
	white matter		-30.5	-52.0	-37.0		<0.001	3.71
2	Extended cluster	right V (191), left V (160), left VI (109), vermal VI (97), right VI (86), right Crus I (40), right I-IV (14), white matter (2)						
	V	right	2.5	-67.0	-5.5	699	<0.001	3.73
	VI	right	8.5	-80.5	-20.5		0.001	3.33
	V	left	-6.5	-62.5	-10.0		0.001	3.30
3	Extended cluster	right V (207), right VI (199), white matter (194), right I-IV (126), right Crus I (12)						
	V	right	28.0	-41.5	-28.0	738	0.001	3.33
	white matter		20.5	-40.0	-31.0		0.001	3.18
	I-IV	right	10.0	-47.5	-25.0		0.002	3.14
4	Extended cluster	white matter (120), right VIIb (115), right Crus II (68), right VIIIa (58), right Crus I (25)						
	white matter		28.0	-49.0	-41.5	386	0.001	3.17
	VIIb	right	38.5	-47.5	-46.0		0.002	3.09
	VIIIa	right	32.5	-52.0	-53.5		0.006	2.65
5	VIIIb	right	23.5	-50.5	-56.5	38	0.002	3.07
6	Extended cluster	right Crus I (311), right VI (222)						
	VI	right	22.0	-68.5	-28.0	533	0.002	2.99
	VI	right	32.5	-67.0	-26.5		0.003	2.84
	VI	right	28.0	-59.5	-28.0		0.012	2.33
7	IX	right	5.5	-49.0	-59.5	11	0.003	2.88
8	Extended cluster	white matter (119), left DN (20), left I-IV (15), left IN (13), left V (12)						
	DN	left	-9.5	-56.5	-29.5	179	0.003	2.87
	I-IV	left	-8.0	-47.5	-25.0		0.016	2.21
9	I-IV	right	14.5	-43.0	-11.5	15	0.005	2.71
10	Crus I	left	-51.5	-67.0	-37.0	15	0.005	2.68
11	VTA	right	2.5	-16.0	-13.0	19	0.008	2.53
12	VIIIa	right	17.5	-65.5	-58.0	27	0.008	2.50
13	Extended cluster	left VIIb (40), left VIIIa (36)						

	VIIb	left	-38.0	-62.5	-59.5	76	0.009	2.48
	VIIIa	left	-32.0	-52.0	-56.5		0.017	2.18
14	VIIIb	left	-23.0	-38.5	-53.5	12	0.01	2.42
15	I-IV	left	-0.5	-52.0	2.0	1	0.012	2.33
16	VIIIa	left	-20.0	-64.0	-59.5	35	0.013	2.29
17	VTA	left	-8.0	-17.5	-10.0	7	0.014	2.28
18	Crus I	right	23.5	-83.5	-22.0	10	0.015	2.24
19	Crus II	left	-9.5	-74.5	-34.0	15	0.016	2.23
20	VIIb	left	-18.5	-79.0	-53.5	11	0.016	2.22
21	VIIIa	right	29.5	-62.5	-53.5	8	0.017	2.19
22	VI	right	28.0	-59.5	-19.0	20	0.02	2.12
23	Extended cluster	right IX (18), vermal VIIIb (4), vermal VIIIa (2), right VIIIa (1)						
	IX	right	5.5	-58.0	-43.0	25	0.02	2.12
	VIIIa	right	7.0	-67.0	-46.0		0.042	1.76
24	V	left	-21.5	-49.0	-16.0	3	0.021	2.10
25	Crus II	right	4.0	-77.5	-37.0	8	0.022	2.07
26	white matter		5.5	-71.5	-11.5	1	0.024	2.03
27	VIIb	right	20.5	-77.5	-55.0	5	0.025	2.01
28	VI	right	20.5	-74.5	-17.5	1	0.027	1.97
29	VI	vermal	2.5	-62.5	-25.0	16	0.029	1.94
30	V	left	-21.5	-41.5	-23.5	6	0.03	1.93
31	VI	right	23.5	-71.5	-17.5	3	0.032	1.90
32	VIIIb	right	14.5	-56.5	-52.0	4	0.034	1.86
33	VIIb	left	-5.0	-71.5	-43.0	3	0.036	1.83
34	V	left	-20.0	-53.5	-16.0	6	0.037	1.82
35	VI	right	20.5	-59.5	-28.0	5	0.038	1.81
36	VIIb	right	13.0	-71.5	-53.5	9	0.039	1.80
37	V	left	-23.0	-34.0	-22.0	2	0.039	1.80
38	I-IV	right	10.0	-50.5	-5.5	1	0.041	1.78
39	VIIb	left	-42.5	-52.0	-53.5	1	0.041	1.77
40	DN	right	14.5	-62.5	-37.0	1	0.044	1.73
41	white matter		-11.0	-38.5	-35.5	1	0.046	1.72
42	VIIIb	left	-21.5	-52.0	-58.0	1	0.047	1.70
43	I-IV	right	5.5	-53.5	0.5	1	0.048	1.69

Supplementary table 7: FMRI activations related to the unexpected omission of the US. TFCE and FWE corrected.

FMRI activation clusters (p<0.05, FWE and TFCE corrected) related to the unexpected omission of the US in the cerebellar cortex, DCN and VTA (Figure 3). Up to three maxima in each cluster are shown separated by at least 8 mm. Coordinates are indicated in MNI space (x,y,z). The cluster size is shown by number of voxels (volume of 1 voxel = 3.375 mm^3). US: Unconditioned stimulus; CS: Conditioned stimulus; VTA: Ventral tegmental area; DCN: Deep cerebellar nuclei; DN: Dentate nucleus; IN: Interposed Nucleus; FN: Fastigial nucleus; MNI: Montreal Neurological Institute standard brain; TFCE t: Threshold-free cluster-enhanced t-statistic; *pFWE*: family-wise error corrected *p*-value.

Index	Location (lobule, DCN, VTA)	Side	MNI coordinates/mm			Cluster size (number of voxels)	p_{FWE}	TFCE t
			x	y	z			
First 3 no US post CS+ > no US post CS- during extinction (Figure 3A), t-test, TFCE, p<0.05, FWE corr.								
1	Extended cluster	left Crus I (2540), left Crus II (2266), white matter (1957), left VI (1531), right VI (1403), right Crus I (1144), left VIIb (811), left DN (273), right V (240), right I-IV (208), left I-IV (185), right DN (154), left VIIIa (138), vermal VI (126), vermal VIIIa (115), left V (114), left IX (93), right Crus II (79), left VIIIb (57), vermal IX (29), right IX (29), left IN (20), left X (15), vermal VIIb (9), vermal Crus I (5), vermal Crus II (4), vermal VIIIb (4), right IN (4), vermal X (3), right VIIb (1), left FN (1)						
	Crus I	left	-38.0	-53.5	-35.5	13558	<0.001	3262
	VI	left	-20.0	-68.5	-26.5		0.001	3214
	VI	left	-24.5	-50.5	-31.0		0.001	3073
2	Extended cluster	right VIIb (193), right Crus II (113), right VIIIa (11)						
	Crus II	right	7.0	-79.0	-43.0	317	0.007	2053
	VIIb	right	22.0	-71.5	-52.0		0.013	1773
	VIIb	right	14.5	-76.0	-50.5		0.014	1746
3	I-IV	right	4.0	-52.0	0.5	2	0.018	1642
4	Extended cluster	left VTA (35), right VTA (22)						
	VTA	right	8.5	-17.5	-10.0	57	0.022	1562
	VTA	left	-8.0	-17.5	-10.0		0.022	1550
	VTA	left	-0.5	-16.0	-14.5		0.031	1413
5	Extended cluster	right VIIb (197), right Crus II (171), right VIIIa (146), white matter (31), right Crus I (24), right X (11), right VI (9)						

	VIIIa	right	35.5	-52.0	-52.0	589	0.022	1551
	Crus II	right	43.0	-49.0	-46.0		0.027	1470
	VIIb	right	35.5	-44.5	-43.0		0.028	1451
6	VI	right	20.5	-74.5	-17.5	1	0.023	1545
7	I-IV	right	5.5	-49.0	-1.0	3	0.023	1545
8	I-IV	left	-5.0	-49.0	-1.0	2	0.023	1545
9	VTA	right	1.0	-20.5	-8.5	5	0.031	1412
10	VTA	left	-0.5	-20.5	-17.5	2	0.036	1348
11	VI	left	-8.0	-67.0	-10.0	1	0.039	1315
12	Crus II	right	28.0	-83.5	-46.0	52	0.042	1281
First 3 no US post CS+ > no US post CS- during recall (Figure 3B), t-test, TFCE, p<0.05, FWE corr.								
1	Extended cluster	left Crus I (1340), left VI (1298), left Crus II (599), left VIIb (142), vermal VI (132), white matter (55), left DN (20), left VIIIa (17), right VI (9), left V (6), vermal Crus I (4)						
	VI	left	-21.5	-71.5	-28.0	3622	0.001	2073
	VI	left	-29.0	-67.0	-26.5		0.002	2046
	VI	left	-8.0	-76.0	-26.5		0.002	1988
2	Extended cluster	vermal VIIIa (140), vermal VIIIb (138), vermal IX (137), left IX (55), left VIIIb (43), white matter (31), left VIIIa (9), vermal X (8), left DN (1)						
	IX	vermal	-0.5	-59.5	-35.5	562	0.021	1318
	VIIIb	vermal	-0.5	-65.5	-44.5		0.028	1245
	VIIIb	left	-9.5	-61.0	-43.0		0.028	1243
3	Extended cluster	right VI (344), white matter (159), right DN (46), right Crus I (30), right IN (8)						
	VI	right	34.0	-55.0	-29.5	587	0.021	1317
	VI	right	32.5	-55.0	-20.5		0.024	1291
	VI	right	20.5	-58.0	-28.0		0.024	1289
4	I-IV	right	14.5	-43.0	-11.5	43	0.024	1291
5	V	right	20.5	-53.5	-13.0	7	0.024	1288
6	Extended cluster	right VIIIa (295), right VIIb (230), right Crus II (94), right VIIIb (66), white matter (16), vermal VIIIa (2)						
	VIIb	right	19.0	-73.0	-49.0	703	0.027	1256
	VIIIa	right	23.5	-64.0	-49.0		0.027	1249
	VIIIa	right	32.5	-52.0	-52.0		0.03	1224
7	VTA	right	2.5	-17.5	-14.5	39	0.033	1192
8	Crus I	left	-36.5	-80.5	-25.0	1	0.035	1178
9	Extended cluster	left VIIb (194), left VIIIa (43), left Crus II (27), left VIIIb (1)						
	VIIb	left	-36.5	-47.5	-50.5	265	0.037	1164
	VIIb	left	-38.0	-55.0	-56.5		0.037	1162
	Crus II	left	-42.5	-62.5	-50.5		0.042	1130
10	VI	right	23.5	-77.5	-19.0	2	0.039	1151
11	V	right	8.5	-56.5	-4.0	2	0.039	1151

12	Extended cluster	right IX (86), white matter (32), right VIIIb (23), right X (17)						
	IX	right	13.0	-53.5	-46.0	158	0.039	1151
	VIIIb	right	19.0	-43.0	-49.0		0.045	1112
13	VIIIb	left	-17.0	-52.0	-50.5	41	0.04	1140
14	VI	right	13.0	-76.0	-16.0	3	0.042	1127
15	I-IV	right	4.0	-46.0	-5.5	52	0.044	1118
16	VTA	left	-8.0	-19.0	-11.5	1	0.044	1115
17	Extended cluster	left X (49), white matter (16), left VIIIb (12)						
	VIIIb	left	-24.5	-38.5	-47.5	77	0.045	1111
	X	left	-15.5	-40.0	-44.5		0.045	1110
18	VI	right	29.5	-47.5	-20.5	1	0.046	1102
19	VI	right	20.5	-71.5	-16.0	1	0.046	1102
20	V	right	23.5	-49.0	-16.0	1	0.046	1102
21	V	left	-17.0	-46.0	-13.0	1	0.048	1092
22	X	right	22.0	-38.5	-46.0	4	0.048	1090
First 3 no US post CS+ > no US post CS- during reacquisition (Figure 3C), t-test, TFCE, p<0.05, FWE corr.								
1	Extended cluster	right VTA (74), left VTA (71)						
	VTA	left	-2.0	-17.5	-7.0	145	0.001	7243
	VTA	right	8.5	-16.0	-11.5		0.001	6425
	VTA	left	-0.5	-20.5	-17.5		0.002	4461
2	Extended cluster	left Crus I (3033), left Crus II (2504), left VI (2143), right VI (2121), right Crus I (1081), left VIIb (982), white matter (896), right VIIb (878), left IX (695), right VIIIa (604), right Crus II (582), right IX (351), vermal IX (252), left VIIIb (246), right X (244), vermal VI (176), left X (175), right I-IV (153), right DN (152), left DN (151), left I-IV (148), right V (130), right VIIIb (121), left VIIIa (75), left V (61), vermal VIIIb (54), vermal VIIIa (47), vermal X (45), right IN (6), vermal Crus I (5), vermal Crus II (2), left FN (2), left IN (1)						
	Crus I	left	-9.5	-82.0	-28.0	18116	0.001	6274
	VI	left	-26.0	-65.5	-28.0		0.001	6189
	VI	left	-29.0	-59.5	-32.5		0.001	6171
3	white matter		-9.5	-38.5	-31.0	20	0.005	2394
4	white matter		-12.5	-37.0	-41.5	4	0.01	988
First 3 no US post CS+ > no US post CS- during reextinction (Figure 3D), t-test, TFCE, p<0.05, FWE corr.								
1	Extended cluster	left Crus I (1030), left VI (807), left Crus II (63), white matter (1), vermal VI (1)						
	VI	left	-8.0	-76.0	-26.5	1902	0.004	2229
	Crus I	left	-15.5	-79.0	-25.0		0.005	2151
	VI	left	-30.5	-58.0	-31.0		0.007	2020
2	Extended cluster	left VTA (47), right VTA (34)						

	VTA	right	4.0	-14.5	-13.0	81	0.027	1432
	VTA	left	-5.0	-16.0	-13.0		0.028	1425
3	VTA	right	4.0	-14.5	-7.0	4	0.034	1340
4	Crus I	right	38.5	-53.5	-31.0	4	0.049	1194
No US post CS+ x prediction error during extinction (Figure 3E), t-test, TFCE, p<0.05, FWE corr.								
1	Extended cluster	left Crus I (2341), left Crus II (1671), left VI (1220), white matter (529), left VIIb (337), left IX (269), vermal VIIIa (135), vermal IX (135), left DN (133), right I-IV (123), left I-IV (122), left VIIIb (64), left X (56), left VIIIa (44), vermal X (33), left V (30), vermal VIIIb (26), right V (23), vermal VI (15), left IN (10), vermal VIIb (9), vermal Crus I (6), vermal Crus II (4), right FN (4), left FN (2)						
	Crus I	left	-11.0	-79.0	-26.5	7341	0.002	2645
	VI	left	-23.0	-68.5	-28.0		0.003	2422
	Crus I	left	-20.0	-76.0	-31.0		0.003	2410
2	Extended cluster	left VTA (54), right VTA (52)						
	VTA	left	-5.0	-17.5	-13.0	106	0.011	1808
	VTA	right	5.5	-16.0	-14.5		0.013	1770
3	I-IV	right	5.5	-49.0	-1.0	3	0.021	1569
4	Extended cluster	right V (9), left V (2)						
	V	right	1.0	-62.5	-1.0	11	0.025	1496
	V	right	5.5	-67.0	-8.5		0.025	1484
5	I-IV	left	-5.0	-49.0	-1.0	3	0.026	1482
6	Extended cluster	right Crus I (600), right VI (246), right Crus II (16), vermal Crus II (1)						
	VI	right	37.0	-50.5	-31.0	863	0.034	1368
	Crus I	right	38.5	-76.0	-25.0		0.035	1356
	Crus I	right	13.0	-80.5	-26.5		0.036	1344
7	I-IV	right	4.0	-52.0	0.5	1	0.039	1315
8	Crus I	left	-45.5	-43.0	-31.0	1	0.043	1275
9	DN	right	16.0	-58.0	-34.0	136	0.044	1263
10	Crus I	right	23.5	-83.5	-22.0	2	0.046	1251
11	VI	right	16.0	-80.5	-19.0	4	0.046	1251
12	V	right	29.5	-44.5	-22.0	41	0.046	1248
	VI	right	35.5	-52.0	-22.0		0.049	1226
No US post CS+ x prediction error during recall test (Figure 3F), t-test, TFCE, p<0.05, FWE corr.								
1	Extended cluster	left VI (357), left Crus I (325), white matter (2)						
	VI	left	-33.5	-55.0	-32.5	684	0.003	1981
	VI	left	-29.0	-64.0	-29.5		0.006	1772
	VI	left	-38.0	-40.0	-35.5		0.043	1198
2	Extended cluster	left VI (56), vermal VI (11), left Crus I (9)						

	VI	vermal	-3.5	-79.0	-19.0	76	0.038	1231
	VI	left	-12.5	-80.5	-20.5		0.041	1213
	VI	left	-20.0	-77.5	-23.5		0.045	1180
3	Crus I	left	-14.0	-79.0	-29.5	60	0.043	1193
4	Crus II	left	-14.0	-79.0	-35.5	2	0.05	1151
No US post CS+ x prediction error during reacquisition (Figure 3G), t-test, TFCE, p<0.05, FWE corr.								
	No significant voxels							
No US post CS+ x prediction error during reextinction (Figure 3H), t-test, TFCE, p<0.05, FWE corr.								
	No significant voxels							

Supplementary table 8: FMRI activations related to the unexpected omission of the US. Uncorrected.

FMRI activation clusters (p<0.05, uncorrected) related to the unexpected omission of the US in the cerebellar cortex, DCN and VTA (Figure 3). Up to three maxima in each cluster are shown separated by at least 8 mm. Coordinates are indicated in MNI space (x,y,z). The cluster size is shown by number of voxels (volume of 1 voxel = 3.375 mm^3). US: Unconditioned stimulus; CS: Conditioned stimulus; VTA: Ventral tegmental area; DCN: Deep cerebellar nuclei; DN: Dentate nucleus; IN: Interposed Nucleus; FN: Fastigial nucleus; MNI: Montreal Neurological Institute standard brain; t: t-statistic; p_{unc}: uncorrected p-value.

Index	**Location (lobule, DCN, VTA)**	**Side**	**MNI coordinates/mm**			**Cluster size (number of voxels)**	**p_{unc}**	**t**
			x	**y**	**z**			
First 3 no US post CS+ > no US post CS- during extinction (Figure 3A), t-test, p<0.05, uncorrected								
1	Extended cluster	left Crus I (3015), white matter (2887), left Crus II (2640), right VI (1855), left VI (1794), right Crus I (1739), left VIIb (1040), right Crus II (838), right VIIb (580), right V (447), right I-IV (333), right VIIIa (327), left DN (289), left V (283), left I-IV (272), left VIIIa (258), left IX (255), vermal VI (232), vermal VIIIa (227), right DN (225), right VIIIb (166), left VIIIb (134), right IX (103), vermal IX (75), right X (57), vermal VIIIb (50), left X (41), vermal Crus II (29), left IN (22), vermal VIIb (17), right IN (11), vermal X (9), vermal Crus I (7), left FN (1)						
	VI	left	-20.0	-68.5	-26.5	20258	<0.001	6.92
	Crus I	left	-38.0	-53.5	-35.5		<0.001	6.77
	Crus II	left	-29.0	-77.5	-41.5		<0.001	6.08

2	Extended cluster	left VTA (53), right VTA (49)						
	VTA	left	-8.0	-17.5	-10.0	102	<0.001	3.82
	VTA	right	8.5	-17.5	-10.0		<0.001	3.74
	VTA	left	-0.5	-16.0	-14.5		0.004	2.77
3	I-IV	left	-5.0	-49.0	-1.0	6	0.012	2.34
4	I-IV	left	-0.5	-52.0	2.0	1	0.021	2.08
5	IX	right	5.5	-49.0	-59.5	1	0.027	1.97
6	VIIIb	right	20.5	-46.0	-56.5	6	0.029	1.94
7	Crus I	left	-33.5	-86.5	-32.5	2	0.031	1.91
8	white matter		22.0	-32.5	-37.0	5	0.031	1.91
9	V	left	-18.5	-47.5	-14.5	1	0.036	1.84
10	Crus II	left	-26.0	-89.5	-37.0	3	0.038	1.81
11	white matter		32.5	-62.5	-38.5	3	0.04	1.79
First 3 no US post CS+ > no US post CS- during recall (Figure 3B), t-test, p<0.05, uncorrected								
1	Extended cluster	left Crus I (1983), left VI (1831), left Crus II (1548), right VI (1164), white matter (1145), left VIIb (683), right VIIIa (557), right VIIb (554), right Crus II (384), left VIIIa (353), right I-IV (350), left VIIIb (343), right VIIIb (335), vermal VIIIa (294), vermal VI (273), right Crus I (205), left IX (197), vermal IX (197), right IX (189), vermal VIIIb (182), left X (162), right V (153), right DN (153), left I-IV (145), left DN (137), right X (121), left V (93), vermal X (25), right IN (21), vermal Crus II (19), vermal VIIb (9), vermal Crus I (7), left FN (3), left IN (1), right FN (1)						
	VI	left	-21.5	-71.5	-28.0	13817	<0.001	5.60
	VI	left	-8.0	-76.0	-26.5		<0.001	5.45
	VI	left	-35.0	-53.5	-31.0		<0.001	5.37
2	Extended cluster	right VTA (51), left VTA (47)						
	VTA	right	2.5	-17.5	-14.5	98	<0.001	4.75
	VTA	left	-8.0	-19.0	-11.5		<0.001	3.57
3	I-IV	right	13.0	-34.0	-22.0	26	0.002	3.09
4	V	left	-17.0	-46.0	-13.0	4	0.004	2.75
5	V	left	-14.0	-50.5	-10.0	6	0.01	2.44
6	Extended cluster	left I-IV (45)						
	I-IV	left	-8.0	-38.5	-20.5	45	0.012	2.34
	I-IV	left	-6.5	-41.5	-11.5		0.014	2.28
7	V	left	-3.5	-58.0	-13.0	13	0.013	2.31
8	Crus I	right	47.5	-53.5	-44.5	5	0.017	2.18
9	IX	right	5.5	-58.0	-55.0	8	0.022	2.07
10	VIIIa	right	10.0	-68.5	-53.5	6	0.032	1.90
11	VI	right	23.5	-71.5	-17.5	1	0.036	1.84
12	IX	left	-6.5	-56.5	-53.5	5	0.037	1.83

13	VI	right	10.0	-74.5	-14.5	1	0.038	1.81
14	V	left	-8.0	-58.0	-4.0	1	0.038	1.81
15	VI	left	-23.0	-62.5	-16.0	1	0.042	1.75
16	V	left	-0.5	-68.5	-8.5	1	0.046	1.71
17	white matter		-9.5	-41.5	-50.5	1	0.048	1.69
First 3 no US post CS+ > no US post CS- reacquisition (Figure 3C), t-test, p<0.05, uncorrected								
1	Extended cluster	left Crus I (2890), left Crus II (2337), left VI (2089), right VI (1996), right Crus I (986), left VIIb (932), right VIIb (789), white matter (747), left IX (650), right VIIIa (546), right Crus II (468), right IX (263), vermal IX (240), right X (240), left VIIIb (225), vermal VI (159), left X (157), left DN (132), right DN (121), left I-IV (106), right I-IV (90), right VIIIb (87), right V (70), left VIIIa (63), vermal VIIIa (41), vermal VIIIb (41), vermal X (37), left V (14), vermal Crus I (5), right IN (4), vermal Crus II (2), left FN (2)						
	Crus I	left	-38.0	-58.0	-31.0	16529	<0.001	9.00
	Crus I	left	-9.5	-82.0	-28.0		<0.001	8.92
	VI	left	-26.0	-65.5	-28.0		<0.001	8.24
2	Extended cluster	right VTA (72), left VTA (67)						
	VTA	left	-2.0	-17.5	-7.0	139	<0.001	6.35
	VTA	left	-0.5	-20.5	-17.5		<0.001	5.10
	VTA	right	8.5	-16.0	-11.5		<0.001	4.52
3	V	left	-0.5	-59.5	-1.0	126	<0.001	4.07
4	white matter		-9.5	-38.5	-31.0	17	0.002	3.08
5	I-IV	right	28.0	-31.0	-31.0	11	0.007	2.57
6	VI	right	35.5	-34.0	-35.5	3	0.029	1.94
7	I-IV	right	1.0	-55.0	-10.0	6	0.036	1.84
8	white matter		-12.5	-37.0	-41.5	1	0.036	1.84
9	V	left	-2.0	-61.0	-14.5	3	0.041	1.77
10	Crus II	right	14.5	-74.5	-35.5	3	0.042	1.76
11	VI	right	32.5	-34.0	-37.0	1	0.046	1.71
First 3 no US post CS+ > no US post CS- reextinction (Figure 3D), t-test, p<0.05, uncorrected								
1	Extended cluster	left Crus I (2250), left Crus II (1542), left VI (1426), left VIIb (606), white matter (460), left I-IV (322), right I-IV (241), left IX (220), vermal IX (147), left DN (118), right V (79), left VIIIa (73), left VIIIb (67), left V (56), right DN (44), vermal VI (29), right IN (18), vermal VIIIa (15), left IN (14), vermal Crus I (7), vermal VIIIb (6), vermal X (6), right IX (4), left FN (4), right FN (2), right VI (1)						
	VI	left	-8.0	-76.0	-26.5	7757	<0.001	6.40
	VI	left	-30.5	-58.0	-31.0		<0.001	5.84
	Crus I	left	-15.5	-79.0	-25.0		<0.001	5.76
2	Extended cluster	left VTA (73), right VTA (69)						

	VTA	left	-5.0	-16.0	-13.0	142	<0.001	5.04
	VTA	right	4.0	-14.5	-13.0		<0.001	5.03
3	Extended cluster	right VI (905), right Crus I (585), right VIIb (498), right VIIIa (433), right X (161), white matter (135), right VIIIb (40), vermal VI (34), right Crus II (29), right V (11), right IX (1)						
	Crus I	right	38.5	-53.5	-31.0	2832	<0.001	4.58
	Crus I	right	43.0	-61.0	-29.5		<0.001	3.54
	VIIb	right	14.5	-74.5	-47.5		0.001	3.51
4	white matter		-23.0	-47.5	-43.0	48	0.008	2.51
5	VIIIa	vermal	7.0	-64.0	-38.5	21	0.017	2.20
6	IX	right	11.5	-59.5	-47.5	27	0.017	2.19
7	white matter		-20.0	-40.0	-37.0	14	0.018	2.15
8	VI	vermal	4.0	-70.0	-16.0	13	0.025	2.01
9	VIIIb	right	11.5	-49.0	-61.0	5	0.028	1.96
10	white matter		-15.5	-34.0	-40.0	4	0.032	1.90
11	I-IV	left	-11.0	-41.5	-16.0	5	0.032	1.89
12	I-IV	left	-8.0	-50.5	-10.0	3	0.036	1.83
13	VI	left	-35.0	-35.5	-35.5	1	0.043	1.75
14	VI	vermal	-0.5	-68.5	-26.5	1	0.045	1.72
15	VI	vermal	1.0	-70.0	-28.0	1	0.046	1.71
16	Crus I	right	23.5	-73.0	-29.5	1	0.049	1.68
No US post CS+ x prediction error during extinction (Figure 3E), t-test, p<0.05, uncorrected								
1	Extended cluster	left Crus I (3530), left Crus II (2289), white matter (1583), left VI (1506), right Crus I (1298), right VI (798), left VIIb (606), left IX (536), left I-IV (254), vermal VIIIa (246), right I-IV (232), left DN (215), right DN (198), vermal IX (177), left VIIIb (173), right V (136), left X (127), vermal VI (126), right Crus II (85), left VIIIa (85), vermal VIIIb (69), left V (66), vermal X (60), vermal Crus II (55), vermal VIIb (41), right IX (20), left IN (18), right IN (16), right FN (8), left FN (7), vermal Crus I (6)						
	Crus I	left	-11.0	-79.0	-26.5	14566	<0.001	6.39
	VI	left	-23.0	-68.5	-28.0		<0.001	5.55
	VI	left	-33.5	-50.5	-32.5		<0.001	5.20
2	Extended cluster	right VTA (81), left VTA (71)						
	VTA	left	-5.0	-17.5	-13.0	152	<0.001	4.45
	VTA	right	5.5	-17.5	-14.5		<0.001	3.77
3	Extended cluster	right Crus II (410), right VIIb (296), right VIIIa (4)						
	Crus II	right	29.5	-82.0	-49.0	710	<0.001	4.04
	Crus II	right	8.5	-79.0	-43.0		<0.001	3.74
	VIIb	right	20.5	-71.5	-52.0		0.001	3.42
4	Extended cluster	right X (112), white matter (45), right VI (25), right VIIIa (19), right VIIIb (17), right VIIb (2)						

	VI	right	31.0	-41.5	-41.5	220	0.001	3.40
	X	right	20.5	-37.0	-49.0		0.006	2.61
	X	right	22.0	-32.5	-40.0		0.027	1.98
5	Extended cluster	right VIIb (107), right VIIIa (92), right Crus II (39), right VIIIb (8), white matter (4)						
	VIIb	right	41.5	-56.5	-53.5	250	0.001	3.16
	VIIIa	right	32.5	-52.0	-49.0		0.008	2.51
	VIIIb	right	28.0	-44.5	-55.0		0.022	2.07
6	Extended cluster	right V (31), left V (8)						
	V	right	1.0	-62.5	-1.0	39	0.005	2.68
	V	right	5.5	-67.0	-8.5		0.006	2.60
7	Extended cluster	right I-IV (23)						
	I-IV	right	5.5	-49.0	-1.0	23	0.006	2.60
	I-IV	right	2.5	-56.5	0.5		0.019	2.14
8	I-IV	left	-5.0	-49.0	-1.0	7	0.008	2.49
9	Crus II	right	31.0	-68.5	-41.5	83	0.01	2.44
10	Crus I	left	-50.0	-70.0	-40.0	12	0.014	2.28
11	IX	right	8.5	-58.0	-53.5	18	0.014	2.27
12	V	left	-26.0	-31.0	-29.5	6	0.019	2.14
13	white matter		5.5	-71.5	-11.5	9	0.024	2.03
14	VI	right	38.5	-38.5	-29.5	5	0.028	1.95
15	VI	right	26.5	-58.0	-29.5	9	0.033	1.87
16	Crus II	right	46.0	-47.5	-46.0	2	0.034	1.86
17	VIIIa	left	-32.0	-47.5	-56.5	1	0.038	1.82
18	I-IV	left	-8.0	-46.0	-4.0	2	0.042	1.76
19	VI	left	-38.0	-37.0	-31.0	1	0.042	1.76
20	VI	right	41.5	-41.5	-32.5	3	0.042	1.75
No US post CS+ x prediction error during recall (Figure 3F), t-test, p<0.05, uncorrected								
1	Extended cluster	left Crus I (1637), left VI (1505), right VI (992), white matter (767), left Crus II (418), vermal VI (364), left VIIIb (322), vermal VIIIa (308), left X (221), left VIIIa (190), vermal IX (186), left IX (175), vermal VIIIb (154), right DN (151), right X (140), right Crus I (112), left I-IV (110), left DN (92), right I-IV (67), right Crus II (64), right V (62), vermal Crus II (62), vermal VIIb (55), left V (53), right VIIIb (49), right IX (41), vermal X (38), right VIIb (25), right VIIIa (18), left VIIb (10), left IN (10), vermal Crus I (4), right IN (1), right FN (1)						
	VI	left	-33.5	-55.0	-32.5	8404	<0.001	7.24
	VI	left	-29.0	-64.0	-29.5		<0.001	5.98
	VIIIb	vermal	-3.5	-64.0	-41.5		<0.001	4.74
2	Extended cluster	left VTA (51), right VTA (32)						
	VTA	left	-0.5	-16.0	-13.0	83	<0.001	4.50

	VTA	right	7.0	-20.5	-14.5		0.019	2.13
3	Extended cluster	left Crus II (535), left VIIb (170), left VIIIa (16), left Crus I (9), white matter (1)						
	Crus II	left	-27.5	-82.0	-43.0	731	<0.001	3.84
	Crus II	left	-23.0	-76.0	-46.0		0.006	2.60
	VIIIa	left	-18.5	-70.0	-55.0		0.015	2.23
4	Extended cluster	right VIIb (278), right VIIIa (273), right VIIIb (135), right Crus II (125), white matter (93), right Crus I (2)						
	VIIIb	right	29.5	-46.0	-53.5	906	<0.001	3.83
	VIIb	right	22.0	-67.0	-44.5		0.001	3.43
	VIIb	right	40.0	-44.5	-50.5		0.002	3.04
5	IX	left	-6.5	-58.0	-53.5	39	0.002	2.97
6	Extended cluster	right I-IV (29), left V (6), right V (6), left I-IV (3)						
	I-IV	right	4.0	-52.0	0.5	44	0.003	2.84
	V	left	-0.5	-61.0	-1.0		0.01	2.43
7	Crus II	left	-33.5	-59.5	-44.5	62	0.004	2.82
8	Extended cluster	left Crus II (89), left VIIb (56)						
	Crus II	left	-45.5	-52.0	-50.5	145	0.004	2.77
	Crus II	left	-39.5	-74.5	-50.5		0.033	1.88
	Crus II	left	-42.5	-67.0	-50.5		0.038	1.81
9	VIIb	left	-3.5	-76.0	-49.0	2	0.009	2.47
10	Crus I	right	34.0	-79.0	-22.0	21	0.012	2.33
11	I-IV	right	13.0	-35.5	-23.5	11	0.012	2.33
12	Crus I	right	43.0	-55.0	-34.0	34	0.014	2.28
13	I-IV	right	2.5	-58.0	-5.5	29	0.017	2.18
14	VIIIb	right	13.0	-47.5	-64.0	5	0.018	2.17
15	Crus I	right	43.0	-64.0	-34.0	21	0.018	2.15
16	Crus I	right	49.0	-73.0	-38.5	1	0.033	1.89
17	VI	right	37.0	-43.0	-25.0	1	0.036	1.83
18	VI	right	13.0	-73.0	-25.0	2	0.037	1.82
19	VIIIa	left	-9.5	-65.5	-56.5	1	0.037	1.82
20	Crus II	right	41.5	-68.5	-52.0	5	0.038	1.81
21	I-IV	left	-3.5	-50.5	-8.5	4	0.039	1.80
22	VIIb	right	34.0	-65.5	-56.5	1	0.041	1.77
23	Crus I	left	-21.5	-86.5	-25.0	2	0.041	1.77
24	IX	right	5.5	-58.0	-55.0	1	0.043	1.75
25	V	left	-6.5	-58.0	-13.0	1	0.047	1.70
26	VIIIa	right	17.5	-64.0	-58.0	1	0.048	1.69
No US post CS+ x prediction error during reacquisition (Figure 3G), t-test, p<0.05, uncorrected								
1	Extended cluster	left Crus I (1123), left VI (925), left Crus II (863), left VIIb (381), white matter (53), left DN (5), left VIIIa (4)						
	Crus I	left	-27.5	-68.5	-31.0	3354	<0.001	3.91

	VI	left	-30.5	-56.5	-32.5		<0.001	3.77
	Crus I	left	-35.0	-49.0	-35.5		0.001	3.52
2	Extended cluster	right VIIb (287), right Crus II (154), right VIIIa (154)						
	VIIIa	right	32.5	-61.0	-53.5	595	<0.001	3.70
	VIIb	right	17.5	-74.5	-46.0		<0.001	3.59
	VIIb	right	31.0	-71.5	-55.0		0.002	3.01
3	Extended cluster	right VTA (32), left VTA (9)						
	VTA	right	5.5	-13.0	-11.5	41	<0.001	3.61
	VTA	left	-0.5	-20.5	-17.5		<0.001	3.60
4	Extended cluster	right VI (270), right Crus I (124)						
	VI	right	37.0	-52.0	-31.0	394	0.001	3.35
	VI	right	32.5	-64.0	-25.0		0.039	1.80
5	Extended cluster	left IX (175), vermal IX (77), right IX (70), left VIIIb (67), white matter (11), vermal VIIIa (4), vermal VIIIb (4), vermal X (2), left VIIIa (1)						
	IX	right	2.5	-58.0	-56.5	411	0.001	3.29
	white matter		-9.5	-58.0	-41.5		0.005	2.71
	VIIIb	left	-9.5	-62.5	-52.0		0.008	2.51
6	X	left	-24.5	-34.0	-46.0	32	0.001	3.23
7	white matter		-24.5	-41.5	-40.0	77	0.003	2.91
8	white matter		26.5	-43.0	-43.0	52	0.005	2.68
9	VTA	left	-5.0	-13.0	-11.5	11	0.012	2.33
10	DN	left	-15.5	-50.5	-35.5	13	0.018	2.15
11	IX	right	5.5	-49.0	-59.5	3	0.024	2.02
12	white matter		-9.5	-40.0	-38.5	4	0.027	1.98
13	X	right	20.5	-35.5	-46.0	9	0.028	1.96
14	VTA	left	-3.5	-16.0	-14.5	3	0.031	1.91
15	Crus I	right	47.5	-64.0	-26.5	5	0.033	1.88
16	VTA	left	-8.0	-16.0	-10.0	2	0.036	1.84
17	Crus II	right	44.5	-71.5	-44.5	3	0.038	1.81
18	white matter		-9.5	-38.5	-31.0	2	0.039	1.80
19	Crus II	right	11.5	-73.0	-35.5	1	0.039	1.80
20	DN	right	17.5	-59.5	-34.0	2	0.039	1.80
21	VIIIb	right	10.0	-44.5	-61.0	4	0.039	1.79
22	Crus I	left	-42.5	-41.5	-41.5	2	0.043	1.75
23	VIIIb	right	14.5	-55.0	-56.5	2	0.048	1.70
24	VTA	right	1.0	-20.5	-7.0	1	0.048	1.70

No US post CS+ x prediction error during recall (Figure 3H), t-test, p<0.05, uncorrected								
1	Extended cluster	right VIIb (160), right Crus II (67), right VIIIa (31)						
	VIIb	right	16.0	-74.5	-47.5	258	0.002	3.12
	VIIb	right	31.0	-71.5	-53.5		0.014	2.28
	VIIIa	right	32.5	-61.0	-53.5		0.017	2.19
2	VIIIb	right	11.5	-46.0	-61.0	41	0.003	2.92
3	Extended cluster	left Crus II (216), left VIIb (179), white matter (46), left VIIIa (8), left Crus I (5)						
	VIIb	left	-32.0	-62.5	-49.0	454	0.005	2.70
	Crus II	left	-27.5	-71.5	-47.5		0.005	2.67
	VIIb	left	-15.5	-73.0	-49.0		0.007	2.54
4	VTA	left	-0.5	-20.5	-17.5	12	0.005	2.66
5	white matter		-24.5	-41.5	-40.0	63	0.006	2.61
6	Extended cluster	left IX (26), right IX (26), left VIIIb (6), right VIIIb (3)						
	IX	left	-5.0	-58.0	-59.5	61	0.008	2.51
	IX	right	2.5	-58.0	-56.5		0.014	2.26
	IX	right	7.0	-56.5	-64.0		0.026	1.99
7	X	left	-26.0	-35.5	-47.5	8	0.012	2.35
8	Crus I	left	-38.0	-62.5	-31.0	37	0.016	2.22
9	VI	left	-35.0	-35.5	-35.5	25	0.018	2.17
10	VIIIb	right	23.5	-49.0	-50.5	4	0.023	2.06
11	VIIIa	vermal	-0.5	-73.0	-40.0	10	0.023	2.06
12	I-IV	left	-5.0	-55.0	-16.0	4	0.023	2.06
13	Crus II	left	-21.5	-86.5	-46.0	21	0.023	2.04
14	I-IV	left	-9.5	-37.0	-22.0	11	0.024	2.03
15	VI	left	-6.5	-73.0	-26.5	20	0.026	2.00
16	Extended cluster	white matter (16), left DN (9), left VI (1)						
	white matter		-24.5	-55.0	-35.5	26	0.027	1.97
	white matter		-17.0	-58.0	-32.5		0.038	1.81
17	VI	left	-32.0	-55.0	-34.0	21	0.028	1.96
18	Crus II	right	44.5	-73.0	-43.0	7	0.028	1.96
19	white matter		-9.5	-40.0	-40.0	1	0.029	1.95
20	Crus I	left	-15.5	-80.5	-25.0	9	0.03	1.92
21	Crus I	left	-36.5	-49.0	-37.0	9	0.033	1.89
22	white matter		-12.5	-50.5	-25.0	7	0.034	1.86
23	VIIIb	left	-8.0	-61.0	-40.0	2	0.035	1.85

24	Crus I	right	40.0	-52.0	-31.0	10	0.036	1.83
25	VIIIa	vermal	5.5	-67.0	-38.5	5	0.037	1.83
26	V	right	4.0	-58.0	-26.5	3	0.038	1.80
27	VTA	left	-5.0	-13.0	-11.5	1	0.04	1.78
28	white matter		-11.0	-68.5	-32.5	9	0.04	1.78
29	VTA	right	4.0	-14.5	-13.0	1	0.042	1.76
30	white matter		-15.5	-40.0	-40.0	3	0.042	1.76
31	IX	vermal	-3.5	-58.0	-38.5	3	0.042	1.75
32	VIIb	right	40.0	-68.5	-55.0	1	0.046	1.72
33	Crus II	right	40.0	-67.0	-43.0	1	0.047	1.70
34	Crus II	right	35.5	-71.5	-47.5	1	0.049	1.68

Supplementary table 9: FMRI activations related to PPI connectivity during unexpected US omissions with a VTA seed. Uncorrected.

FMRI PPI positive and negative activation clusters (p<0.05, uncorrected) related to connectivity with the VTA during unexpected omission of the US in the cerebellar cortex and DCN (Figure 4). Up to three maxima in each cluster are shown separated by at least 8 mm. Coordinates are indicated in MNI space (x,y,z). The cluster size is shown by number of voxels (volume of 1 voxel = 3.375 mm^3). US: Unconditioned stimulus; CS: Conditioned stimulus; VTA: Ventral tegmental area; DCN: Deep cerebellar nuclei; DN: Dentate nucleus; IN: Interposed Nucleus; FN: Fastigial nucleus; MNI: Montreal Neurological Institute standard brain; t: t-statistic; p_{unc}: uncorrected p-value.

Index	**Location (lobule, DCN)**	**Side**	**MNI coordinates/mm**			**Cluster size (number of voxels)**	**p_{unc}**	**t**
			x	**y**	**z**			
No US post CS+ x prediction error PPI positive connectivity with VTA during extinction (Figure 4A), t-test, p<0.05, uncorrected								
1	VIIIa	left	-24.5	-68.5	-59.5	107	<0.001	4.14
2	VI	left	-29.0	-59.5	-25.0	48	0.002	3.10
3	VI	left	-35.0	-35.5	-34.0	12	0.002	3.04
4	VIIIa	right	10.0	-70.0	-55.0	10	0.007	2.58
5	VIIb	left	-14.0	-73.0	-53.5	12	0.008	2.51
6	VIIIa	vermal	-2.0	-68.5	-44.5	6	0.009	2.47

7	VIIIb	right	17.5	-40.0	-53.5	9	0.009	2.45
8	V	right	19.0	-47.5	-20.5	8	0.01	2.42
9	VIIIb	right	17.5	-59.5	-59.5	8	0.011	2.39
10	V	right	10.0	-56.5	-19.0	17	0.012	2.36
11	VI	vermal	-3.5	-67.0	-23.5	6	0.013	2.32
12	VI	right	35.5	-34.0	-35.5	5	0.014	2.28
14	Crus II	left	-30.5	-79.0	-50.5	2	0.019	2.13
15	Crus I	left	-23.0	-89.5	-32.5	1	0.021	2.09
16	Crus II	right	16.0	-83.5	-35.5	1	0.021	2.09
17	Crus I	right	32.5	-86.5	-34.0	1	0.022	2.08
18	Crus II	left	-47.0	-53.5	-49.0	3	0.022	2.08
19	Crus II	vermal	4.0	-74.5	-32.5	1	0.024	2.03
20	Crus I	right	29.5	-88.0	-34.0	1	0.025	2.02
No US post CS+ x prediction error PPI negative connectivity with VTA during extinction (Figure 4A), t-test, p<0.05, uncorrected								
1	white matter		29.5	-65.5	-44.5	84	0.001	3.36
2	Extended cluster	white matter (216), left VI (12), left VIIIa (1)						
	white matter		-20.0	-38.5	-37.0	229	0.002	3.14
	white matter		-23.0	-52.0	-40.0		0.003	2.91
	white matter		-26.0	-43.0	-40.0		0.008	2.51
3	Extended cluster	white matter (37), right IX (29), vermal X (15), right IN (10), vermal IX (8), vermal VIIIa (2)						
	IN	right	7.0	-58.0	-31.0	101	0.002	3.12
	X	vermal	5.5	-49.0	-34.0		0.007	2.57
4	DN	left	-12.5	-50.5	-32.5	82	0.002	3.07
5	Extended cluster	white matter (124), right X (4), right IX (1)						
	white matter		11.5	-41.5	-40.0	129	0.002	3.04
	white matter		23.5	-52.0	-43.0		0.011	2.39
6	Extended cluster	white matter (127), left Crus II (38), left Crus I (15), left DN (9)						
	white matter		-17.0	-70.0	-40.0	189	0.002	2.99
	white matter		-18.5	-61.0	-38.5		0.006	2.60
7	IX	right	5.5	-56.5	-64.0	10	0.004	2.83
8	V	right	8.5	-55.0	-4.0	38	0.005	2.70
9	Crus I	right	47.5	-67.0	-34.0	32	0.006	2.60
10	Crus II	right	37.0	-58.0	-43.0	19	0.006	2.60

11	Crus I	left	-36.5	-58.0	-31.0	34	0.006	2.60
12	I-IV	left	-20.0	-32.5	-22.0	2	0.011	2.39
13	Crus I	left	-26.0	-79.0	-26.5	10	0.011	2.37
14	Crus I	right	17.5	-85.0	-25.0	35	0.011	2.36
15	VIIIb	vermal	4.0	-61.0	-40.0	2	0.012	2.33
16	Crus I	left	-14.0	-86.5	-23.5	23	0.013	2.31
17	VIIIa	right	34.0	-49.0	-46.0	8	0.014	2.28
18	Crus II	left	-30.5	-67.0	-47.5	9	0.014	2.27
19	I-IV	right	19.0	-34.0	-19.0	1	0.015	2.25
20	white matter		23.5	-62.5	-40.0	13	0.015	2.24
21	Crus II	left	-38.0	-70.0	-43.0	3	0.016	2.22
22	VIIIb	right	10.0	-62.5	-55.0	4	0.016	2.20
23	Crus I	left	-42.5	-61.0	-37.0	4	0.017	2.20
24	IX	right	2.5	-55.0	-56.5	4	0.017	2.18
25	Crus II	left	-3.5	-88.0	-29.5	1	0.018	2.17
26	white matter		-3.5	-55.0	-29.5	1	0.018	2.16
27	VIIIb	left	-18.5	-53.5	-50.5	5	0.019	2.14
28	VI	right	28.0	-43.0	-32.5	3	0.019	2.13
29	VIIb	right	22.0	-77.5	-55.0	1	0.02	2.11
30	IX	right	4.0	-64.0	-53.5	2	0.02	2.11
31	Crus I	left	-45.5	-59.5	-25.0	6	0.02	2.11
32	Crus II	right	10.0	-80.5	-50.5	1	0.021	2.10
33	VIIb	left	-5.0	-74.5	-50.5	1	0.022	2.06
34	Crus I	left	-45.5	-65.5	-34.0	1	0.023	2.05
35	Crus II	right	13.0	-82.0	-50.5	1	0.024	2.04
36	white matter		29.5	-50.5	-41.5	1	0.024	2.04
37	IX	vermal	2.5	-50.5	-40.0	1	0.025	2.02
No US post CS+ x prediction error PPI positive connectivity with VTA during recall (Figure 4A), t-test, p<0.05, uncorrected								
1	Extended cluster	left VI (203), left Crus I (65), left V (52)						
	V	left	-21.5	-50.5	-20.5	320	<0.001	4.07
	Crus I	left	-39.5	-59.5	-26.5		<0.001	3.58
	VI	left	-32.0	-58.0	-23.5		0.001	3.21
2	Extended cluster	left VIIIa (94), left VIIIb (69), left IX (63), vermal VIIIa (25), left VIIb (15), vermal VIIIb (5), white matter (2), left X (2)						
	VIIIa	left	-5.0	-68.5	-46.0	275	0.001	3.53
	VIIIb	left	-14.0	-44.5	-49.0		0.004	2.81
	VIIIa	left	-11.0	-65.5	-50.5		0.006	2.65
3	Extended cluster	left I-IV (60), right I-IV (54)						

	I-IV	left	-0.5	-43.0	-14.5	114	0.001	3.41
	I-IV	right	4.0	-46.0	-23.5		0.001	3.26
	I-IV	left	-6.5	-43.0	-23.5		0.013	2.31
4	Extended cluster	right VI (134), right Crus I (67), white matter (11)						
	VI	right	25.0	-68.5	-29.5	212	0.001	3.29
	Crus I	right	34.0	-68.5	-28.0		0.003	2.90
	VI	right	19.0	-61.0	-29.5		0.004	2.75
5	I-IV	left	-15.5	-37.0	-25.0	69	0.001	3.28
6	Extended cluster	vermal VI (104), left VI (28), right VI (17), left Crus II (12), vermal Crus II (12), vermal Crus I (5), right Crus I (3), left Crus I (1)						
	Crus II	vermal	-0.5	-79.0	-28.0	182	0.001	3.24
	VI	right	7.0	-71.5	-20.5		0.004	2.78
	VI	left	-6.5	-73.0	-20.5		0.004	2.77
7	Extended cluster	right IX (107), right VIIIa (70), vermal VIIIb (41), vermal VIIIa (39), vermal IX (36), right VIIIb (30), right VIIb (7), white matter (4)						
	VIIIa	right	13.0	-67.0	-47.5	334	0.002	3.08
	VIIIb	vermal	7.0	-62.5	-37.0		0.003	2.90
	IX	right	11.5	-56.5	-49.0		0.003	2.89
8	Extended cluster	right VI (198), right V (155), right I-IV (26)						
	V	right	20.5	-46.0	-17.5	379	0.002	3.01
	VI	right	29.5	-55.0	-28.0		0.003	2.94
	V	right	7.0	-56.5	-7.0		0.003	2.92
9	VIIb	right	41.5	-53.5	-49.0	46	0.003	2.86
10	IX	left	-2.0	-55.0	-46.0	76	0.005	2.68
11	VI	left	-24.5	-73.0	-22.0	49	0.005	2.68
12	Extended cluster	left Crus I (59), white matter (5)						
	Crus I	left	-39.5	-76.0	-34.0	64	0.006	2.64
13	VI	left	-32.0	-44.5	-29.5	25	0.006	2.61
14	Crus II	right	22.0	-86.5	-41.5	17	0.006	2.59
15	VIIIa	right	31.0	-44.5	-49.0	14	0.007	2.59
16	VI	left	-17.0	-62.5	-29.5	7	0.007	2.55
17	VI	right	34.0	-41.5	-28.0	24	0.007	2.54
18	V	right	4.0	-64.0	-7.0	31	0.008	2.50
19	Crus II	left	-47.0	-55.0	-49.0	20	0.009	2.45
20	Crus I	left	-33.5	-74.5	-25.0	26	0.01	2.40
21	VIIIb	right	17.5	-56.5	-55.0	12	0.01	2.40
22	V	left	-9.5	-50.5	-8.5	10	0.012	2.35
23	I-IV	left	-8.0	-43.0	-7.0	6	0.012	2.33
24	VIIIb	left	-23.0	-47.5	-59.5	5	0.012	2.32
25	X	left	-21.5	-34.0	-46.0	26	0.013	2.31
26	Crus II	right	28.0	-80.5	-40.0	8	0.014	2.27
27	Crus I	right	41.5	-67.0	-37.0	5	0.014	2.26

28	Crus I	left	-20.0	-83.5	-29.5	8	0.016	2.22
29	Crus I	left	-12.5	-86.5	-28.0	5	0.016	2.22
30	Crus II	right	38.5	-82.0	-40.0	1	0.016	2.22
31	Crus II	left	-36.5	-40.0	-41.5	2	0.016	2.22
32	VI	left	-6.5	-67.0	-10.0	11	0.016	2.21
33	VI	right	38.5	-61.0	-22.0	1	0.016	2.20
34	VI	vermal	1.0	-64.0	-20.5	4	0.016	2.20
35	VIIIb	right	20.5	-43.0	-47.5	6	0.017	2.19
36	VI	left	-15.5	-67.0	-26.5	3	0.017	2.19
37	Crus I	left	-33.5	-70.0	-32.5	4	0.017	2.19
38	VIIb	left	-36.5	-41.5	-47.5	4	0.017	2.18
39	VIIIa	left	-30.5	-47.5	-52.0	3	0.018	2.15
40	X	left	-14.0	-38.5	-46.0	1	0.019	2.14
41	I-IV	right	7.0	-47.5	-7.0	3	0.02	2.12
42	V	left	-11.0	-59.5	-19.0	2	0.022	2.08
43	VI	left	-24.5	-64.0	-28.0	1	0.022	2.07
44	VI	right	35.5	-59.5	-22.0	1	0.023	2.05
45	VI	right	16.0	-74.5	-20.5	1	0.023	2.05
46	VI	left	-36.5	-41.5	-28.0	1	0.023	2.05
47	VIIIa	right	22.0	-61.0	-59.5	1	0.023	2.05
48	I-IV	right	13.0	-40.0	-28.0	1	0.024	2.03
49	white matter		-9.5	-59.5	-38.5	1	0.024	2.03
50	Crus II	left	-36.5	-80.5	-43.0	1	0.024	2.02
51	V	right	10.0	-61.0	-19.0	1	0.025	2.02
No US post CS+ x prediction error PPI negative connectivity with VTA during recall (Figure 4A), t-test, p<0.05, uncorrected								
1	white matter		-20.0	-34.0	-32.5	17	0.002	2.98
2	white matter		-8.0	-68.5	-34.0	15	0.003	2.84
3	VIIb	right	40.0	-64.0	-53.5	24	0.004	2.83
4	Crus II	right	4.0	-80.5	-44.5	13	0.004	2.77
5	Crus II	left	-8.0	-91.0	-35.5	3	0.011	2.40
6	VIIb	left	-39.5	-59.5	-58.0	33	0.011	2.38
7	white matter		26.5	-44.5	-41.5	9	0.011	2.37
8	Crus II	right	8.5	-89.5	-34.0	2	0.012	2.34
9	VI	left	-27.5	-38.5	-32.5	5	0.015	2.25
10	Crus I	right	28.0	-83.5	-26.5	1	0.02	2.11
11	I-IV	right	20.5	-32.5	-22.0	1	0.021	2.09
12	Crus I	right	44.5	-77.5	-31.0	2	0.022	2.08
13	VIIb	right	26.5	-68.5	-55.0	1	0.023	2.05
14	white matter		-15.5	-34.0	-37.0	1	0.023	2.05

15	Crus I	right	44.5	-59.5	-29.5	1	0.024	2.03
No US post CS+ x prediction error PPI positive connectivity with VTA during reacquisition (Figure 4A), t-test, p<0.05, uncorrected								
1	I-IV	left	-18.5	-32.5	-22.0	52	<0.001	3.95
2	VIIb	left	-5.0	-67.0	-32.5	82	0.001	3.26
3	Extended cluster	right Crus II (108), right VIIb (9)						
	Crus II	right	25.0	-80.5	-44.5	117	0.001	3.16
	Crus II	right	28.0	-71.5	-47.5		0.014	2.29
4	Extended cluster	left Crus I (96)						
	Crus I	left	-45.5	-58.0	-35.5	96	0.002	3.06
	Crus I	left	-39.5	-65.5	-26.5		0.015	2.25
5	VIIb	left	-39.5	-59.5	-55.0	25	0.003	2.88
6	white matter		7.0	-62.5	-28.0	34	0.003	2.88
7	Crus II	right	7.0	-82.0	-46.0	9	0.004	2.75
8	VI	left	-21.5	-62.5	-28.0	93	0.005	2.71
9	Extended cluster	right IX (20), left IX (12), left VIIIb (1)						
	IX	right	2.5	-62.5	-56.5	33	0.005	2.68
	IX	left	-6.5	-59.5	-58.0		0.014	2.29
10	V	right	16.0	-47.5	-23.5	86	0.005	2.67
11	I-IV	left	-11.0	-41.5	-10.0	15	0.006	2.65
12	VI	right	34.0	-46.0	-34.0	31	0.007	2.58
13	I-IV	right	17.5	-32.5	-20.5	25	0.007	2.57
14	white matter		17.5	-47.5	-41.5	11	0.007	2.56
15	VIIIa	right	26.5	-58.0	-61.0	6	0.007	2.54
16	VIIIa	right	11.5	-70.0	-56.5	3	0.009	2.48
17	white matter		31.0	-61.0	-43.0	9	0.009	2.47
18	white matter		25.0	-67.0	-41.5	37	0.009	2.46
19	Crus I	right	41.5	-70.0	-26.5	8	0.011	2.40
20	white matter		41.5	-55.0	-38.5	31	0.011	2.37
21	VI	vermal	2.5	-77.5	-16.0	3	0.012	2.34
22	VIIIb	right	25.0	-52.0	-58.0	5	0.013	2.32
23	I-IV	right	25.0	-32.5	-34.0	10	0.013	2.32
24	VI	right	19.0	-65.5	-28.0	4	0.014	2.28
25	I-IV	right	2.5	-43.0	-22.0	16	0.014	2.27
26	I-IV	right	11.5	-43.0	-16.0	14	0.015	2.25
27	VI	right	31.0	-61.0	-22.0	2	0.016	2.23
28	Crus II	left	-20.0	-82.0	-50.5	6	0.016	2.22

29	VI	right	28.0	-49.0	-20.5	4	0.016	2.22
30	Crus I	right	40.0	-53.5	-29.5	5	0.016	2.21
31	Crus II	left	-45.5	-65.5	-52.0	2	0.016	2.21
32	VI	right	35.5	-56.5	-23.5	6	0.016	2.21
33	Crus II	left	-5.0	-83.5	-43.0	4	0.018	2.17
34	Crus II	left	-33.5	-82.0	-47.5	1	0.018	2.16
35	I-IV	right	11.5	-46.0	-10.0	8	0.018	2.15
36	VI	left	-32.0	-67.0	-26.5	10	0.019	2.15
37	VI	left	-27.5	-53.5	-32.5	1	0.02	2.12
38	VIIb	right	20.5	-70.0	-52.0	1	0.022	2.07
39	VIIb	left	-38.0	-47.5	-50.5	1	0.023	2.05
40	VIIIb	right	28.0	-38.5	-50.5	1	0.023	2.05
41	VI	right	29.5	-74.5	-20.5	1	0.023	2.05
42	Crus II	left	-14.0	-80.5	-49.0	1	0.023	2.05
43	Crus I	left	-50.0	-61.0	-26.5	1	0.023	2.05
44	DN	left	-14.0	-55.0	-32.5	1	0.024	2.03
45	VI	left	-35.0	-53.5	-28.0	1	0.024	2.03
46	I-IV	right	14.5	-38.5	-25.0	1	0.025	2.02
No US post CS+ x prediction error PPI negative connectivity with VTA during reacquisition (Figure 4A), t-test, p<0.05, uncorrected								
1	white matter		-11.0	-47.5	-23.5	52	0.001	3.46
2	I-IV	right	4.0	-52.0	-13.0	27	0.001	3.15
3	Crus I	right	43.0	-47.5	-28.0	5	0.002	3.04
4	VIIb	right	44.5	-52.0	-49.0	15	0.002	2.98
5	VIIIb	left	-8.0	-44.5	-58.0	27	0.002	2.98
6	Extended cluster	white matter (66), left Crus I (1), left Crus II (1)						
	white matter		-30.5	-58.0	-40.0	68	0.002	2.97
	white matter		-21.5	-50.5	-37.0		0.004	2.80
7	white matter		8.5	-46.0	-31.0	12	0.003	2.91
8	VI	right	34.0	-40.0	-26.5	7	0.009	2.48
9	Crus II	right	11.5	-83.5	-40.0	12	0.009	2.47
10	Crus II	left	-12.5	-85.0	-40.0	9	0.009	2.46
11	white matter		-15.5	-40.0	-31.0	20	0.012	2.35
12	V	left	-21.5	-37.0	-29.5	9	0.014	2.27
13	VIIIb	right	16.0	-49.0	-52.0	12	0.014	2.26
14	VIIb	right	38.5	-44.5	-44.5	5	0.015	2.25
15	VIIIa	right	8.5	-70.0	-50.5	2	0.016	2.20
16	Crus I	left	-48.5	-47.5	-40.0	1	0.019	2.13
17	I-IV	left	-2.0	-46.0	-16.0	1	0.023	2.04

No US post CS+ x prediction error PPI positive connectivity with VTA during reextinction (Figure 4A), t-test, p<0.05, uncorrected								
1	white matter		22.0	-32.5	-34.0	20	0.002	2.97
2	VIIIa	right	11.5	-70.0	-56.5	11	0.003	2.87
3	I-IV	left	-18.5	-32.5	-23.5	17	0.004	2.78
4	VIIIb	left	-18.5	-46.0	-61.0	21	0.007	2.57
5	Extended cluster	left VIIb (28), left VIIIa (11)						
	VIIb	left	-38.0	-53.5	-58.0	39	0.008	2.53
	VIIb	left	-38.0	-61.0	-53.5		0.017	2.20
	VIIIa	left	-29.0	-49.0	-58.0		0.018	2.16
6	VIIIb	right	11.5	-50.5	-61.0	9	0.008	2.52
7	I-IV	right	2.5	-43.0	-22.0	21	0.008	2.48
8	VI	left	-23.0	-59.5	-29.5	26	0.009	2.48
9	X	left	-15.5	-37.0	-49.0	3	0.011	2.37
10	VIIIa	left	-29.0	-40.0	-50.5	11	0.012	2.34
11	VIIb	right	41.5	-59.5	-55.0	17	0.012	2.33
12	Crus I	left	-50.0	-68.5	-41.5	2	0.014	2.28
13	Crus I	left	-47.0	-58.0	-34.0	8	0.014	2.27
14	VI	left	-36.5	-53.5	-28.0	9	0.014	2.26
15	VIIIb	right	14.5	-56.5	-61.0	7	0.016	2.21
16	VIIIb	right	23.5	-50.5	-58.0	5	0.016	2.21
17	IX	left	-6.5	-62.5	-56.5	4	0.017	2.18
18	Crus II	left	-6.5	-85.0	-43.0	3	0.019	2.14
19	VIIb	left	-32.0	-62.5	-52.0	3	0.019	2.13
20	VIIIb	right	26.5	-40.0	-52.0	1	0.02	2.12
21	Crus II	left	-8.0	-91.0	-35.5	2	0.02	2.11
22	I-IV	right	11.5	-40.0	-10.0	1	0.021	2.08
23	Crus I	right	50.5	-62.5	-32.5	3	0.022	2.07
24	VIIIa	left	-32.0	-43.0	-52.0	1	0.023	2.05
25	I-IV	right	11.5	-38.5	-13.0	1	0.024	2.04
26	VI	right	37.0	-58.0	-23.5	2	0.024	2.03
27	X	left	-24.5	-34.0	-41.5	1	0.024	2.03
28	IX	left	-6.5	-46.0	-50.5	1	0.024	2.02
No US post CS+ x prediction error PPI negative connectivity with VTA during reextinction (Figure 4A), t-test, p<0.05, uncorrected (i076 and i082)								
1	I-IV	right	4.0	-50.5	-14.5	38	0.001	3.33
2	VIIIb	left	-9.5	-43.0	-58.0	18	0.001	3.20
3	white matter		-12.5	-47.5	-26.5	31	0.002	3.03
4	Extended cluster	left V (20), white matter (9), left I-IV (9)						
	white matter		-18.5	-31.0	-31.0	38	0.003	2.93

	V	left	-26.0	-35.5	-28.0		0.016	2.22
5	V	right	31.0	-38.5	-25.0	24	0.003	2.86
6	VI	left	-35.0	-38.5	-32.5	42	0.003	2.86
7	Crus II	right	7.0	-80.5	-41.5	29	0.004	2.79
8	Extended cluster	right IX (116), right VIIIb (90), white matter (22), right VIIIa (17)						
	IX	right	14.5	-55.0	-50.5	245	0.004	2.76
	IX	right	8.5	-56.5	-44.5		0.005	2.69
	VIIIb	right	17.5	-44.5	-50.5		0.016	2.22
9	Extended cluster	white matter (187), left Crus II (25), left Crus I (17), left VIIIa (9), left VI (4), left DN (1)						
	white matter		-30.5	-59.5	-40.0	243	0.005	2.72
	white matter		-24.5	-55.0	-37.0		0.006	2.60
	VIIIa	left	-29.0	-52.0	-46.0		0.014	2.26
10	V	right	32.5	-34.0	-34.0	6	0.005	2.67
11	white matter		-12.5	-40.0	-31.0	92	0.007	2.55
12	I-IV	left	-5.0	-49.0	-13.0	19	0.008	2.53
13	VI	vermal	1.0	-77.5	-25.0	4	0.008	2.51
14	VIIb	right	11.5	-71.5	-49.0	29	0.009	2.48
15	VIIIa	left	-8.0	-70.0	-53.5	24	0.009	2.44
16	white matter		-14.0	-53.5	-40.0	15	0.011	2.38
17	Crus I	right	32.5	-77.5	-37.0	11	0.011	2.36
18	VIIIb	left	-18.5	-44.5	-52.0	11	0.012	2.35
19	Crus II	right	14.5	-85.0	-37.0	7	0.013	2.31
20	Crus I	left	-17.0	-82.0	-25.0	5	0.014	2.26
21	Crus I	left	-48.5	-47.5	-40.0	1	0.014	2.26
22	IX	left	-5.0	-52.0	-41.5	5	0.015	2.24
23	X	vermal	-2.0	-50.5	-32.5	5	0.016	2.22
24	Crus I	right	44.5	-65.5	-43.0	2	0.019	2.14
25	V	left	-23.0	-46.0	-17.5	1	0.02	2.12
26	Crus II	left	-14.0	-85.0	-40.0	6	0.02	2.11
27	IX	left	-5.0	-49.0	-37.0	1	0.021	2.10
28	Crus I	left	-11.0	-71.5	-31.0	4	0.021	2.09
29	white matter		-27.5	-44.5	-35.5	1	0.023	2.06
30	Crus I	right	46.0	-61.0	-43.0	1	0.023	2.04
31	Crus II	right	40.0	-44.5	-44.5	1	0.023	2.04
No US post CS+ x prediction error PPI positive connectivity with VTA during extinction, recall, reacquisition and reextinction (Figure 4B), t-test, p<0.05, uncorrected								
1	Extended cluster	left Crus I (158), left VI (142), left V (14)						

	VI	left	-32.0	-58.0	-25.0	314	0.001	3.53
	VI	left	-21.5	-52.0	-19.0		0.002	2.99
	Crus I	left	-38.0	-65.5	-32.5		0.003	2.90
2	I-IV	left	-14.0	-37.0	-25.0	105	0.001	3.30
3	Extended cluster	left X (23), left VIIIb (11), left VIIIa (6)						
	X	left	-21.5	-34.0	-46.0	40	0.001	3.25
	VIIIa	left	-29.0	-40.0	-50.5		0.016	2.21
4	Extended cluster	right V (225), right VI (32), white matter (21), right I-IV (16)						
	V	right	17.5	-47.5	-22.0	294	0.001	3.19
	V	right	13.0	-53.5	-19.0		0.003	2.94
5	Extended cluster	left I-IV (33), right I-IV (32)						
	I-IV	left	-5.0	-43.0	-22.0	65	0.002	3.13
	I-IV	right	4.0	-43.0	-20.5		0.004	2.76
6	VIIIb	left	-24.5	-46.0	-58.0	31	0.002	3.08
7	VIIIb	right	19.0	-59.5	-59.5	53	0.002	3.03
8	VIIb	left	-36.5	-41.5	-47.5	24	0.002	3.01
9	VI	left	-23.0	-61.0	-28.0	151	0.003	2.85
10	VIIIb	right	25.0	-52.0	-58.0	13	0.005	2.69
11	Crus II	vermal	-2.0	-79.0	-29.5	16	0.005	2.68
12	white matter		41.5	-53.5	-38.5	29	0.005	2.67
13	VIIIb	right	13.0	-40.0	-52.0	3	0.005	2.67
14	V	right	2.5	-61.0	-23.5	36	0.006	2.65
15	VI	left	-6.5	-73.0	-22.0	25	0.006	2.62
16	VI	right	8.5	-73.0	-22.0	23	0.007	2.59
17	VIIb	left	-26.0	-68.5	-55.0	8	0.007	2.57
18	Extended cluster	right Crus I (33), right VI (27)						
	Crus I	right	32.5	-67.0	-32.5	60	0.007	2.55
	VI	right	22.0	-62.5	-29.5		0.014	2.26
19	VIIIb	left	-15.5	-38.5	-50.5	4	0.009	2.47
20	VI	right	34.0	-56.5	-23.5	22	0.009	2.45
21	V	right	10.0	-61.0	-19.0	11	0.009	2.45
22	Crus II	left	-21.5	-79.0	-52.0	6	0.01	2.41
23	Crus II	left	-29.0	-79.0	-52.0	21	0.01	2.41
24	V	right	2.5	-65.5	-7.0	20	0.01	2.41
25	I-IV	left	-8.0	-43.0	-8.5	12	0.01	2.41
26	Crus I	left	-45.5	-58.0	-32.5	9	0.01	2.41
27	VI	right	28.0	-67.0	-23.5	50	0.013	2.32
28	VIIIa	right	10.0	-70.0	-56.5	3	0.013	2.30
29	VIIIa	left	-8.0	-68.5	-44.5	6	0.014	2.27
30	VIIIb	right	23.5	-46.0	-58.0	3	0.015	2.25

31	VI	left	-9.5	-67.0	-26.5	5	0.015	2.24
32	VI	left	-33.5	-43.0	-25.0	6	0.015	2.23
33	IX	right	2.5	-55.0	-47.5	5	0.017	2.20
34	VIIIa	left	-30.5	-47.5	-52.0	3	0.017	2.18
35	I-IV	right	14.5	-40.0	-28.0	3	0.018	2.15
36	VIIIa	vermal	5.5	-70.0	-44.5	4	0.019	2.15
37	Crus II	left	-33.5	-80.5	-47.5	2	0.022	2.08
38	Crus II	left	-15.5	-80.5	-50.5	1	0.022	2.08
39	IX	right	1.0	-62.5	-55.0	2	0.022	2.07
40	Crus I	left	-32.0	-79.0	-31.0	1	0.022	2.07
41	Crus II	left	-17.0	-85.0	-49.0	1	0.023	2.04
42	Crus II	right	26.5	-80.5	-41.5	1	0.024	2.03
43	X	right	23.5	-34.0	-47.5	1	0.024	2.03
44	Crus II	left	-47.0	-56.5	-46.0	1	0.025	2.02
No US post CS+ x prediction error PPI negative connectivity with VTA during extinction, recall, reacquisition and reextinction (Figure 4B), t-test, p<0.05, uncorrected								
1	Extended cluster	white matter (515), left V (72), left IX (25), left I-IV (14), left DN (12), left VI (10), vermal X (7), left Crus I (6), left Crus II (4), left X (2)						
	white matter		-18.5	-31.0	-32.5	667	0.001	3.24
	white matter		-24.5	-53.5	-37.0		0.002	3.12
	V	left	-26.0	-37.0	-31.0		0.002	3.00
2	white matter		-9.5	-70.0	-34.0	21	0.004	2.77
3	I-IV	right	4.0	-52.0	-13.0	16	0.006	2.62
4	white matter		10.0	-70.0	-35.5	6	0.006	2.62
5	Extended cluster	white matter (35), right DN (2)						
	white matter		23.5	-52.0	-37.0	37	0.006	2.61
	white matter		16.0	-49.0	-35.5		0.017	2.18
6	white matter		7.0	-46.0	-32.5	10	0.009	2.48
7	VIIIa	right	8.5	-70.0	-50.5	9	0.009	2.47
8	VIIIa	left	-9.5	-68.5	-55.0	4	0.009	2.44
9	Crus II	right	13.0	-82.0	-50.5	2	0.011	2.38
10	Crus II	right	8.5	-80.5	-40.0	9	0.013	2.32
11	Crus II	left	-21.5	-80.5	-43.0	5	0.013	2.30
12	VIIIb	left	-8.0	-46.0	-59.5	12	0.013	2.30
13	white matter		2.5	-59.5	-29.5	5	0.013	2.29
14	Crus I	right	41.5	-46.0	-41.5	5	0.015	2.26

15	white matter		-11.0	-46.0	-25.0	3	0.016	2.21
16	IX	right	5.5	-50.5	-62.5	3	0.017	2.19
17	white matter		34.0	-46.0	-43.0	4	0.018	2.15
18	VIIIb	right	13.0	-61.0	-55.0	1	0.019	2.14
19	VIIIb	right	26.5	-43.0	-44.5	2	0.02	2.12
20	Crus II	left	-12.5	-85.0	-40.0	2	0.021	2.10